OCCURRENCE AND DISTRIBUTION OF AU AND AG IN THE CARIBOU-CROSS MINING AREA, BOULDER COUNTY, COLORADO

by

Sage Langston-Stewart

A thesis submitted to the Faculty and Board of Trustees of the Colorado School of Mines in partial fulfillment of the requirements for the degree of Master of Science (Geology).

Golden, Colorado

Date _____

Signed: _____

Sage Langston-Stewart

Signed: _____

Dr. Katharina Pfaff

Thesis Advisor

Golden, Colorado

Date _____

Signed: _____

Dr. Wendy Bohrson

Professor and Department Head

Department of Geology and Geological Engineering

ABSTRACT

The Caribou-Cross deposit is part of the historical Grand-Island mining district in southwest Boulder County, Colorado, just west of the town of Nederland, approximately 21 miles west of Boulder. The Grand Island district includes at least 15 historic silver and gold mines with the Caribou and the Cross mines being the two primary mines. The Caribou-Cross and legacy mines scattered about the property of Grand Island Resources was intermittently mined for Au and Ag since the 1870's and is currently undergoing brownfield redevelopment by Grand Island Resources.

The Grand Island mining district is in the northernmost part of the Colorado Mineral Belt (CMB), a northeast-southwest trend of mineral deposits stretching across Colorado. Structurally controlled precious metal bearing veins are hosted in Laramide age Caribou monzonite and in Precambrian Idaho Springs gneiss. It is the goal of this study to improve the understanding of ore zonation, related alteration assemblages, the occurrence, mineralogy, and spatial distribution of precious metals, and the development of a conceptual model for the Caribou-Cross deposit in the Grand Island mining district.

One hundred samples from across the district ranging from igneous host rock lithologies, primary veins, to waste rock samples were collected and investigated using optical petrography, micro-X-ray fluorescence, cathodoluminescence microscopy, fluid inclusion petrography and microthermometry, FE-SEM-BSE and -EDS, and SEM based automated mineralogy.

Six different intrusive rock types were identified and distinguished based on petrography and automated mineralogy, including magnetite dunite, monzonite, quartz monzonite, amphibolite, magnetite amphibolite, and lamprophyre. The monzonite shows an alkaline evolution path and evidence suggests the mafic bodies originated from magmatic differentiation. Alteration consists of large-scale, early-stage hydrothermal K-feldspar alteration along fractures prior to vein formation. Subsequent sericitization of plagioclase is present proximal to the veins whereas chlorite alteration is present distal to the vein. Early pyrite and quartz (Q1) veins were followed by ankerite and second-stage quartz (Q2). Fluid inclusions in Q1 quartz are CO_2 rich suggesting that vein formation took place deep below the paleosurface. In contrast, rare fluid inclusion assemblages present in Q2 quartz are low in CO_2. Homogenization temperatures range from 210 to 225°C and salinities range from 7.9 to 13.9 wt.% NaCl equivalent. Base metal minerals (chalcopyrite, galena, iron-poor sphalerite) and precious metal phases (stromeyerite and

Ag-rich gold) formed in fractures and vugs contemporaneously with and after the Q2 quartz. Late barren carbonate veins and a final supergene stage, which includes malachite and azurite, conclude the formation of the Caribou-Cross deposit. It is interesting to note that Ag-bearing gold was only found at Cross, but not at Caribou.

Veins show strong structural control and complex overprinting relationships that are indicative of a system that evolved through space and time with multiple changes between lithostatic and hydrostatic conditions. The Caribou-Cross deposit is interpreted to be a deep seated magmatic-hydrothermal system that formed from fluids having an intermediate sulfidation state

TABLE OF CONTENTS

LIST OF FIGURES

LIST OF TABLES

LIST OF ABBREVIATIONS AND ACROYNYMS

Locations:

CMB	Colorado Mineral Belt
IRSZ	Idaho Springs-Ralston shear zone
NS	Native Silver
SI	San Isabel
SWP	Southwest Pandora
CR	county road

Methods:

FE	field-emission
SEM	scanning electron microscope
AM	automated mineralogy
EDS	energy-dispersive spectroscopy
BSE	backscattered electron
TIMA	TESCAN Integrated Mineral Analyzer
XPL	cross-polarized light
PPL	plane-polarized light
FI	fluid inclusion
CL	cathodoluminescence

Mineral abbreviations:

qtz	quartz
Q1	early-stage quartz

Q2	late-stage quartz
ank	ankerite
bt	biotite
amph	amphibole
chl	chlorite
Kfs	potassium feldspar
ser	sericite
ms	muscovite
el	electrum; Ag-bearing gold
smy	stromeyerite
cpy	chalcopyrite
py	pyrite
gn	galena
sp	sphalerite
pl	plagioclase
brt	barite
peg	pegmatite
dol	dolomite
cc	chalcocite

Elements:

Ag	silver
Au	gold
Ti	titanium

Fe	iron
Cu	copper
Pb	lead

Miscellaneous:

fg	fine-grained
MSPC	muscovite-sericite-phengite-chlorite
MSPCAA	muscovite-sericite-phengite-chlorite-ankerite-adularia
N	number (total number of analyses)
IS	intermediate sulfidation
LS	low sulfidation
HS	high sulfidation
GIR	Grand Island Resources

ACKNOWLEDGEMENTS

From climbing mountains to academic pursuits, I couldn't do it without the support of my tribe. I specially thank my advisor, Dr. Katharina Pfaff for being my guide and providing feedback while always being positive and encouraging. I thank Sean Muller and Grand Island Resources for allowing me to conduct this research on their deposit and allow me the opportunity gain valuable experience working at an underground mine. I'd like to thank Thomas Monecke and Jim Reynolds for helping with cathodoluminescence and fluid inclusion work. Special thanks to all my fellow grad students: Filip Kasprowicz for keeping the mood light with your sense of humor, Paul Henderson and Reji Raghavan for discussing all aspects of mineral exploration over beers, Noah Fleischer and Ben Magnin for sharing their office space and hosting much needed lunch breaks, and everyone else who made Mines a great experience. I'd like to specially thank Kelsey Livingston for always going above and beyond for students by helping with research and being the go-to woman for any job. Thanks to all my undergraduate friends for the love and support through the process and putting together weekend getaways. Thanks to everyone else who has been a part of my life for encouraging me and keeping my spirits high throughout the process. It takes a village to raise a child, and similarly, it takes a community to raise a grad student.

Thanks to Grand Island Resources for fully sponsoring this project. Thanks to the National Science Foundation and the Barrick Endowment at Colorado School of Mines for providing additional funding that allowed me to focus on my academic pursuits.

CHAPTER 1: INTRODUCTION

Colorado has attracted prospectors since the mid 1800's and the Pikes Peak or Bust gold rush flooded this new frontier with people trying to strike it rich in the Colorado Rocky Mountains. Throughout history, metals such as gold, silver, molybdenum, lead, zinc, tungsten, uranium, copper, iron, and many more have been mined in Colorado. Most of these metals have come from what is called the Colorado Mineral Belt (CMB). The CMB is a southwest-northeast trend of mining districts stretching across Colorado from the San Juan mountains to the front range near Boulder (Figure 2.1). The CMB is characterized by Tertiary igneous intrusive bodies and related ore deposits which are typically porphyries, epithermal veins, and replacement bodies (Tweto and Sims, 1963). Although gold initially brought many people to Colorado, silver had its time in the spotlight during the silver boom beginning in 1879 when silver was discovered in Leadville, Colorado. During this time, Caribou-Cross was discovered. Gold and silver were the source of the wealth in the west and have significantly contributed to the economic and social growth of Colorado. With gold rising to an average price of nearly $1800 per ounce in 2021, gold has shifted to the focus of exploration.

The CMB is host to many vein-type gold and silver deposits. The Idaho Springs deposits are vein-type deposits with pyrite, sphalerite, galena, chalcopyrite, and tennantite as the principal ore minerals along with gold and silver (Moench and Drake, 1966). At Central City, Au-Ag bearing veins show complex progressive re-opening and overprinting textures that display district-wide metal zoning as a result of the progression of the magmatic-hydrothermal system, which is thought to be genetically related to a deep alkaline intrusion (Alford et al. 2019). Gold and silver are related to the polymetallic base metal stage which overprints an earlier quartz-pyrite stage (Alford et al. 2019).

The northeastern portion of the CMB in Boulder County exhibits unusual tungsten and telluride deposits which have attracted both prospectors and scholars who conducted studies describing this mineralized area, which is known as the Tungsten District. The district consists of northeast-trending veins containing dominantly ferberite and quartz while some veins contain ferberite and gold tellurides (Lovering and Tweto, 1953). The Tungsten District lies adjacent to

the Caribou-Cross deposit which are dominantly silver and gold bearing veins of magmatic-hydrothermal origin.

The Caribou-Cross silver and gold deposits are hosted in Precambrian and younger metasedimentary rocks and in Laramide age monzonitic intrusions. Precious and base metals are associated with sulfide-rich, near vertical, fault-controlled veins (Holland, 1994). Gold is thought to occur deeper in the deposit whereas silver has been observed to occur at high grades shallow in the deposit (S. Muller, pers. commun., 2021). Since the Grand-Island mining district is thought to represent a magmatic-hydrothermal system, alteration assemblages should show well-defined zoning patterns with respect to the intrusion, as seen in the nearby Central City vein deposits. Metal and alteration zoning is caused by factors such as temperature gradients, varying host rocks, and variations in fluid-rock ratio. Mineralization is structurally controlled, similar to the Central City and Tungsten District deposits, but determining the lithologic controls on mineralization will be imperative for further exploration.

It is the goal of this study to improve the current understanding of ore zonation, related alteration assemblages, and the occurrence, mineralogy, and spatial distribution of precious metals, and develop of a conceptual model for the Caribou-Cross deposit in the Grand-Island mining district.

CHAPTER 2: THE GRAND ISLAND MINING DISTRICT

The Grand Island mining district is located northwest of Nederland, Colorado in west-central Boulder County, Colorado (Figure 2.1). The district includes at least 15 historic silver and gold mines, with the Caribou and the Cross being the two primary mines. The current operation is a brownfield redevelopment of the Caribou and Cross mines and exploration of the legacy mines scattered about the property of Grand Island Resources.

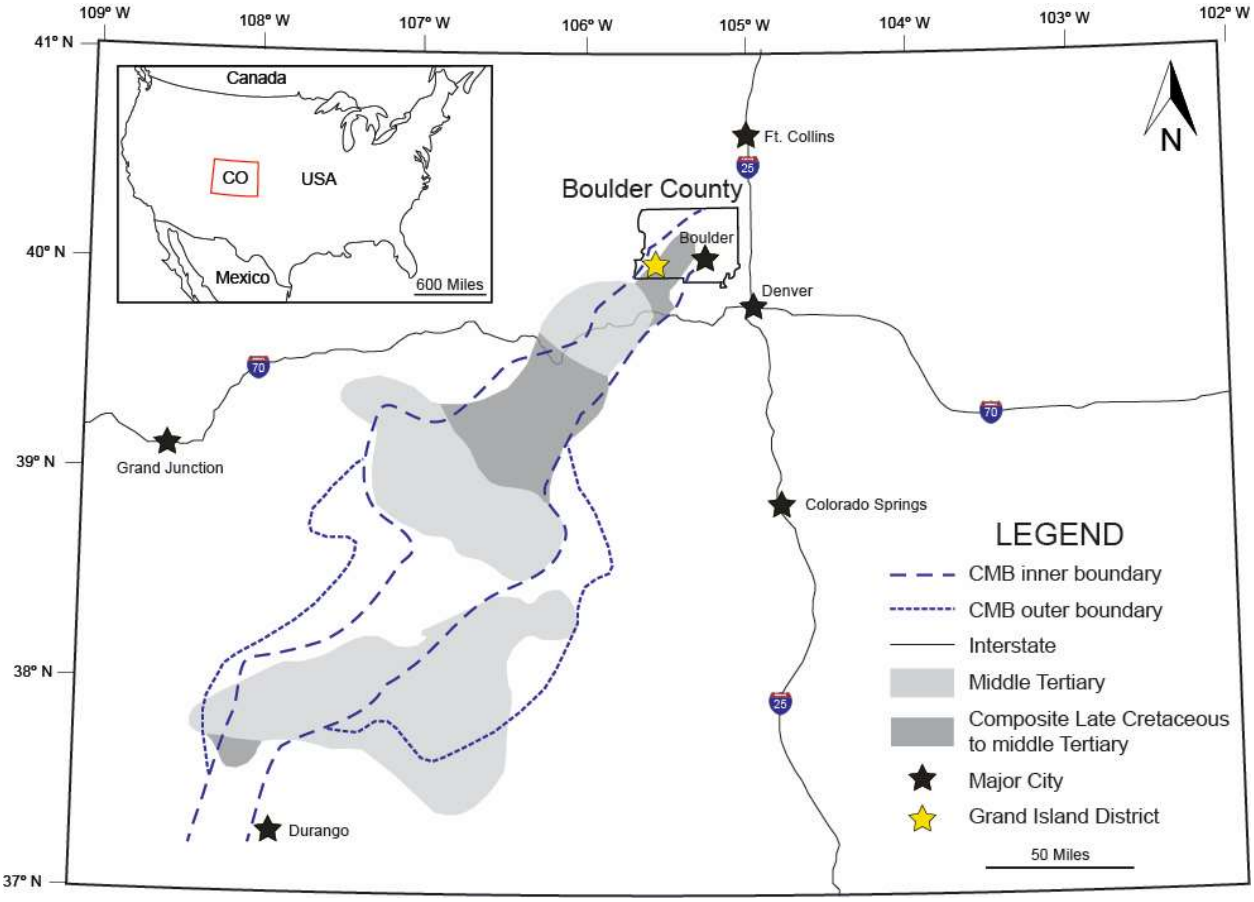

Figure 2.1 Location of Caribou-Cross mines (after Wilson and Sims, 2003).

The Caribou and Cross mines are located approximately 5.2 miles up county road (CR) 128 from Nederland, which is a well-kept, graded road that provides access to the mine year-round. The main office space and logging area is located at the entrance of the Idaho Tunnel, also known as the Caribou Tunnel (Figure 2.2). The Idaho Tunnel connects back to the Caribou shaft and the Caribou workings; however, the Idaho Tunnel and Caribou mine are currently

under rehabilitation. Just down the hill (9,800 feet elevation) is the entrance into the underground workings of the Cross mine (the Cross) (Figure 2.2). The first level tunnel at the Cross mine is fully accessible year-round whereas lower levels at the Cross are usually flooded. Drill core is kept in buildings on-site and those are fully accessible year-round; however, some historical high-grade intercepts are missing. The Comstock shaft, core warehouse, and core logging area are located just a half mile up CR 128 (Figure 2.2). Further roads allow access to waste-rock piles and remains of historical operations, which are only accessible during the summer months when there is no snow coverage. The historical Caribou mine and most waste-rock piles are on Caribou Hill, with a peak of 10,300 feet elevation (Figure 2.2). The Silver Point mine and associated dumps are located just east of Caribou Hill (Figure 2.2). The Congo Chief mine and Pandora hill, also called Pomeroy Mountain, are located northeast of Caribou hill, across from the Caribou Park bog (Figure 2.2). These are accessible from Forest Service Road 505 during the summer months. Figure 2.2 shows the infrastructure and mine locations described above.

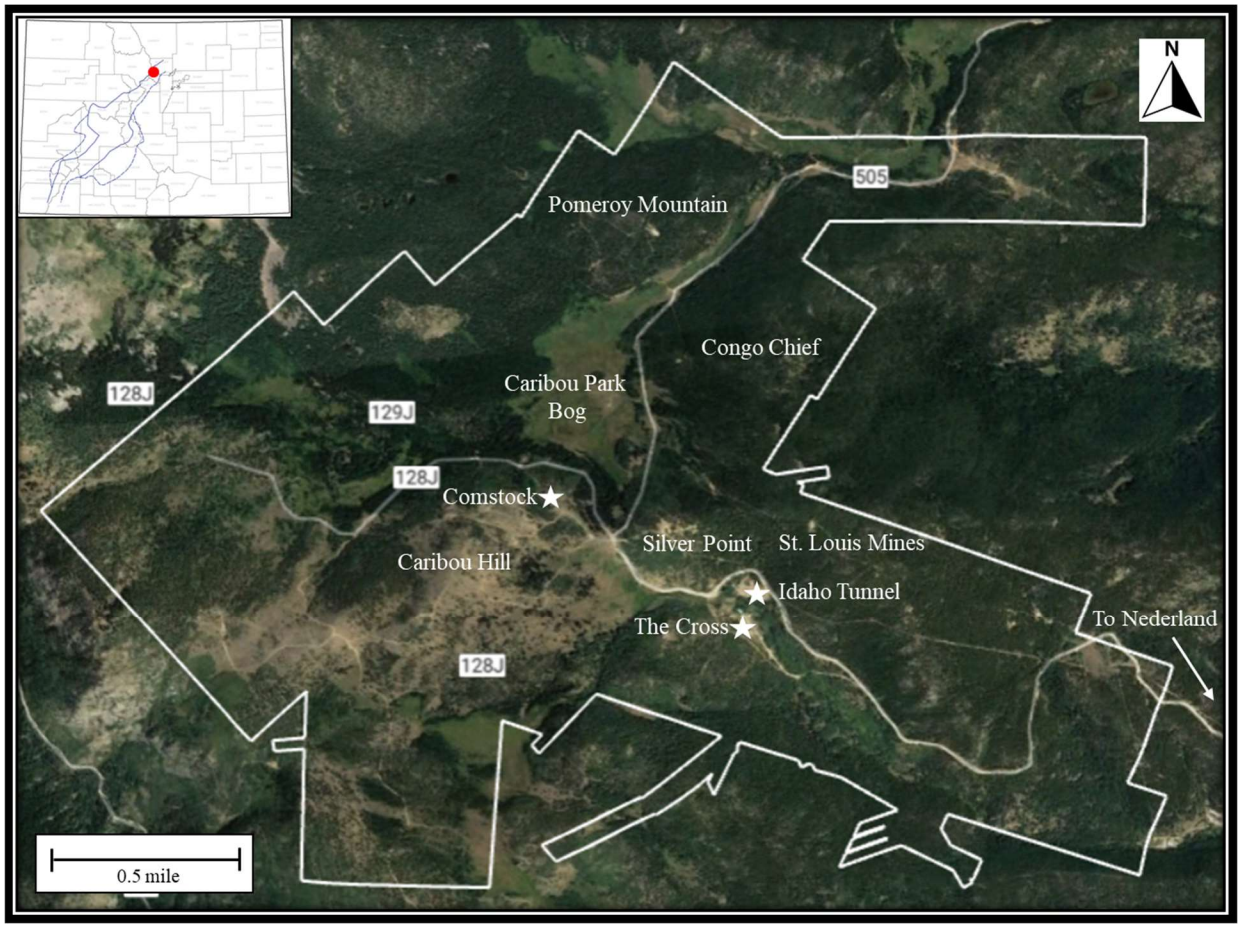

Figure 2.2 Google Earth satellite image with important district locations and claim area boundary.

2.1 Mine History

Prospecting began in the Grand Island district as early as 1859, and the first claim in the area was filed in March of 1861 (Smith, 2003). Samuel Conger, a gold prospector granted the credit for discovering the Caribou silver deposit, visited the region in the 1860's where he discovered a piece of high-grade silver float while he was hunting near Pomeroy Mountain (Figure 2.2; Smith, 2003). Although he did not recognize the silver, he knew the piece of float was something important due to the weight of the rock sample, so he held on to this rock out of curiosity. On his mission out west, he stopped in Virginia City, Nevada, where he saw people mining ore that was similar to what he had seen at Caribou. After learning about silver mining in Virginia City, he assembled a team of prospectors to return to Caribou and bring silver mining to Colorado (Smith, 2003; Raines pers. commun., 2022).

In 1869, Samuel Conger relocated the place where he found the high-grade silver rock and he brought along his friends William Martin, George Lytle, Hugh McCammon, John Pickel, and Harvey Mishler (Smith, 2003). Martin discovered the Caribou vein and Lytle discovered the Poorman vein, both with rich lodes (Smith, 2003). At that time, there were no roads or infrastructure in the district. Over the next decade, roads were built to Caribou along with a mill in Nederland (Smith, 2003). Many prospectors and miners looking to get rich flooded to the Caribou area and the small town of Caribou grew and gained popularity. The town of Caribou reached its peak in the 1870's with a school, newspaper, saloons, post office, a church, and many other businesses (Smith, 2003). The town had multiple fires and with the fall of the silver price, Caribou dwindled to a ghost town by the 1890's (Smith, 2003). Many of the mines were worked on intermittently by various owners until 1939 (Smith, 2003).

During the silver rush in the Grand Island district, the Cross mine was worked on by C.M. Carol (1876 to 1886) and was reopened in 1915 by George W. Teal (S. Muller, pers. commun., 2021). The Teal family partnered with Todd Dofflemeyer and worked on the Cross forming the Cross Gold Mining Company until a disagreement caused its closure in 1939 (S. Muller, pers. commun., 2021).

The mines were not reopened until 1974 when Tom Hendricks gained a long-term mining lease from the Dofflemeyer family. Tom Hendricks formed Calais Resources and partnered with many other companies including Columbine Minerals of Denver (Colorado), Good Mining Co., Power Petroleum, East West Minerals of Sidney in Australia, Gwalia USA, Minerals Canada Ltd, Echo Bay Mines, and Grand Island Resources (S. Muller, pers. commun., 2021). During his time, Hendricks consolidated all of what is now known as the Grand Island District under one entity and opened many of the historical underground workings. Tom Hendricks pursued multiple drilling programs and mining phases while operating the Cross. Grand Island Resources acquired the entire project in 1998 with Hendricks as Vice President, member of the Board of Directors, and project manager. From working on the property for roughly 50 years, Tom Hendricks had valuable knowledge of the property, led significant rehabilitation and exploration efforts, and understood the geology of the deposit (S. Muller, pers. commun., 2021). Grand Island Resources still owns and operates the project today. Grand Island Resources holds 3.5 square miles of patented and unpatented claims for the project area and has continued mine rehabilitation, reclamation, and exploration efforts.

CHAPTER 3: GEOLOGY

The Grand Island district ore deposits in the northern CMB are hosted in two primary host rocks, the Precambrian Idaho Springs gneiss and the Laramide age Caribou monzonite. The Cross veins are hosted in the Idaho Springs gneiss and the Caribou monzonite, with prominent occurrences of stockwork at the contact, whereas the Caribou veins are hosted solely in the heterogeneous Caribou monzonite stock. Structures provided conduits for hydrothermal fluids to form veins and stockwork zones within these host rocks. The Cross was mined historically for gold whereas the Caribou was mined historically for high-grade silver and both deposits exhibit supergene enrichment, especially noted at Caribou. Veins vary in width from a few inches (centimeters) to tens of feet (meters) and commonly have strike lengths greater than 300 feet (100 meters). There has been extensive research on the Cross and the Caribou deposits, and they have historically been interpreted as entirely separate systems, although this study looks at both deposits to be of the same system. The following sections provide more detail on the regional geology, host rocks, and deposit geology.

3.1 Regional Geology and Structure

The Grand-Island mining district is located in the northern most part of the CMB, and more specifically, the northern margin of the Idaho Springs-Ralston shear zone (IRSZ) of the Colorado lineament in the Front Range mineral belt (Figure 3.1). The CMB is a northeast-southwest trend of mineral occurrences and ore deposits throughout Colorado following ancient Precambrian weakness zones (Tweto and Sims, 1963). The IRSZ is a cataclastically deformed zone that is one to two miles (~1.5-3.5 km) wide and trends north 55° to 60° east for 23 miles (~37 km) from Idaho Springs to the mountain front at Coal Creek where it terminates beneath the Fountain Formation (Figure 3.1; Tweto and Sims, 1963). The northwest side of the shear zone contains broad, upright anticlines and synclines that trend north-northeast, whereas the southeast side of the shear zone contains primary folds that trend east-northeast (Figure 3.1; Tweto and Sims, 1963). In the northeast area of the shear zone, near Coal Creek, the shearing was more intense than to the southwest area, near Idaho Springs. New foliation that strikes north 60° to 70° east and steeply dips southeast crosscuts older gneissic structures (Tweto and Sims, 1963).

Movement occurred over multiple generations, showing that there was an initial stage with horizontal movement, then a later stage with vertical movement which is when the cataclasis and cross-folding occurred (Tweto and Sims, 1963). Younger northwest trending faults crosscut the dominant northeast trending shear zones. These faults are mostly barren, but they affected the distribution of the northeast-trending veins and ore minerals (Tweto and Sims, 1963).

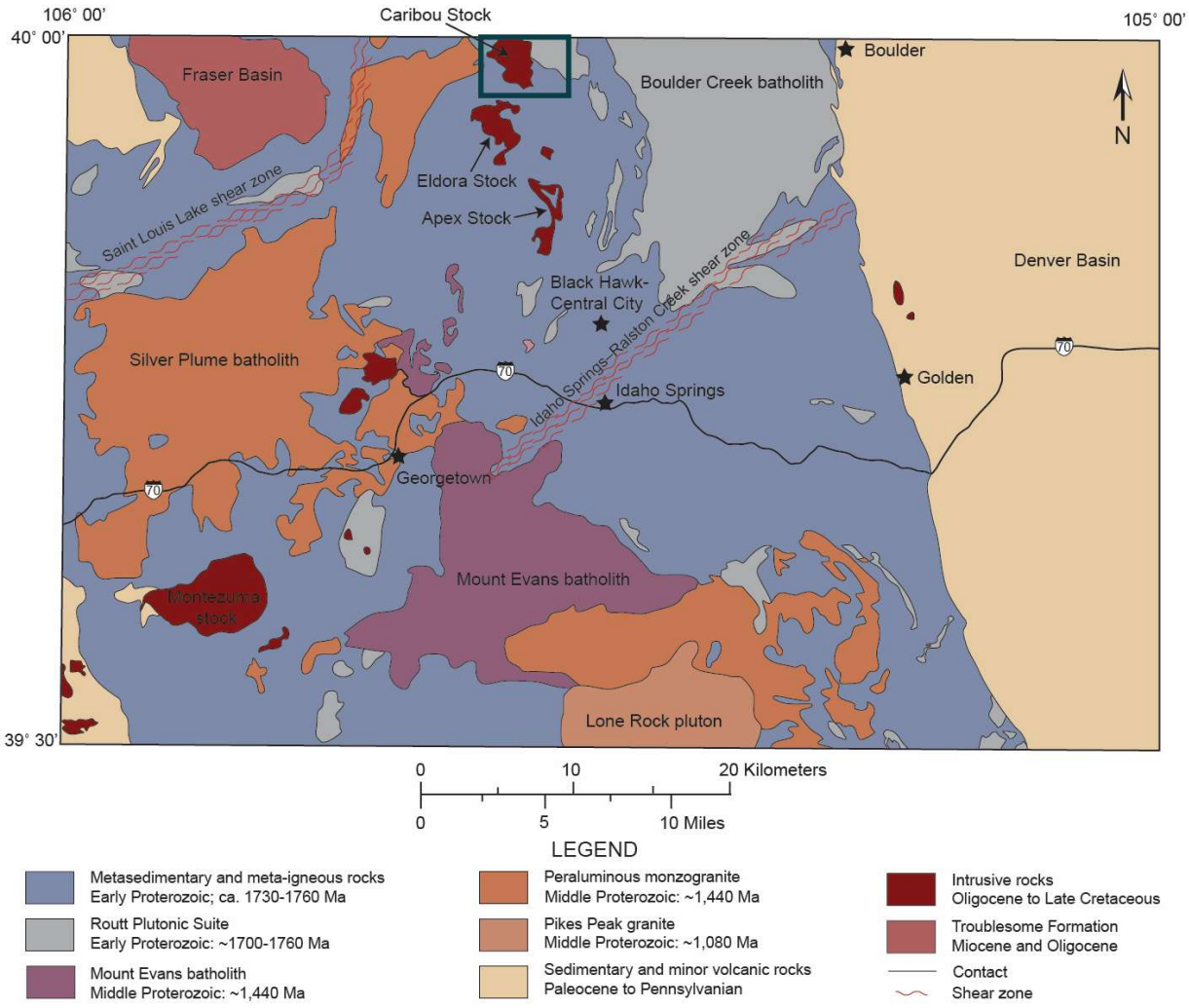

Figure 3.1 Simplified regional geologic map of the Denver west quadrangle in north-central Colorado (modified after Kellog et al., 2008)

During the Laramide Orogeny in the Late Cretaceous (approximately 72 Ma), alkaline and calc-alkaline igneous rocks intruded Precambrian rocks. Opposing Tweto and Sims (1963) conclusion that Precambrian fault zones provided fluid pathways for mineral deposition as faults were reactivated and dilated, Caine et al. (2010) provided evidence that suggest the structures hosting and controlling mineral deposits in the eastern central Front Range are related to the

shallow, brittle Laramide stress field and gradual strain localization with accompanying hydrothermal fluid flow rather than reactivation of Proterozoic ductile shear zones. Lytle (2016) interpreted that the IRSZ did not form as a result of a subduction zone or from a continental suture zone related to pre-existing crustal scale weakness, but rather is the result of folding associated with the Picuris orogeny ~1.43 Ga.

During the first main period of magmatism between 70 to 60 Ma, magmatism occurred throughout the entire CMB (Gable, 1984). During the second period of magmatism, from 54 to 44 Ma, magmatism occurred on a smaller scale with few scattered plutons in the central and northeast CMB (Gable, 1984). Magmatism may have been continuous and may have continued after these dates, but there is not sufficient age data to establish that (Gable, 1984). There are multiple intrusive bodies near the Caribou area, which include most notably the Apex and Buckeye Mountain stocks, Long Gulch stock, Eldora stock, Caribou stock, Audubon-Albion stock, Jamestown stock, and Bald Mountain stock, among others (Gable, 1984). According to spectrographic analyses, the intrusions in the area have below-average amounts of most base-metal trace elements compared to the published averages, except for uranium, thorium, barium, copper, strontium, vanadium, and zirconium (Gable, 1984). Gable (1984) also noted that most mineable ore deposits, in and associated with the stocks and dikes, may not be directly associated to the intrusions.

Based on geophysical data, Wilson and Sims (2003) concluded that the northeast trending ductile shear zones are more abundant than previously known. The shear zones formed from transpressional tectonics around 1.4 Ga in the Mesoproterozoic and locally followed pre-existing Paleoproterozoic structures (Wilson and Sims, 2003). A second set of northwest trending Mesoproterozoic shears represents a secondary control on intrusion emplacement. The two major periods of mineralization are during Late-Cretaceous to early Tertiary and mid-Tertiary, both of which were superposed by a minor late Tertiary ore-forming event (Figure 2.1; Wilson and Sims, 2003). Gravity lows were interpreted as long-lived magma chambers following a northwest-trending basement shear zone separating each magma body (Wilson and Sims, 2003).

Holland (1994) conducted a detailed structural analysis at the Cross and determined that the major faults strike east-southeast and dip steeply north to vertical with two major episodes of fault movement. The first is left-lateral strike-slip along east-west striking structures which is overprinted by right lateral strike-slip movement along minor east-northeast striking structures

(Holland, 1994). Holland (1994) concluded regional east-trending compression created left-lateral movement of the Arapahoe Pass-Junction Ranch fault. The Caribou stock and quartz monzonite dikes were localized in dilation zones that developed on the Arapahoe Pass-Junction Ranch fault (Holland, 1994). When the direction of compression rotated to the northeast, northeast-trending tensional cross structures, which were cemented by hydrothermal minerals, formed between east-trending left-lateral shear zone boundaries (Holland, 1994). Sigmoidal structures were formed by the counter-clockwise rotation of the central portions of the northeast-trending structures, and east-trending structures developed at left-lateral shear zone boundaries (Holland, 1994). Domino-style rotation occurred as left-lateral movement continued on the east-trending structures (Holland, 1994). Northeastern compression ended after the first stage of mineralization and late unmineralized faults formed in conjugate sets at N23W/88W and N35E/57W (Holland, 1994). Holland (1994) suggested that ore formation was strongly structurally controlled, which confirms the findings of Barrett and Schuiling (1988).

Ore-bearing veins show two main orientations: one set of veins strikes east and dips nearly vertical, and the other set of veins strikes northeast and has variable dips to the northwest (Holland, 1994). The northeast-trending structures are hypothesized to curve into the east-trending structures and depth (Holland, 1994). There is evidence that the veins formed in reactivated fault planes and the structures potentially merge into a deep trunk or root zone (Holland, 1994). Although the trunk zone has not yet been tested to depth, the regional and deposit-scale structure is a critical component in the localization of ore. The two dominant structural orientations on both the regional and deposit-scale are northwest-trending and northeast-trending (Barrett and Schuiling, 1988; Holland, 1994; S. Muller, pers. commun, 2021).

3.2 Host Rock Lithologies

The host rocks in the Grand Island mining district are dominantly the Idaho Springs gneiss and the Caribou monzonite (Gable, 1969). Other distinct units include the “iron dike” (S. Muller, pers. commun., 2021), lamprophyre, diabase, gabbro, pyroxenite, and multiple other intrusive bodies (Gable, 1969), which adds complexity to the igneous evolution, as described below. Figure 3.2 displays the geologic map with the primary units.

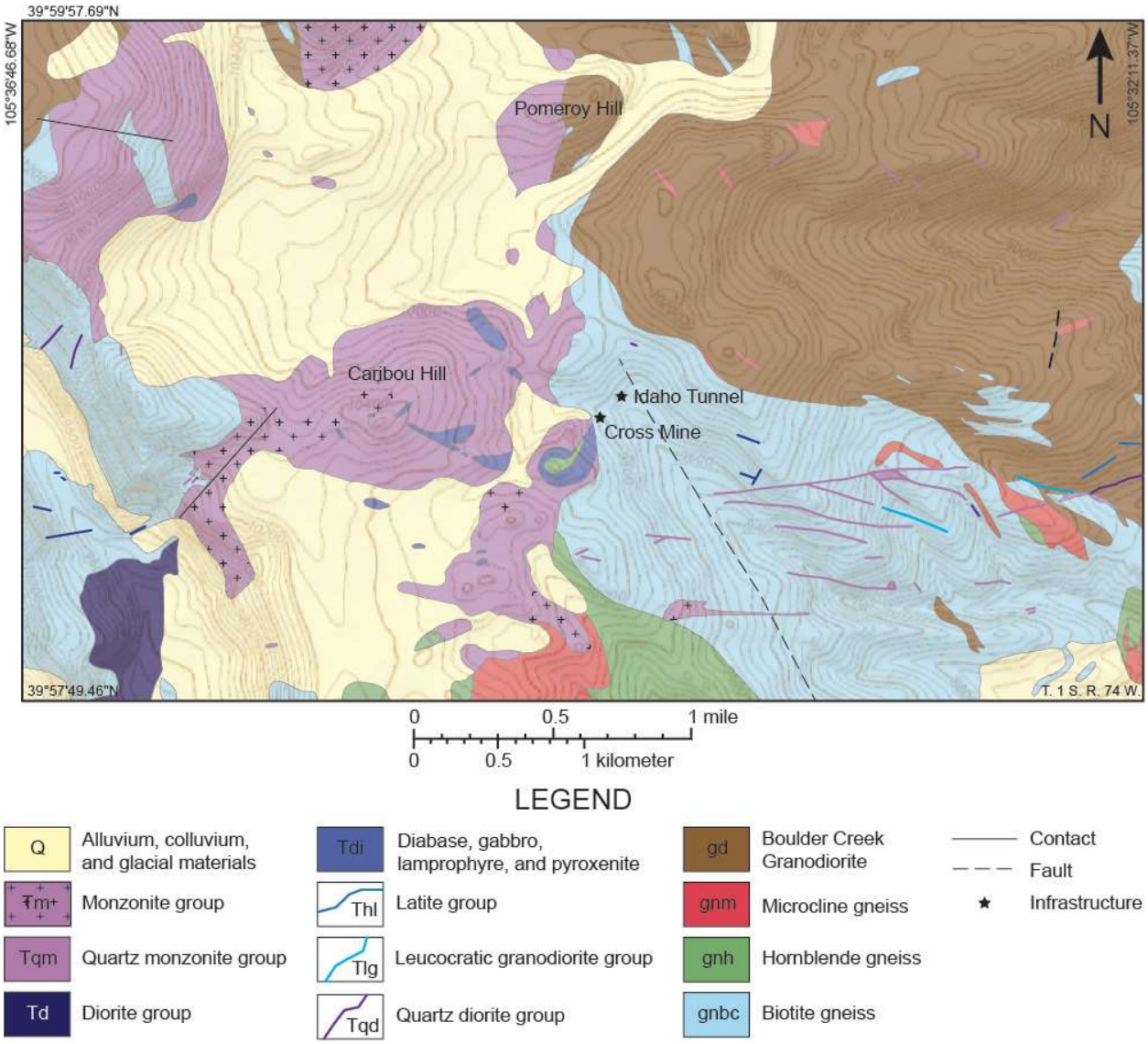

Figure 3.2 Geologic map of the project area (modified after Gable, 1969) with locations of the Cross mine and the Idaho Tunnel.

The underlying Precambrian basement rocks in the Grand-Island mining district have exhibited multiple periods of deformation including both ductile and brittle regimes. The dominant Precambrian rock type in the project area is the Idaho Springs gneiss which generally refers to the Precambrian basement rock in the Front Range but has been mapped as distinct sub-units including microcline gneiss, hornblende gneiss, and biotite gneiss (Gable, 1969). The Idaho Springs gneiss formed from a shaly sedimentary protolith and reached peak metamorphism around 1.75 Ga (Rb-Sr; Hedge et al., 1967). Subsequently, this unit was intensely folded and

altered to quartz-biotite gneiss and quartz-biotite sillimanite schist (Lovering and Goddard, 1950).

The primary igneous intrusive rocks associated with the Laramide activity in the Grand Island district is the heterogeneous Caribou stock, which is dominantly monzonite to quartz monzonite in composition but also includes rocks with mafic compositions (Holland, 1994). The Caribou stock is Paleocene, dated at roughly 62.6 +/- 6.3 Ma by zircon fission track (Marvin et al., 1974). Smith (1938) described the Caribou stock as a composite intrusion that is a biotitic augite monzonite enclosing small volumes of gabbroic and ultramafic rock and titaniferous magnetite masses. Lovering and Goddard (1950) described the Caribou stock to be calcic monzonite to quartz monzonite with mafic rocks composing more than five percent of the stock. Gable (1984) identified mafic bodies of pyroxenite and gabbro that have titaniferous magnetite rich lenses.

As observed by Smith (1938) and Lovering and Goddard (1950), the contact between the monzonite and mafic rocks is sharp in some locations and gradational in others. The largest body of titaniferous iron rocks, which has recently been called the “iron dike” by current mine employees consists of magnetite pyroxenite with biotite amphibolite and gabbro (Lovering and Goddard, 1950). This magnetite body contains 30%-65% magnetite and 2.6%-4.5% titanium oxide, which was historically observed for the potential of being iron and titanium ore (Lovering and Goddard, 1950). Thus far, no connection of the magnetite and mafic rocks with the base- and precious-metal veins has been identified.

3.3 Ore Mineralogy

The Caribou and Cross are both structurally controlled gold, silver, and base-metal vein deposits approximately 0.5 miles (~1 km) apart. The veins are structurally controlled by two sets of strike-slip faults. The east-west trending faults are steeply dipping, and the northeast trending faults vary from a steep southeast dip to shallow northwest dip (Barrett and Schuiling, 1988; Holland, 1994). The faults show evidence of a reversal of strain from right lateral to left lateral, which provided a tensional environment for vein formation (Barret and Schuiling, 1988; Holland, 1994).

The Cross and the Caribou deposits have historically been interpreted as unique systems due to different gold to silver ratios between the deposits. The Cross deposit, dominantly gold-

bearing, is hosted in both the Idaho Springs gneiss and the Caribou monzonite with exceptional mineralization in the stockwork zone at the lithologic contact. The Caribou deposit, dominantly silver bearing, is hosted entirely in the Caribou monzonite. Supergene enrichment of silver has played a critical role forming the high-grade zones in the district, particularly at the Caribou (Barrett and Schuiling, 1988; Moore et al., 1957), although the depth to which the supergene mineralization extends is debated as well as if the zoning that is present in these deposits is due to hypogene or supergene processes (Miller, 1983; Francis, 1987; Barrett, 1989; Holland, 1994;), which is discussed in more detail in the following sections.

3.3.1 The Caribou Deposit

The Caribou is a silver, gold, and base-metal vein deposit hosted in the Caribou monzonite and has been historically mined for high-grade silver, but little gold has been recognized. Native silver was reported in all ore from the Caribou even at depth (Lovering and Goddard, 1950). The lead-silver ore bodies are described as vertical or steeply dipping veins as wide as 7 feet, but only mineralized at the centers with 18 inches in thickness (Moore et al. 1957). The upper portions of veins at the Caribou deposit have been strongly oxidized and enriched in silver above the 300 level (Lovering and Goddard, 1950; Moore et al. 1957; Miller, 1983). The veins are mostly fissure fillings and ore zones are localized by changes in dip or strike of the vein and by vein junctions (Lovering and Goddard, 1950; Moore et al., 1957;). The main veins at the Caribou deposit include the No Name, Nelson (East, Intermediate, and West Nelson), Caribou, Poorman, and around 30 other minor veins, of note is the Radium vein.

The No Name vein is the most notorious at the Caribou as it was the most productive silver vein and extended over 1,800 feet along strike (Lovering and Goddard, 1950). It has a northeast trend of north 65° east and dips 55° to 60° northwest (Lovering and Goddard, 1950). The No Name vein had considerably more carbonate minerals than did the Caribou vein (Moore et al., 1957). A particular occurrence of massive pink carbonate minerals occurs on the 500 level of the No Name vein with a thickness greater than one foot (Moore et al., 1957). The junction of the No Name vein and the Caribou vein, which has an east trend, was the largest ore shoot in the district (Lovering and Goddard, 1950). All of the east-trending veins terminate at the No Name vein (Lovering and Goddard, 1950).

The Nelson veins strikes parallel to the No Name vein. The Caribou vein and Poorman vein strike approximately east-northeast (Moore and Cavender, 1951). The Caribou vein is most notable on the 360 level (Moore et al., 1957). Quartz is more abundant in the Caribou vein compared to other veins at the Caribou deposit such as the No Name vein (Moore et al., 1957).

The Radium vein on the 920, 1040, and 1140 levels at the Caribou strikes east-northeast and was of interest by the USGS in the 1950's for exploration of uranium, which funded the drive for the Idaho Tunnel (Moore and Cavender, 1951). Although there is not a considerable uranium resource in the Radium vein, it contains unusual mineralogy compared to the other veins in that it has an excess of chalcopyrite contemporaneous with galena and sphalerite and contains pitchblende (Moore et al., 1957).

Although abundances of minerals change in different veins at the Caribou, Francis (1987), who observed 69 thin sections from the veins in the Caribou deposit including the No Name vein, Poorman vein, North Poorman vein, Guadalupe vein, and the Nelson vein, interpreted that all of the veins have a similar paragenesis. Francis (1987) distinguished four periods of vein mineralization (Figure 3.3). The first includes massive white quartz associated with pyrite and hematite (Francis, 1987; Moore et al., 1957). The second is main-stage ore including quartz, galena, sphalerite, and chalcopyrite (Francis, 1987). Late quartz occurs as clear euhedral crystals that fill open vugs and form veinlets that cross-cut other minerals, except for the late-stage carbonates (Moore et al., 1957). Galena and sphalerite are closely associated, but sphalerite increases with depth due to shallow leaching from groundwaters (Moore et al., 1957; Miller, 1983). The third stage is the precious-metal phase which includes polybasite, stromeyerite, jalpaite, and chalcopyrite. The last stage is supergene enrichment, which includes chalcocite, covellite, and bornite (Francis, 1987).

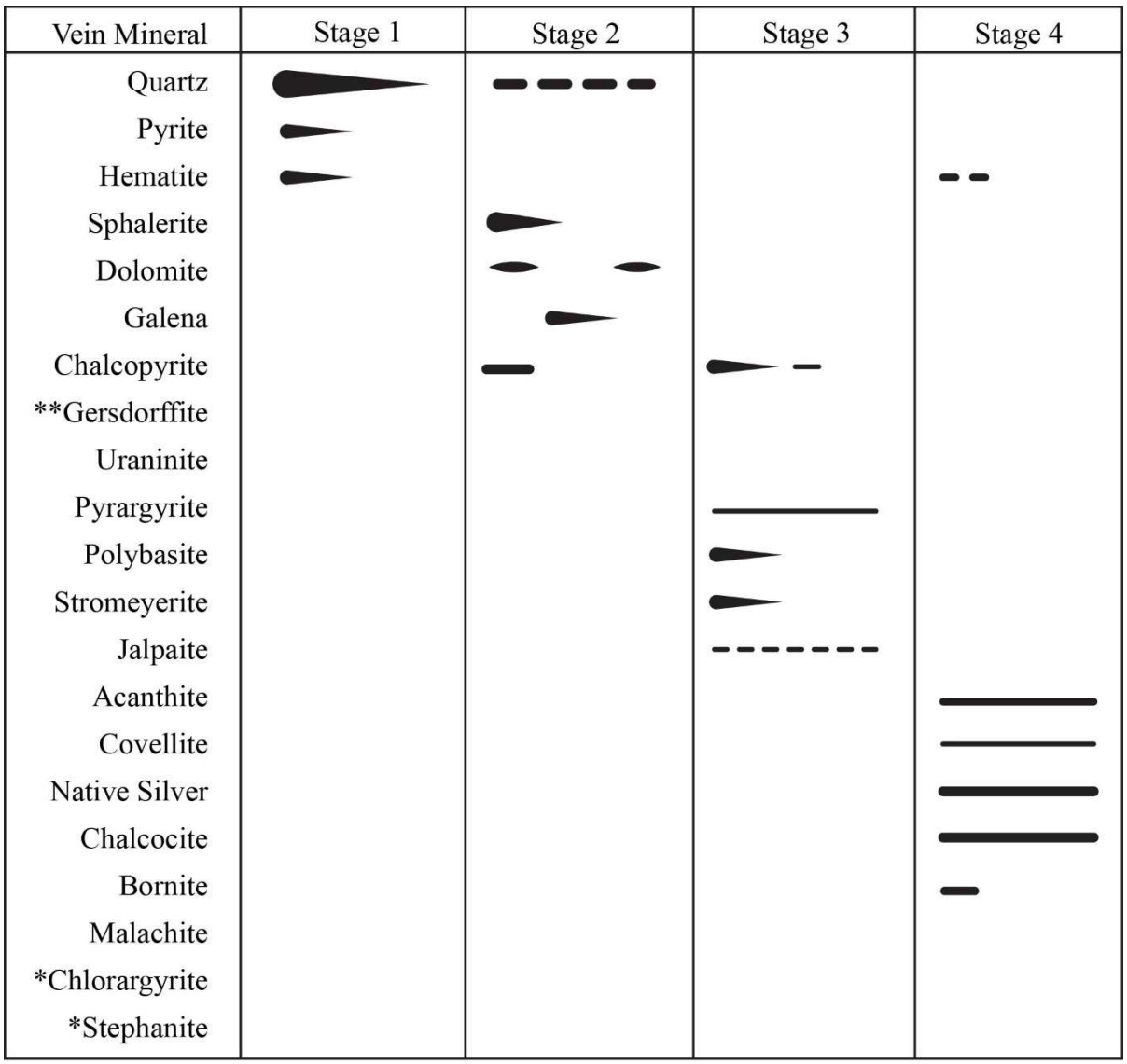

* = minerals reported by Moore et al. (1957)

** = minerals reported by Write (1954)

Figure 3.3 Mineral paragenesis of the veins at the Caribou deposit (modified after Francis, 1987)

Moore et al. (1957) described alteration zoning patterns around the veins at the Caribou, as shown in Figure 3.4. According to his work, the silicified zone ranges from a few inches to 2 feet wide from the center of the vein. This zone is characterized by the complete destruction of original texture, cryptocrystalline quartz, sericite or illite or both, and carbonates. The ratio of sericite to illite decreases outward from the vein. The silicified zone grades into slightly altered rock characterized by chlorite that ranges from 6 inches to 2 feet wide. The chlorite zone grades outward into fresh rock. An argillic zone sometimes occurs between the silicified zone and the

chlorite zone with sharp boundaries. It is characterized by green-gray and very friable rock with minerals of the montmorillonite group (Moore et al., 1957). Alteration of plagioclase in the wall rock is zoned outward from the veins from sericite to kaolinite to montmorillonite-kaolinite (Francis, 1987).

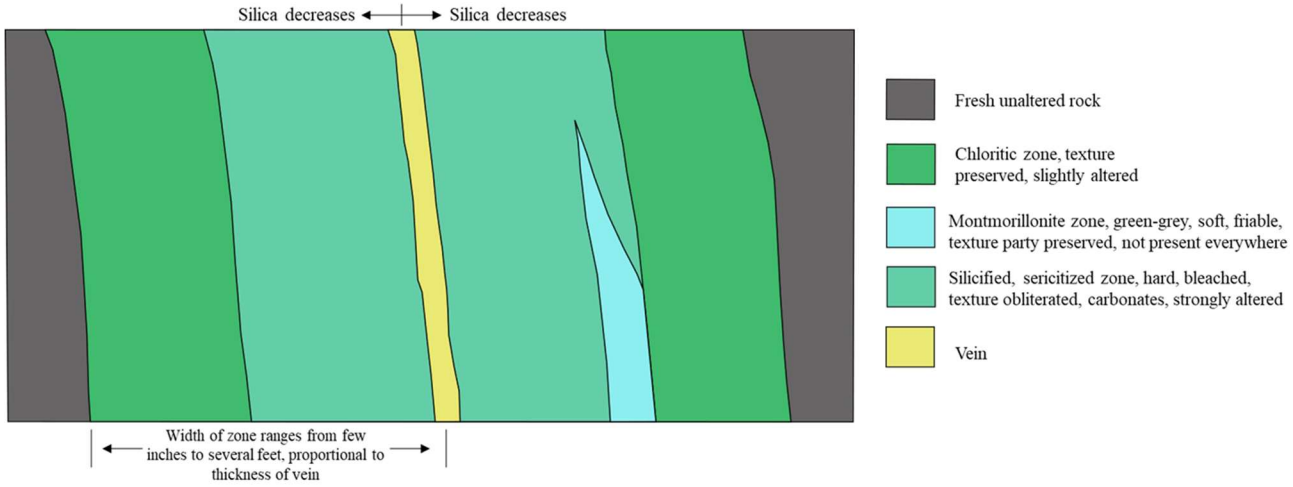

Figure 3.4 Alteration zoning of the Caribou vein in the Caribou deposit (modified after Moore et al., 1957)

To summarize, the Caribou is host to silver and base-metal vein mineralization showing four stages of mineralization (Figure 3.3) and a defined alteration halo (Figure 3.4). The dominant ore minerals are sphalerite, galena, chalcopyrite, and silver-bearing minerals. The supergene effect is prominent at shallow depths.

3.3.2 The Cross Deposit

The Cross deposit consist of gold, silver, and base-metal veins hosted in both the Idaho Springs gneiss and the Caribou monzonite. The main veins at the Cross deposit include the Hopewell (or East Cross), Cross, Crown Point, Rare Metals, Romeo, Juliet Stockwork, South Apache, North Apache, and Potosi veins (Figure 3.5). Many other smaller veins and vein splays are present in underground workings.

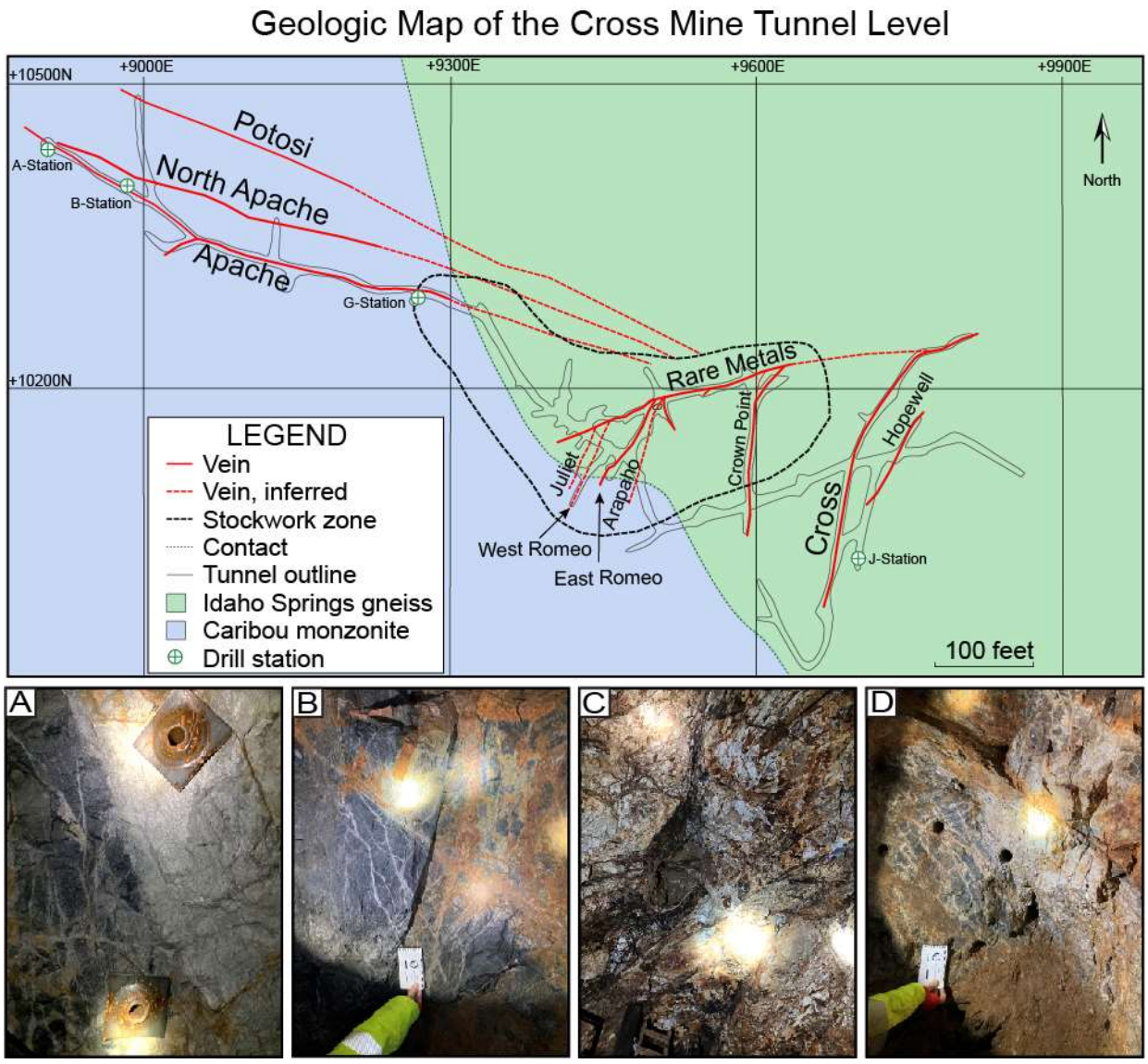

Figure 3.5 Geologic Map of the Cross Mine Tunnel Level with coordinates on the mine grid, locations of veins, the stockwork zone, and 2021 drill stations (modified after Holland, 1994): A) photograph of the back at the Potosi tunnel showing wide alteration halo and stockwork stringer veins; B) photograph of the rib at the Apache tunnel with oxidized stringer veins; C) photograph of the ballroom at Crown Point within the stockwork zone in the Idaho Springs gneiss; D) photograph of the stockwork zone near the Arapaho vein in the Caribou monzonite with a pegmatitic vein and oxidized stringers.

Previously the Hopewell, Cross, Romeo, Juliet, Arapahoe, Crown Point, and Rare Metals veins were thought to coalesce at depth with the legendary “trunk zone” (Barrett and Schuiling, 1988; Holland, 1994). The Hopewell, Cross, Romeo, Juliet, Arapahoe, and Crown Point veins strike northeast-southwest and have a near vertical dip (Barrett and Schuiling, 1988; Holland, 1994). These veins truncate against the Rare Metals vein which strikes east-northeast (Barrett

and Schuiling, 1988). A newly defined large stockwork zone (new interpretation by Dave Young, pers. commun., 2021), located at a bend in the lithologic contact, encompasses the Rare Metals, Crown Point, Romeo, Arapaho, and Juliet veins and extends at depth (D. Young, pers. commun., 2021; Figure 3.5). The Apache and Potosi veins are well-defined vein zones that follow a northwest trend extending out from the primary stockwork zone (Figure 3.5). Based on field work between Spring of 2021 and Spring of 2022, these vein zones consist of multiple generations of parallel and crisscrossing thin vein stringers. Typical vein margins are gradational and are grade-defined, but veins become more discrete and sharply defined at depth (Barrett and Schuiling, 1988). Changes in strike and dip of the veins are high grade zones, as well as areas near the contact (Barrett and Schuiling, 1988). The dominant control on mineralization is "structural channeling along dilatational fault and vein planes within an environment chemically favorable for the precipitation of Ag-bearing gold and base metal sulfides" (Holland, 1994).

Oxidation is noted to 600 feet depth, but unoxidized sulfides occur just under surface (Barrett and Schuiling, 1988). Gold to silver ratios increase with depth but only due to supergene enrichment, since hypogene mineralization is consistent with depth (Barrett and Schuiling (1988). Jobodwana (1991) took trace element geochemistry from four drill holes on the Apache vein at the 4th level and found the Au:Ag ratio to be 1:615. There are lateral variations of mineralization, but no pattern or zoning was recognized. Barrett and Schuiling (1988) credit ore variation due to changes in strike and dip of the veins.

According to Holland (1994), there are seven discrete ore forming events (Figure 3.6). The first stage contains fine-grained quartz and pyrite, with minor molybdenite. Coarse-grained quartz-pyrite of the second stage, locally includes sericite on euhedral quartz, specular hematite, sphalerite, and galena. More than half of the pyrite from this stage is replaced by base- and precious-metal sulfides (Holland, 1994). The third carbonate stage includes dolomite, calcite, and ankerite. The base- and precious-metal stage (stage four) contains sphalerite, galena, and chalcopyrite, in order of decreasing abundance, along with Ag-bearing gold. The Ag-bearing gold is typically less than 20 μm and occurs at base-metal sulfide grain boundaries but is closely related to second stage chalcopyrite (Holland, 1994). Sphalerite, galena, chalcopyrite, and Ag-bearing gold occur as open-space fill in the coarse-grained quartz-pyrite veins and replace pyrite (Holland, 1994). Other minerals which may belong in this stage, but normally appear in the later sulfosalt stage include acanthite, tennantite, tetrahedrite, famatinite, and stromeyerite. Acanthite

and galena show an intergrowth texture, revealing their close paragenetic relationship (Nigbor, 1986). Native silver and associated acanthite are locally abundant in permeable, sheared portions of the Rare Metals vein and in near-surface high grade veins in the northwest zone (Barrett and Schuiling, 1988). High silver assays always occurred with high lead and zinc assays (Dentler, 1984; Nigbor, 1986).

The later sulfosalt stage (stage six) consists of chalcopyrite, tetrahedrite, tennantite, proustite, famatinite, pyrargyrite, and stromeyerite (Holland, 1994). Sulfosalts occur as later replacement of the base metals (Holland, 1994; Barrett and Schuiling, 1988). The dolomite stage consists only of dolomite that is locally pale green or pink and occasionally, dolomite occurs as open space fill in the previous veins but typically crosscuts or offsets previous veins or cements breccias (Holland, 1994). The supergene stage (stage seven) contains covellite, chalcocite (Barrett and Schuiling, 1988; Holland, 1994), bornite, and digenite that replaced dominantly chalcopyrite but also galena and sphalerite. Native sulfur occurs on surfaces of fine-grained quartz and on faulted sulfide surfaces. Native silver occurs as wires and with sieve texture in large, irregular masses. Goethite replaces everything except for quartz (Holland, 1994).

Holland (1994) described five distinct alteration assemblages in regards to time with associated ore forming assemblages as shown in Figure 3.6, whereas previous studies described alteration assemblages spatially in regards to distance from the vein. Generally, K-feldspar alteration occurred first (Nigbor, 1986; Barrett and Schuiling, 1988; Jobodwana, 1991). Silicification and sericitization overprints are proximal to the vein and are often the most abundant (Nigbor, 1986; Barrett and Schuiling, 1988). Argillic alteration is distal from the vein and includes kaolinite, montmorillonite, illite, and smectite (Nigbor, 1986; Barrett and Schuiling, 1988; Holland, 1994). Barrett and Schuiling (1988) include distal chloritization and hydrothermal clay. Jobodwana (1991) observed a weakly developed distal propylitic alteration of chlorite, epidote +/- calcite +/- sericite +/- K-feldspar.

To summarize, the Cross deposit consists of multiple veins and a large stockwork zone consisting of multiple historically mined veins located at the contact between the Caribou monzonite and the Idaho Springs gneiss. The primary ore minerals are base metal sulfides, Ag-bearing gold, acanthite, and silver-sulfosalts. Seven ore-forming stages have been identified by Holland (1994) and alteration generally consists of K-feldspar, sericite, silicification, chlorite, and clays.

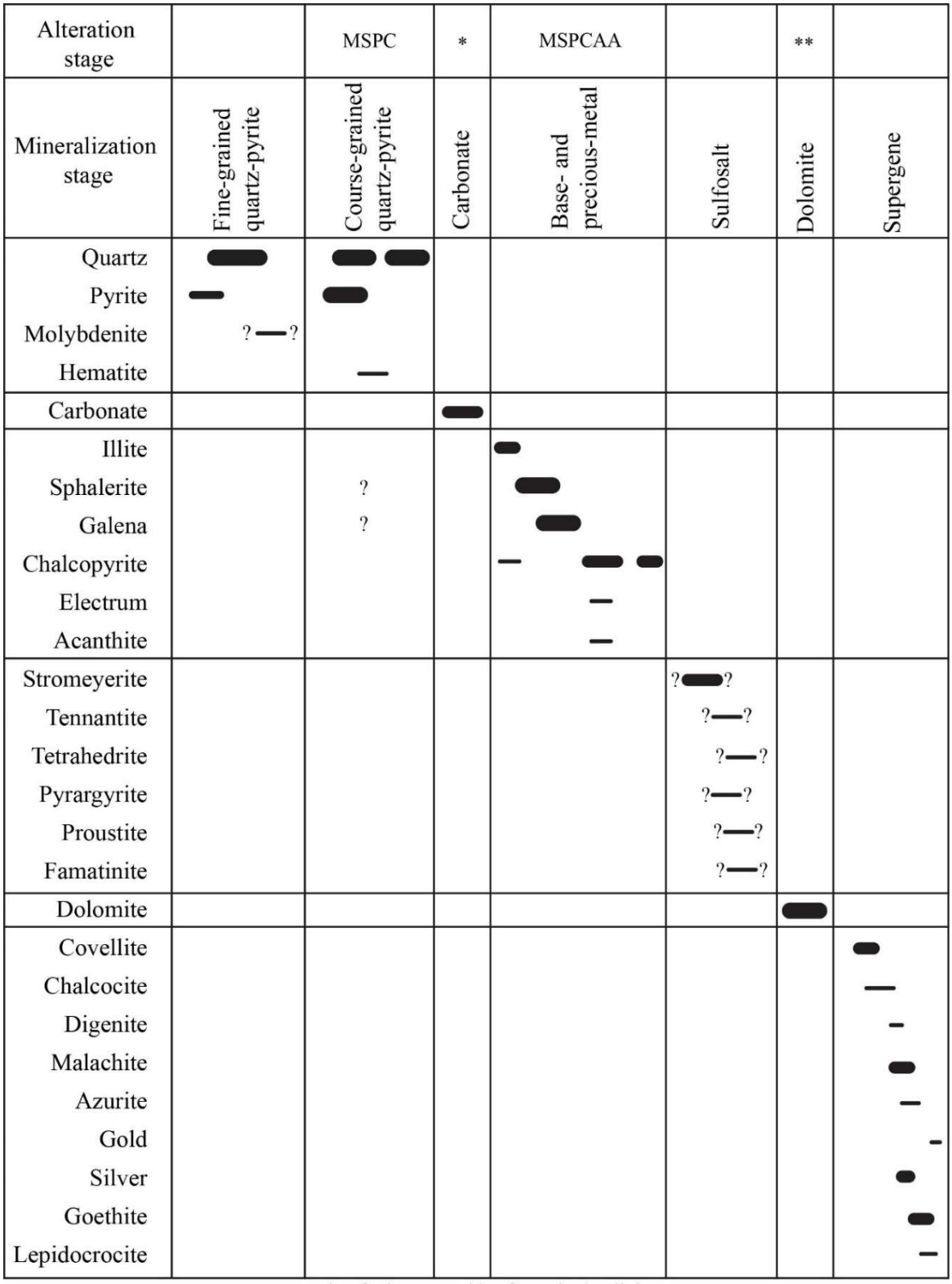

Figure 3.6 Paragenetic table of the Cross deposit (modified after Holland, 1994). Adularia alteration is associated with hematite mineralization. MSPC stands for muscovite-sericite-phengite-chlorite. MSPCAA stands for muscovite-sericite-phengite-chlorite-ankerite-adularia.

CHAPTER 4: MATERIALS AND METHODS

4.1 Sampling Strategy

At the time of this study, the Caribou workings were not accessible, however, the Cross workings on the main tunnel were accessible as well as the waste rock piles across the district. A drilling program operated from January 2021 until November 2021. In May 2021, 35 samples were collected from drill holes and a few waste rock piles. Sampling continued throughout the fall of 2021 to target the remaining waste rock piles, igneous rock types, samples from summer drilling including the stockwork zone, and few historical drill holes. One hundred samples were collected for this study: 35 thick sections and 65 rock chip epoxy mounts. The samples are categorized into three domains: samples targeting precious metal bearing veins, samples targeting the waste rock, and samples targeting the igneous suite. Twenty-eight of the thick sections come from nine diamond core drill holes and the remaining seven thick sections come from grab samples of waste rock piles on Caribou Hill. The 65 rock chip epoxy mounts were added to the suite; 20 samples for investigation of the igneous host rock suite, 21 samples for the opaque mineralogy of the waste rock piles scattered around the district, and 24 samples targeting the stockwork zone and drilling from the 1990's at depths below the workings of the Caribou shaft. All sample locations are shown in Figure 4.1.

Prior to collecting samples from the Grand-Island mining district, the existing LeapFrog model and accompanying geochemical data was studied to identify high-grade Au and Ag drill core intercepts from the spring 2021 underground drilling at the Cross. These high-grade intercepts of core were laid out and examined on site at the Caribou where particular halved core and quarter core samples were collected based on veining and alteration textures in May 2021. These samples range in depth from the first level at the Cross down to 278 feet below the first level from stations A, B, and J, which were all drilled from the tunnel level at the Cross (Figure 3.5).

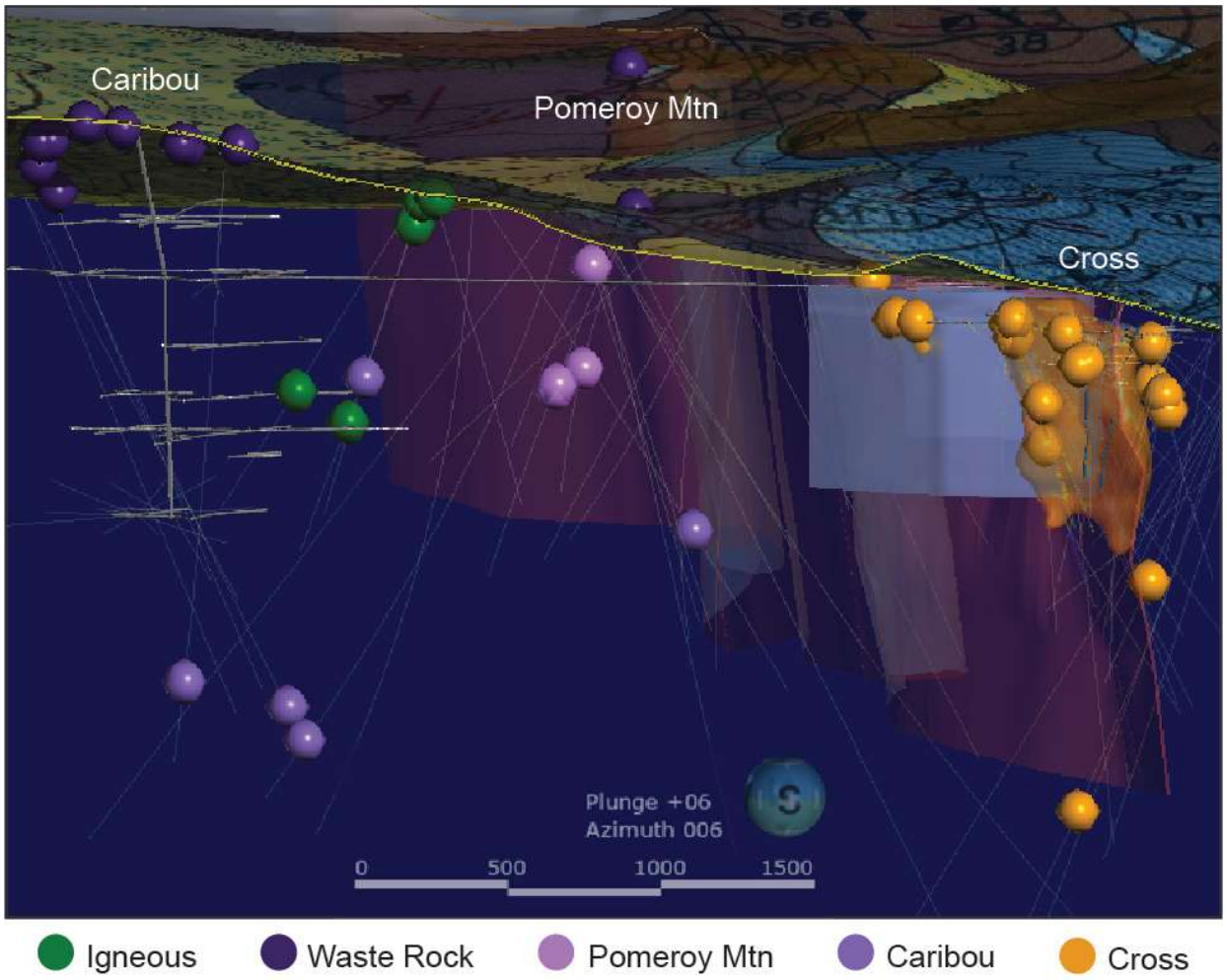

Figure 4.1 Sample location map from LeapFrog looking north. The underground workings, drill hole traces, stockwork zone (orange volume), Apache-Potosi veins (blue surface), and the lithologic contact (red surface) are shown.

Samples from drill holes are named in the format: project name-year-hole number-footage. For example, Sample CR-21-A1-123.5 is from the Cross project, drilled in 2021, drill hole A1 (drill hole 1 at station A), at 123.5 feet depth down hole. Drill stations are labeled in Figure 3.5. Note that many of these drill holes are not collared from the surface. As a result, 123.5 feet downhole is not true depth below surface.

Additional ore samples were collected to include all portions of the Caribou-Cross deposit, in the fall of 2021 after drilling was complete and assay data was available. These samples targeted ore in the newly defined stockwork zone from 2021 drilling at G station and I station and ore below the workings at the Caribou from 2021 drilling at SN station and 1990's

drilling (Table 4.1). Table 4.1 displays the sample name, preparation type, drill hole number, depth from which the sample was taken, and the zone and vein system the sample is from.

Table 4.1 Sample list of samples targeting precious metal bearing veins

No.	Sample ID	Prep type	Drill hole	Depth (ft)	Zone	Vein system
1	CR-21-A1-123.5	Thick section	CR-21-A1	123.5	Cross	Apache-Potosi
2	CR-21-A1-132	Thick section	CR-21-A1	132	Cross	Apache-Potosi
3	CR-21-A1-153	Thick section	CR-21-A1	153	Cross	Apache-Potosi
4	CR-21-A1-77	Thick section	CR-21-A1	77	Cross	Apache-Potosi
5	CR-21-A2-1.0	Thick section	CR-21-A2	1	Cross	Apache-Potosi
6	CR-21-A3-10.5	Thick section	CR-21-A3	10.5	Cross	Apache-Potosi
7	CR-21-A3-11.0	Thick section	CR-21-A3	11	Cross	Apache-Potosi
8	CR-21-A3-4.0	Thick section	CR-21-A3	4	Cross	Apache-Potosi
9	CR-21-A5-177	Thick section	CR-21-A5	177	Cross	Apache-Potosi
10	CR-21-B1-109.5	Thick section	CR-21-B1	109.5	Cross	Apache-Potosi
11	CR-21-B1-110	Thick section	CR-21-B1	110	Cross	Apache-Potosi
12	CR-21-B1-12.5	Thick section	CR-21-B1	12.5	Cross	Apache-Potosi
13	CR-21-B1-13.5	Thick section	CR-21-B1	13.5	Cross	Apache-Potosi
14	CR-21-B1-3.5	Thick section	CR-21-B1	3.5	Cross	Apache-Potosi
15	CR-21-B1-6.5	Thick section	CR-21-B1	6.5	Cross	Apache-Potosi
16	CR-21-G11-44.5	Epoxy mount	CR-21-G11	44.5	Cross	Stockwork Zone
17	CR-21-G14-3.6	Epoxy mount	CR-21-G14	3.6	Cross	Stockwork Zone
18	CR-21-G2-284.5	Epoxy mount	CR-21-G2	284.5	Cross	Stockwork Zone
19	CR-21-G2-287.5	Epoxy mount	CR-21-G2	287.5	Cross	Stockwork Zone
20	CR-21-G4-46.5	Epoxy mount	CR-21-G4	46.5	Cross	Stockwork Zone
21	CR-21-G4-47.5	Epoxy mount	CR-21-G4	47.5	Cross	Stockwork Zone
22	CR-21-G4-6	Epoxy mount	CR-21-G4	6	Cross	Stockwork Zone
23	CR-21-G6-412.5	Epoxy mount	CR-21-G6	412.5	Cross	Stockwork Zone
24	CR-21-G6-5	Epoxy mount	CR-21-G6	5	Cross	Stockwork Zone
25	CR-21-I4-47	Epoxy mount	CR-21-I4	47	Cross	Stockwork Zone
26	CR-21-J11-232	Thick section	CR-21-J11	232	Cross	Hopewell
27	CR-21-J8-236.5	Thick section	CR-21-J8	236.5	Cross	Crown Point
28	CR-21-J8-252.5	Thick section	CR-21-J8	252.5	Cross	Crown Point
29	CR-21-J8-253.5	Thick section	CR-21-J8	253.5	Cross	Crown Point
30	CR-21-J8-255	Thick section	CR-21-J8	255	Cross	Crown Point
31	CR-21-J8-256	Thick section	CR-21-J8	256	Cross	Crown Point
32	CR-21-J8-260.5	Thick section	CR-21-J8	260.5	Cross	Crown Point
33	CR-21-J9A-224	Thick section	CR-21-J9A	224	Cross	Hopewell east
34	CR-21-J9A-275	Thick section	CR-21-J9A	275	Cross	Hopewell east

Table 4.1 Continued.

35	CR-21-J9A-276	Thick section	CR-21-J9A	276	Cross	Hopewell east
36	CR-21-J9A-278.5	Thick section	CR-21-J9A	278.5	Cross	Hopewell east
37	CR-21-J9A-35.2	Thick section	CR-21-J9A	35.2	Cross	Hopewell east
38	CR-21-J9A-38.5	Thick section	CR-21-J9A	38.5	Cross	Hopewell east
39	CR-95-110-1584	Epoxy mount	CR-95-110	1584	Caribou	Deep
40	CR-95-110-1591	Epoxy mount	CR-95-110	1591	Caribou	Deep
41	CR-95-110-1592	Epoxy mount	CR-95-110	1592	Caribou	Deep
42	CR-97-101-947	Epoxy mount	CR-97-101	947	Caribou	Deep
43	CR-97-103-1815	Epoxy mount	CR-97-103	1815	Caribou	Deep
44	CR-97-103-1936	Epoxy mount	CR-97-103	1936	Caribou	Deep
45	CR-97-103-1937	Epoxy mount	CR-97-103	1937	Caribou	Deep
46	CR-97-104-1346.5	Epoxy mount	CR-97-104	1346.5	Caribou	No Name
47	CR-98-108-1782	Epoxy mount	CR-98-108	1782	Cross	Deep
48	CR-98-121-1030	Epoxy mount	CR-98-121	1030	Pomeroy Mtn	Park Hill Breccia
49	CR-98-122-931	Epoxy mount	CR-98-122	931	Pomeroy Mtn	Park Hill Breccia
50	CR-98-122-948	Epoxy mount	CR-98-122	948	Pomeroy Mtn	Park Hill Breccia
51	CR-98-123-545	Epoxy mount	CR-98-123	545	Pomeroy Mtn	Park Hill Breccia
52	SN01-1013	Epoxy mount	CR-21-SN01	1013	Caribou	No Name

Surface samples from waste rock piles were collected for investigation of varying ore mineralogy across the district. Over 29 waste rock piles were mapped and characterized in 2021, and eight of these piles, which contained visible veining with sulfides or interesting alteration textures, were selected for further analysis. Appendix A.1 is a table with waste rock pile field descriptions. Seven thick sections were prepared on samples: S-00, S-5, S-10, S-13, S-18, S-19, and S-25 (Figure 4.2, Figure 4.3) and 21 waste rock pile samples from various stations (Figure 4.2) were made into epoxy mounts (Table 4.2). Some stations were given an arbitrary number such as S-00 or 651, but if the waste rock pile could be confidently matched with a historical mine, then it was given a name such as Native Silver (NS), San Isabel (SI) or Southwest Pandora (SWP).

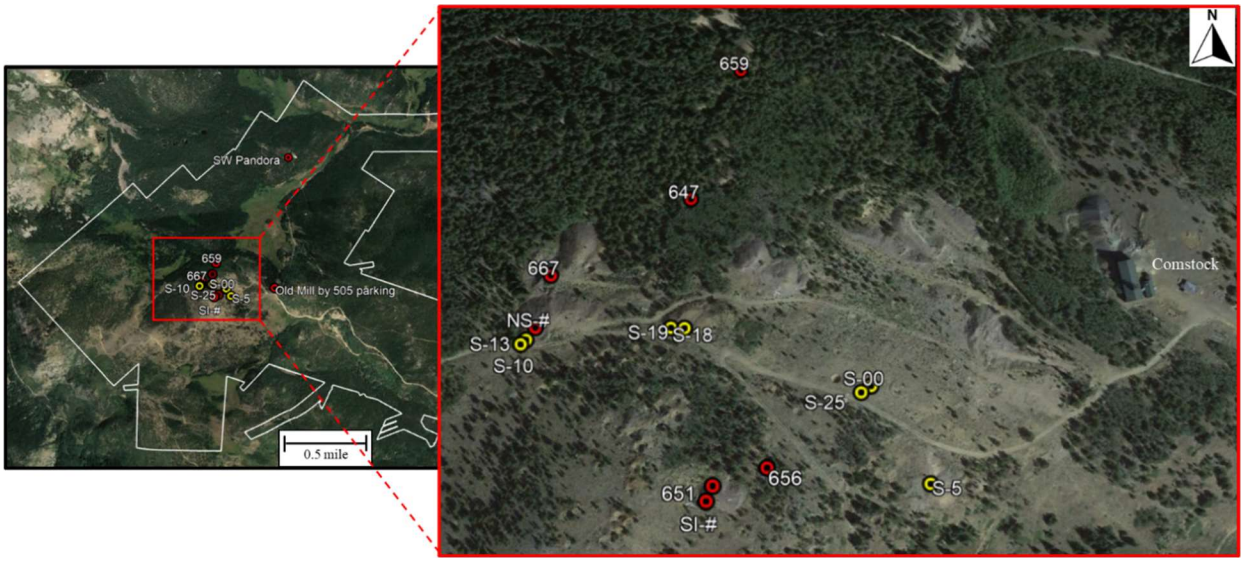

Figure 4.2 Surface sampling locations from various waste rock piles across the Grand Island district. Samples that were made into thick sections are yellow circles and sample locations of samples that were made into epoxy mounts are displayed in red circles.

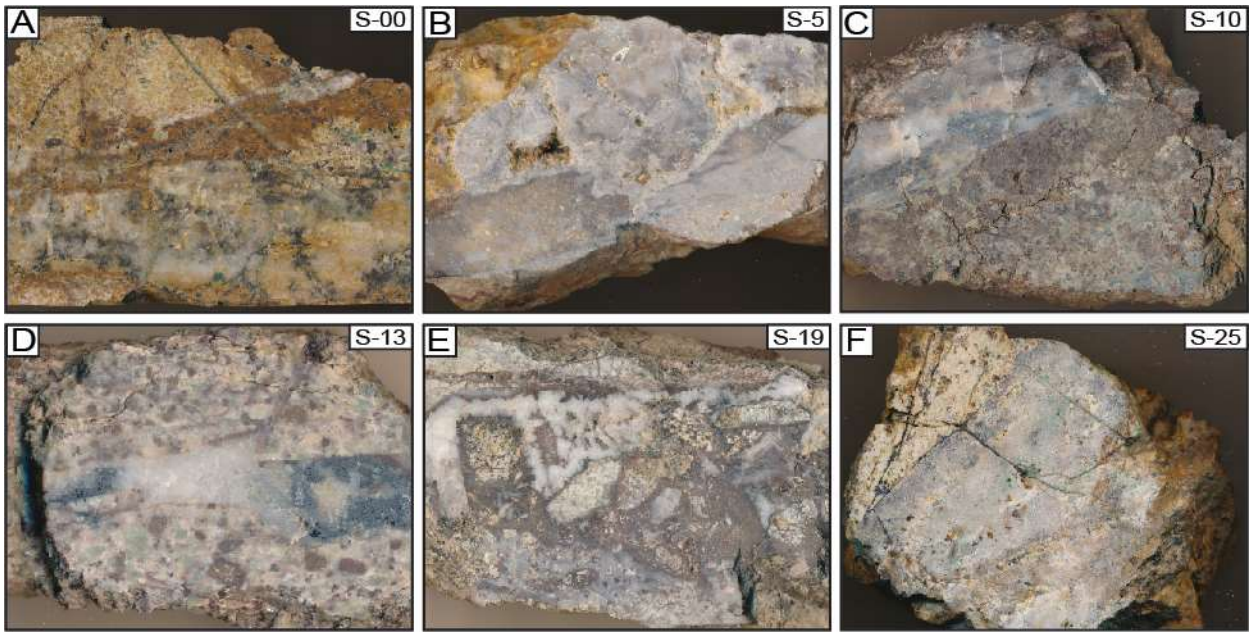

Figure 4.3 Photographs of waste rock pile samples collected in May 2021: A) Oxidized quartz vein; B) course grained quartz with euhedral quartz growing into an open vug; C) vein with oxidation and alteration halo; D) sulfide minerals in a large milky quartz vein with altered and oxidized host rock and fault offsetting the vein; E) Brecciated vein with large euhedral quartz grains and oxidation; F) large milky quartz vein with malachite and azurite in vugs

Table 4.2 Sample list of samples from waste rock piles

No.	Sample ID	Prep type	Latitude	Longitude
1	S-00	Thick section	39.5853780	-105.3523100
2	S-5	Thick section	39.5855100	-105.3449400
3	S-10	Thick section	39.5854500	-105.3520600
4	S-13	Thick section	39.5854500	-105.3520600
5	S-18	Thick section	39.5855100	-105.3520600
6	S-19	Thick section	39.5855100	-105.3520600
7	S-25	Thick section	39.5853780	-105.3523100
8	Old Mill	Epoxy mount	39.9816240	-105.5787700
9	651	Epoxy mount	39.9810090	-105.5852520
10	659	Epoxy mount	39.9837320	-105.5852200
11	SWP	Epoxy mount	39.9925978	-105.5772808
12	667	Epoxy mount	39.9822630	-105.5867400
13	656	Epoxy mount	39.9811100	-105.5848300
14	647	Epoxy mount	39.9827870	-105.5855840
15	SI-1	Epoxy mount	39.9810090	-105.5852520
16	SI-2	Epoxy mount	39.9810090	-105.5852520
17	SI-3	Epoxy mount	39.9810090	-105.5852520
18	SI-4	Epoxy mount	39.9810090	-105.5852520
19	SI-5	Epoxy mount	39.9810090	-105.5852520
20	SI-6	Epoxy mount	39.9810090	-105.5852520
21	SI-7	Epoxy mount	39.9810090	-105.5852520
22	SI-8	Epoxy mount	39.9810090	-105.5852520
23	SI-9.1	Epoxy mount	39.9810090	-105.5852520
24	SI-9.2	Epoxy mount	39.9810090	-105.5852520
25	SI-10	Epoxy mount	39.9810090	-105.5852520
26	SI-11	Epoxy mount	39.9810090	-105.5852520
27	SI-12	Epoxy mount	39.9810090	-105.5852520
28	NS-1	Epoxy mount	39.9819280	-105.5868150

Samples from surface trenching and summer 2021 surface drilling were collected for investigation of the variation of host rock lithologies. Four samples from historical iron dike trenches, with emphasis on altered and fresh rock, were made into epoxy mounts. For example, these samples are named FeD-T1-1 meaning iron dike- trench 1- sample 1. Additional samples were collected from core of various host rock lithologies down to a depth of 1,288 feet drilled from SG station and SN station at the surface at Comstock (Table 4.3; Figure 2.2). Lithologies targeted include monzonite, quartz monzonite, pyroxenite, gabbro, lamprophyre, and the “iron

dike." One final sample comes from a piece of skeleton core of unknown location but was representative of the Caribou monzonite.

Table 4.3 Sample list of samples investigating igneous lithologies

			Sample location			
No.	**Sample ID**	**Prep type**	**Drill hole**	**Depth (ft)**	**Latitude**	**Longitude**
1	FeD-T1-1	Epoxy mount			39.9837060	-105.5823190
2	FeD-T1-2	Epoxy mount			39.9837060	-105.5823190
3	FeD-T1-3	Epoxy mount			39.9837060	-105.5823190
4	FeD-T1-4	Epoxy mount			39.9837060	-105.5823190
5	SG01-90	Epoxy mount	CR-21-SG01	90		
6	SG02-899.5	Epoxy mount	CR-21-SG02	899.5		
7	SG06A-197	Epoxy mount	CR-21-SG06A	197		
8	SG06A-345	Epoxy mount	CR-21-SG06A	345		
9	SG06A-456-1	Epoxy mount	CR-21-SG06A	456		
10	SG06A-456-2	Epoxy mount	CR-21-SG06A	456		
11	SN01-123	Epoxy mount	CR-21-SN01	123		
12	SN01-248.5	Epoxy mount	CR-21-SN01	248.5		
13	SN01-438-1	Epoxy mount	CR-21-SN01	438		
14	SN01-438-2	Epoxy mount	CR-21-SN01	438		
15	SN02-1287.5	Epoxy mount	CR-21-SN02	1287.5		
16	SN02-1282	Epoxy mount	CR-21-SN02	1282		
17	SN03-752-1	Epoxy mount	CR-21-SN03	752		
18	SN03-752-2	Epoxy mount	CR-21-SN03	752		
19	SN03-1029	Epoxy mount	CR-21-SN03	1029		
20	Mz	Epoxy mount	Unknown core sample			

4.2 Micro X-Ray Fluorescence

Core slabs from which billets were made were analyzed for elemental distribution using a micro-X-ray fluorescence (μXRF) spectrometry at the Mineral and Materials Characterization (MMC) facility at the Colorado School of Mines. Seven core slabs were loaded into the Bruker M4 Tornato μXRF spectrometer and ran at standard operating conditions under vacuum at 50keV and 600μA. Element distribution maps were produced with a 40 μm pixel size at a 15 ms/pixel dwell time.

4.3 Optical Microscopy

Reflected and transmitted light microscopy was performed on 35 thick sections to identify ore, gangue, and alteration minerals, observe mineral assemblages, mineral abundances, and textures. Photomicrographs were taken for documentation.

Initially the thick sections were observed under transmitted light in both plane-polarized light (PPL) and cross-polarized light (XPL) to identify and understand the gangue minerals. Next, the thick sections were observed in reflected light in both PPL and XPL to identify and understand the opaque minerals. Notes were recorded about mineralogy, textures, and identified zones of further interest and minerals that needed to be observed at a higher resolution under the FE-SEM.

4.4 Cathodoluminescence Microscopy

Located at the microscopy and fluid inclusion laboratory at Colorado School of Mines, the HC5-LM hot-cathode CL microscope by Lumic Special Microscopes, Germany based on an Olympus BXFM-ILHS microscope was operated at standard conditions of 14 kV with a current density of 10 $\mu A\ mm^{-2}$. The Teledyne Luminera Infinity 5-5 digital camera connected to a Dell OptiPlex 7090 computer was used to capture true color CL images. Upon microscopy, two distinct quartz generations were identified based on textural relationships and fluid inclusion petrography.

4.5 Fluid Inclusion Study

Fluid inclusion petrography was conducted using an Olympus BX51 microscope with a 40x objective. Microthermometric data were collected using a Fluid Inc.-adapted U.S. Geological Survey gas-flow heating and freezing stage with an accuracy to 0.1°C for freezing and accuracy of heating ranging from 2°C at 200°C. Two primary fluid inclusion assemblages (FIA's) were identified in late-stage quartz that was associated with sphalerite inclusions in sample CR-21-A3-10.5. The thick section was broken into smaller pieces so that the temperature gradient within the sample is decreased. Metastability prevents inclusions to immediately freeze, so the sample was rapidly cooled beyond the eutectic temperature to ensure the inclusion was frozen. The first fluid inclusion assemblage which consisted of two fluid inclusions was cooled

with liquid nitrogen down to roughly -60°C. Upon heating, the fluid inclusions cross the eutectic point, which is indicated by a bubble jerk from the first melting liquid unlocking the vapor bubble. The sample was cycled from around -60°C to around 10°C to identify evidence of clathrate and view the bubble jerk that indicates the temperature of last ice melting. Once the temperature of last ice melting was accurately observed and recorded, the FIA was heated up to the point where the bubble disappeared, which gave the homogenization temperature. This was cycled multiple times to identify this point. The second FIA was first heat-cycled to identify the temperature of homogenization. The sample was then cycled through freezing to identify the bubble jerk indicating the temperature of last ice melting.

4.6 Scanning Electron Microscopy

Scanning electron microscopy (SEM) improved the understanding of the occurrence and composition of minerals, mineral associations, textures, and the occurrence and distribution of precious and other metals. The imaging targeted textural relationships between minerals to further delineate the precious metals using high-resolution BSE imaging. The instrument used was the TESCAN MIRA3 LMH Schottky field emission-scanning electron microscope (FE-SEM) located in MMC facility. The FE-SEM was used at an acceleration voltage of 20 kV, beam intensity of 11 nA, and a working distance of 10 mm.

Backscattered electron (BSE) images document findings including textural relationships. The BSE detector is a TESCAN motorized retractable annular, single-crystal YAG located in the FE-SEM. This is characterized by a 0.1 Z atomic number resolution and high sensitivity.

Energy dispersive spectroscopy (EDS) analyses was used to conduct semi-quantitative analyses of the mineral chemistry to unravel the occurrence and distribution of the vein and alteration assemblages. The EDS detector is a Bruker XFlash 6/30 silicon drift detector located in the FE-SEM. The collimator is multi-layer with a 6.0mm aperture.

Samples were loaded into the vacuum chamber and set up under standard operating conditions. The FE-SEM was then driven around the sample to look for different brightness contrasts that show textural relationships and use the EDS to acquire chemical data of point analyses on interesting mineral assemblages. Areas of interest that were identified with reflected and transmitted light microscopy were targeted on the FE-SEM. Once the BSE image was brought into focus and captured on the area of interest, a point was chosen on the best surface

possible for EDS analysis. The spectrum was analyzed for any peak overlaps and elements were selected based on the spectra. The spectra were quantified in both normalized atom percent and unnormalized mass percent. For Ag-bearing gold grains, Au:Ag ratios are reported as the atom percent of Au and Ag, which was collected using semi-quantitative EDS, and this does not account for any trace elements in the Ag-bearing gold grains.

4.7 SEM-based Automated Mineralogy

SEM-based automated mineralogy scans were produced in the MMC facility. The purpose of automated mineralogy analysis was to identify mineral species and textural information as well as quantify the mineral modal abundances and mineral associations.

The mounted billet was loaded into the TESCAN-VEGA-3 Model LMU VP-SEM platform and analysis was started using the TIMA3 control program. Data were collected from four Pulsetor EDS systems which acquire X-ray spectra from each point. The beam stepping interval was user defined at an acceleration voltage of 25 keV, a beam intensity of 14 nA, and a working distance of 10 mm. The sample was scanned at a 5 μm pixel spacing over a cropped portion of the sample, which took approximately 3 hours. The X-ray spectra acquired at each point were compared by the software to a spectrum in the look-up table which assigned each mineral or phase to the corresponding pixel. Results are output by the TIMA software, and a false-color mineral map was generated with mineral assignments grouped appropriately.

Once the data was collected, the data was then verified and reduced. This consisted of looking at pixels and the spectrum as well as the mineral associations. Minerals that did not show up in the sample were grouped into “Other minerals.” Sericite, muscovite, and illite were combined into one group as they are chemically similar. All carbonate minerals were grouped into one carbonate group. All varieties of potassium feldspar were grouped into the K-feldspar group. Minerals containing titanium such as rutile were grouped into a “Ti minerals” group. The spectrum and the texture of the unclassified minerals was observed to determine what they may likely be and deduced, if possible, into another group.

Once the legend and mineral groupings were cleaned up, then images and data were saved and downloaded. The mass percent and volume percent modal analysis were exported and put into graphs. The mineral associations, which are which pixels are touching other pixels, were also exported and graphed. The BSE image as well as the automated mineralogy map were

exported. Minerals of interest were selected and laid over the BSE image to preserve textural relationships.

4.8 Data Analytics

Assay data was observed for district wide trends using ioGas, Geostatistica, and LeapFrog. Assay data was loaded into these software's which were used primarily as visualization tools. The database for assays, drill hole collars, surveys, and pre-existing modeled shapes are kept updated by Grand Island Resources, and these updated databases are what was used for the purposes of this project.

CHAPTER 5: RESULTS

The following section presents the petrographic data from optical microscopy, automated mineralogy, and SEM-BSE and -EDS investigation for the igneous rock suite, and ore, gangue, and alteration mineralogy of the Caribou-Cross deposit. The ore-forming fluid characteristics were derived from cathodoluminescence microscopy and fluid inclusion studies on samples from the Cross.

5.1 Igneous Petrography

The Caribou stock is dominantly a monzonite to quartz monzonite but includes a variety of other rock types such as diorite, gabbro, pyroxenite, magnetite dunite, and lamprophyre. The purpose of this section is to identify and classify unaltered rock types. Core logging and field observations in 2021 also contributed to these results.

Figure 5.1 and Figure 5.2 show automated mineralogy data for five different lithologic groups: Group 1 dominantly consists of olivine and magnetite and is therefore classified as a magnetite dunite (Figure 5.2 A and B). Group 2 represents monzonite and quartz monzonite, which is the main host rock lithology, consisting of K-feldspar, plagioclase, and quartz and is described in further detail below. Group 3 is dominantly composed of actinolite and plagioclase with lesser biotite and magnetite, so it is classified as an amphibolite (Figure 5.2 C and D). Group 3 rocks are texturally very similar to group 4 but contain abundant interstitial plagioclase. Group 4 is dominantly composed of actinolite and magnetite with some hornblende and chlorite (Figure 5.2 E and F). Texturally this group is very similar to group 1, but with amphibole instead of olivine (magnetite amphibolite or altered magnetite dunite). In some instances, the magnetite occurs as congregated irregular masses that appear to consume the amphibolite. Group 5 is a lamprophyre and is dominantly comprised of biotite with lesser actinolite, hornblende, and magnetite (Figure 5.2 G and H).

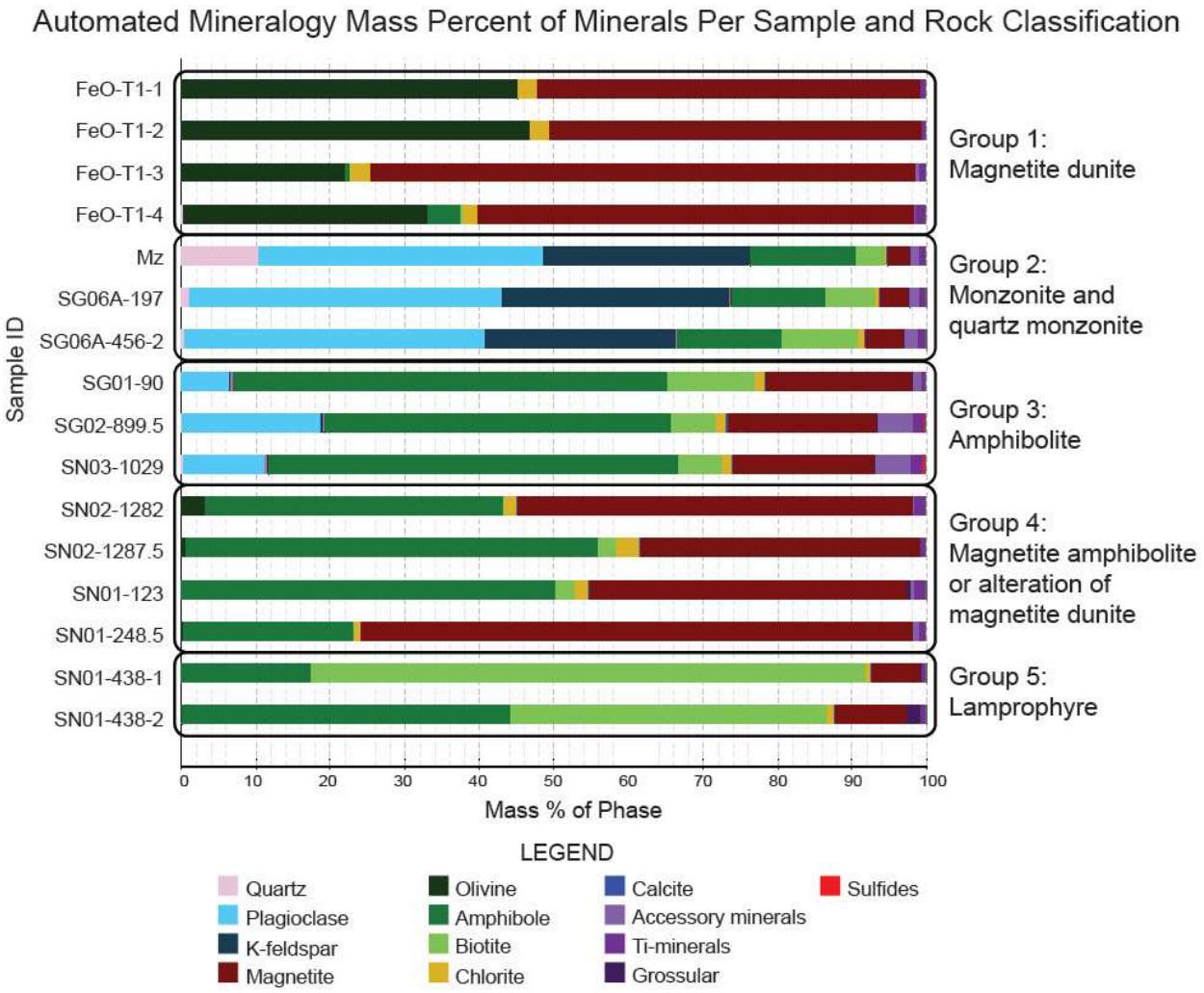

Figure 5.1 Mineral abundance data of the igneous rock suite from automated mineralogy in mass percent. Mass percent of each phase (mineral) is on the horizontal axis and sample IDs are on the vertical axis. Samples composed of more than one rock type of vein material were omitted from this chart.

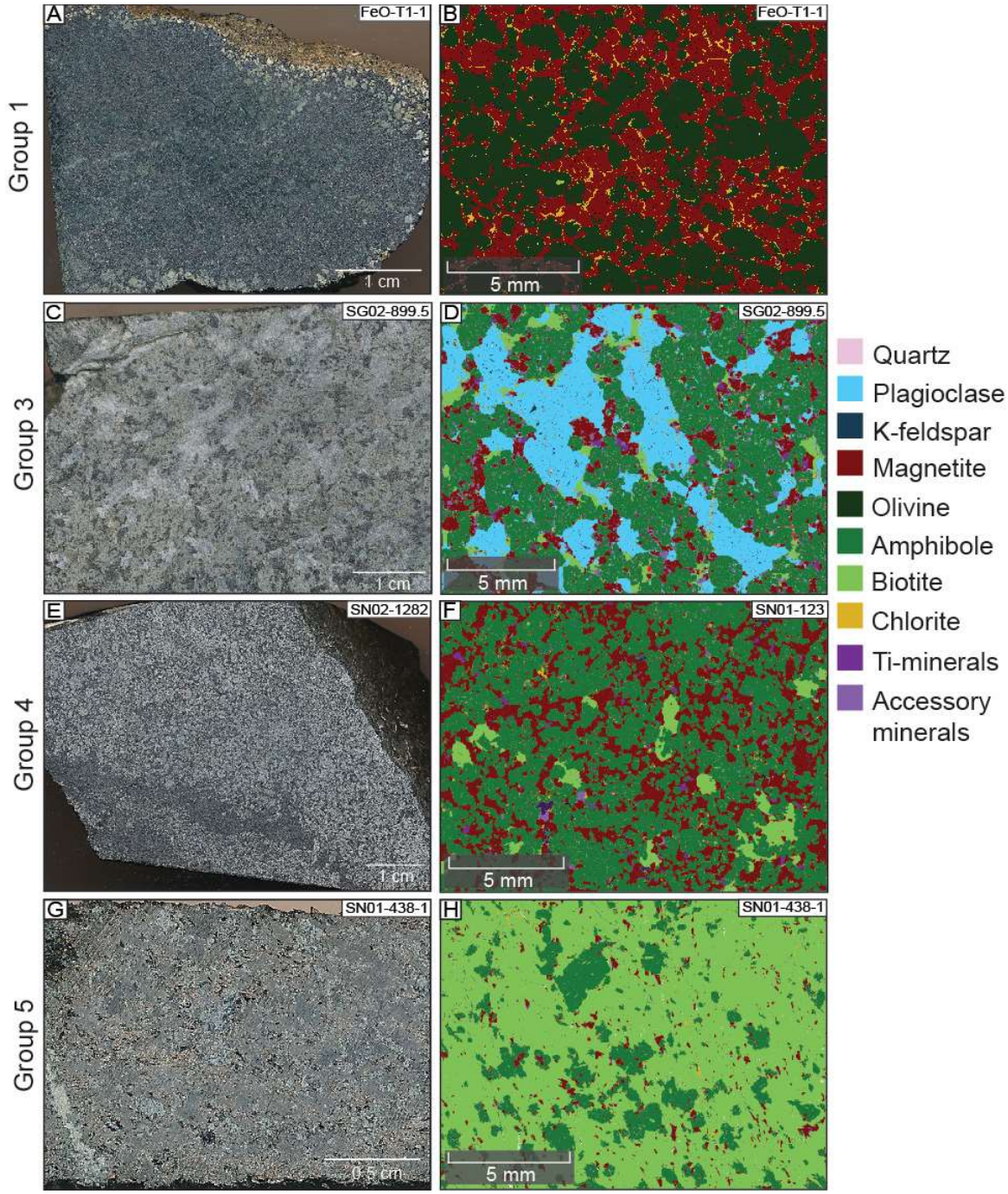

Figure 5.2 Hand sample photographs alongside with false-colored automated mineralogy maps highlighting the mineralogy of each rock type and textures: A) Group 1: magnetite dunite grab sample with weathered edges (photograph) and B) Olivine and magnetite anhedral cumulate grains with interstitial chlorite; C) Group 3: course-grained amphibolite (photograph) and D) Amphibole grains with interstitial plagioclase; E) Group 4: magnetite amphibolite with a larger accumulation of magnetite crystals (photograph) and F) Amphibole with interstitial magnetite and biotite; G) Group 5: lamprophyre with course-grained root beer brown, flaky biotite and a thin chlorite vein (photograph) and H) Largely biotite with some amphibole and magnetite faintly lineated, possibly following biotite cleavage or foliation.

Because the Caribou monzonite is the most common host rock, more detail is provided below. In the typical Caribou monzonite (Figure 5.3), the major minerals are plagioclase, K-feldspar, and quartz with lesser actinolite, hornblende, magnetite, apatite, and biotite. There is trace muscovite, olivine, amphibole, chlorite, calcite, zircon, ilmenite, and titanite, and secondary chalcopyrite and pyrite. Table 5.1 illustrates the major and minor minerals, mineral formulas, and their mass percent in sample Mz. Based on the mineral abundance data, the major elemental components of the Caribou stock are K, Al, and Ca. The monzonite is typically phaneritic with grain sizes ranging from a few millimeters to rarely centimeters. Other textures include flow banding (sample SG06A-197), xenoliths, abrupt changes in grain size(sample SG06A-456-2), and porphyrytic texture in some areas of the district.

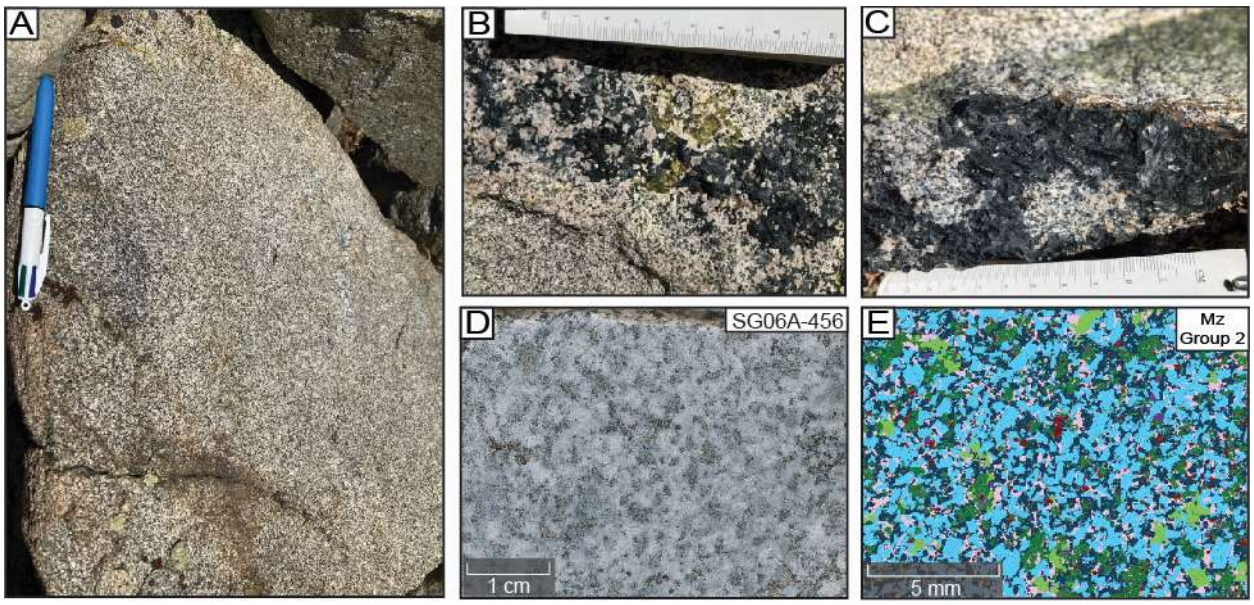

Figure 5.3 Photographs and automated mineralogy images of the Caribou monzonite: A) photograph of monzonite outcrop on the top of Caribou hill; B) Close-up photograph of course-grained black hornblende and green epidote; C) Close-up photograph of course-grained black hornblende occurring on fractured surface of outcrop; D) Photograph of sample SG06A-456 from core; E) Automated mineralogy image of sample Mz (color legend as in Figure 5.2) with plagioclase, K-feldspar, and quartz with lesser actinolite, hornblende, magnetite, apatite, and biotite.

Table 5.1 Mineralogy of representative Caribou monzonite sample Mz, with mass percent of minerals based on automated mineralogy.

Major	Formula	Mass %
Plagioclase	$NaAlSi_3O_8$-$CaAl_2Si_2O_8$	40
Orthoclase	$KAlSi_3O_8$	30
Quartz	SiO_2	10
Actinolite	$Ca_2(Mg,Fe)_5Si_8O_{22}(OH)_2$	5
Hornblende	$(Ca,Na)_2(Mg,Fe,Al)_5(Al,Si)_8O_{22}(OH)_2$	8
Magnetite	$Fe^{2+}Fe^{3+}{}_2O_4$	3
Apatite	$Ca_5(PO_4)_3(Cl,F,OH)$	1
Biotite	$K(Mg,Fe)_3(Al,Si_3O_{10})(F,OH)_2$	4
Minor	**Formula**	**Mass %**
Muscovite	$KAl_2(AlSi_3O_{10})(OH)_2$	<1
Olivine	$(Ca,Fe,Mn,Ni,Mg)_2SiO_4$	<1
Chlorite	$(Al,Fe,Mg,Mn)_{5\text{-}6}(Al,Fe,Si)_4(O,OH)_{18}$	<1
Calcite	$CaCO_3$	<1
Zircon	$Zr(SiO_4)$	<1
Ilmenite	$Fe^{2+}TiO_3$	<1
Titanite	$CaTi(SiO_4)O$	<1
Pyrite	FeS_2	<1
Chalcopyrite	$CuFeS_2$	<1

Quartz, alkali feldspar, and plagioclase modal percent from automated mineralogy have been plotted on a QAP diagram (Figure 5.4). Sample Mz is shown to be a quartz monzonite whereas samples SG06A-197 and SG06A-456-2 are monzonite. All other rock types fall into the mafic igneous classification schemes and are dominantly olivine or amphibole, and thus have not been plotted on such diagrams.

The magnetite dunite contains olivine and magnetite cumulate crystals with interstitial chlorite, which could have likely been amphibole or biotite. The titaniferous magnetite bodies are composed of equigranular, hypidiomorphic olivine and magnetite cumulate crystals (Figure 5.2) sometimes with interstitial chlorite and titanium minerals such as rutile, ilmenite, and titanite. The olivine shows alteration to actinolite and orthoamphibole (sample FeO-T1-4) and the magnetite is changed to hematite. Both rocks have been referred to as “iron dike” in the past.

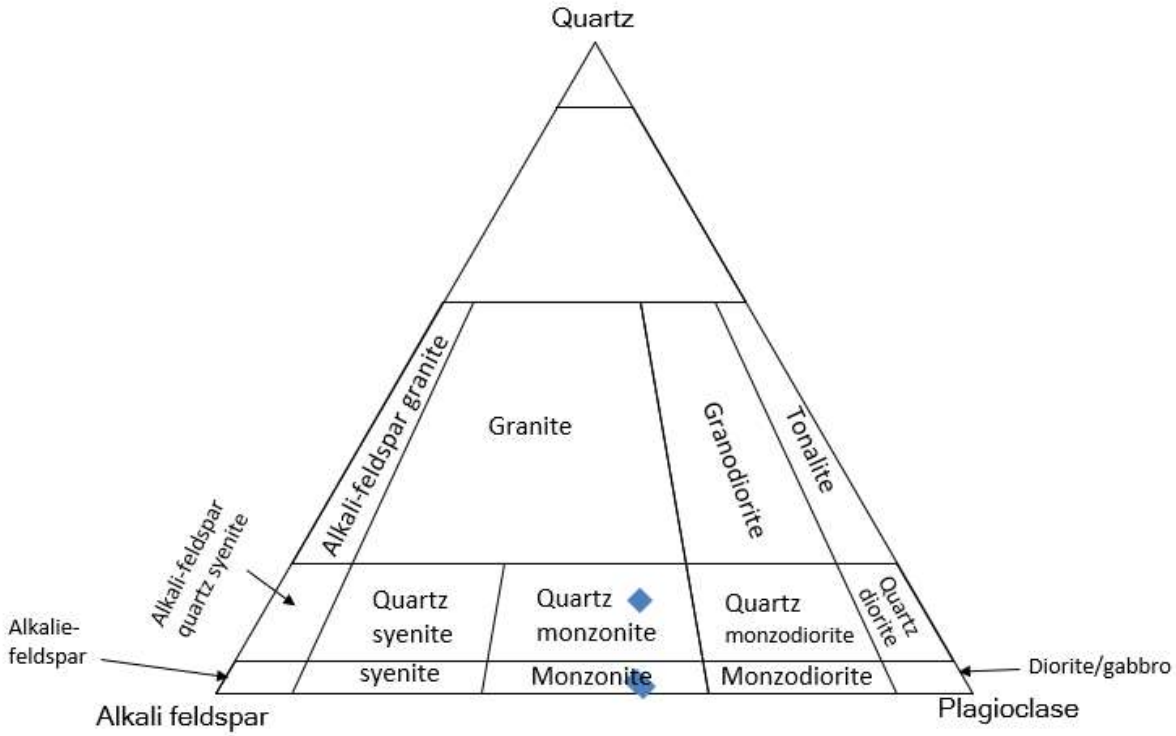

Figure 5.4 QAPF diagram with samples Mz, SG06A-197, SG06A-456-2 using modal percent of minerals from automated mineralogy (classification fields from Streckeisen, 1967)

5.2 Ore Petrography

The following section describes all commonalities between samples from the Apache-Potosi, Stockwork zone, Hopewell, Crown Point, deep Cross, and Caribou ore zones. Subsequently, each zone in the deposit is described with regards to unique or exemplary characteristics.

Generally, veins in the Grand Island district show a wide variety of textures including banding, comb quartz, vugs. open-space fill, brecciation, and stockwork veining (Figure 5.5). The dominant gangue minerals in the veins are quartz and ankerite. Sulfides in the veins are dominantly pyrite, galena, and sphalerite, with lesser chalcopyrite, Ag-bearing gold, and silver sulfosalts. Alteration halos (Figure 5.6) vary in width and consist of K-feldspar and sericite with distal chlorite. Occasionally silicification is present. The host rock of all samples collected for this study is the Caribou monzonite, with the exception of sample CR-21-J9A-224 hosted in pegmatite.

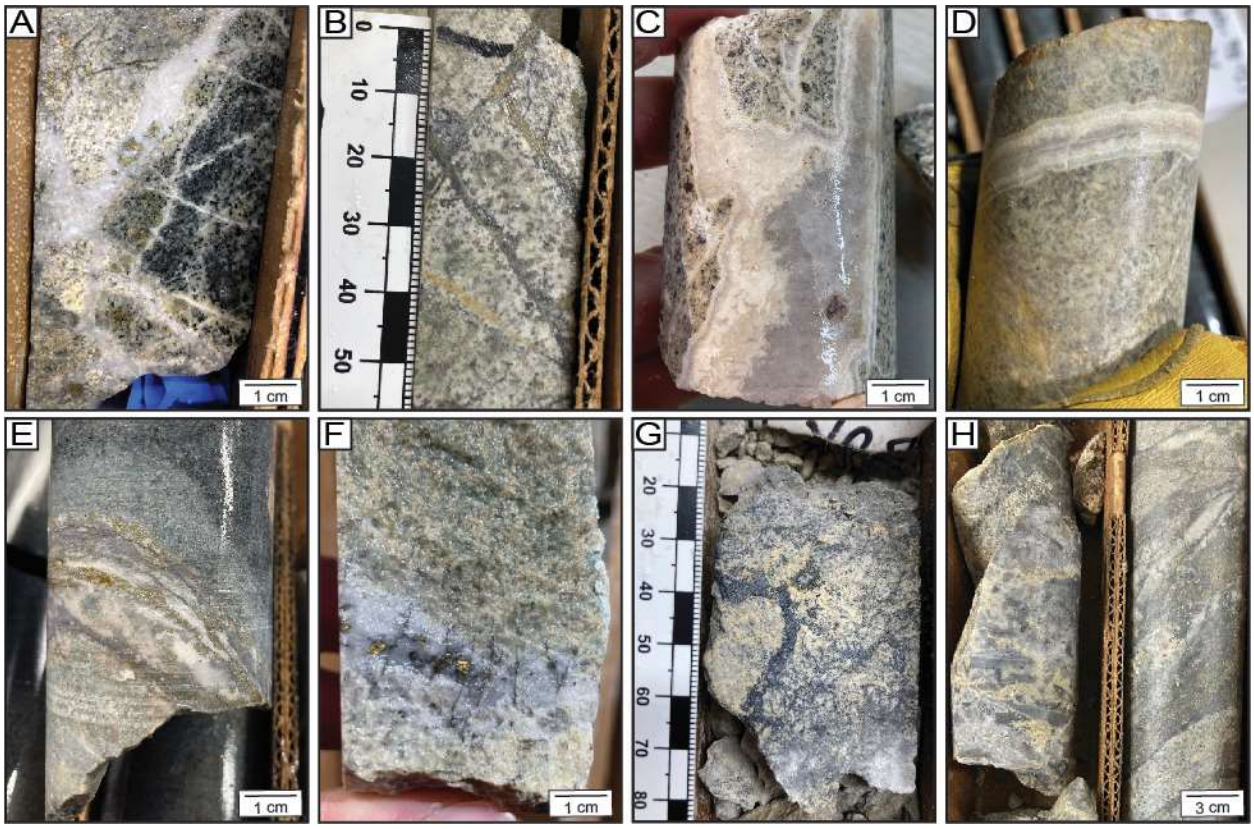

Figure 5.5 Core photographs of various vein textures and structures present at the Cross: A) Stockwork quartz veins with narrow alteration halos; B) Crosscutting stockwork sulfide veins in pervasively altered monzonite; C) Banded undulating quartz vein; D) Banded quartz-carbonate vein with euhedral comb quartz and euhedral carbonate in strongly altered monzonite; E) Well-defined vein zone with multiple generations of cross-cutting gangue and sulfide minerals with K-feldspar and sericite proximal alteration halo and sericite distal alteration halo with a sharp boundary to unaltered monzonite; F) Milky quartz vein with orthogonal crosscutting sulfide mineralization; G) Breccia ore at the bottom of a fault zone with sulfide infill; H) brecciated vein and wide stockwork sulfide-quartz-ankerite veins in pervasively altered monzonite.

5.2.1 Alteration

K-feldspar alteration occurs across the deposit associated with veins and fractures. One stage of hydrothermal K-feldspar alteration occurred early and is fracture controlled as indicated by the presence of K-feldspar alteration halos around hairline fractures without any vein filling and extending inconsistently on each side of veins. Subsequent veining occurred along fractures, which show evidence of offset both prior to and after vein mineralization. There is significant K-feldspar alteration also associated with veins and fractures after vein formation.

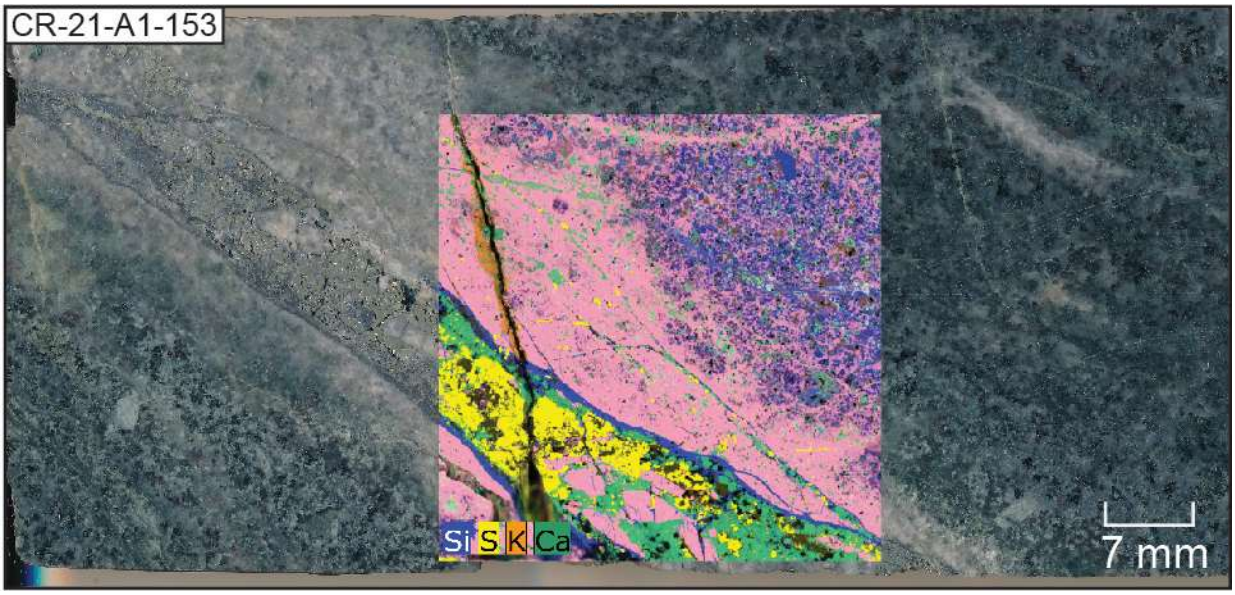

Figure 5.6 Core photograph of sample CR-21-A1-153 (from Apache-Potosi) showing a vein and alteration halo with a µXRF element map overlain on the core photo. Potassium maps out both K-feldspar and sericite. Silica relates to quartz in the vein and silicates in the host rock. Sulfur indicates sulfides in the veins. Calcium accounts for carbonate in the major vein and stringers.

Sericite alteration is exhibited as sericite replacing plagioclase and less commonly, quartz replacing K-feldspar. Primary igneous plagioclase grains are typically 1 mm to 3 mm in size. They are completely sericitized proximal to the vein, but distal from the vein, plagioclase is only partially sericitized and plagioclase twinning may be preserved. This gradient is gradual and alteration width varies significantly between veins (Figure 5.7). Sericite is fine-grained, especially close to the vein (Figure 5.7 F). Changes in sericite grain size from very fine grained to fine grained account for macroscopic halos. Farther away from the vein, sericite is slightly courser grained and is less pervasive. In addition, course-grained muscovite grains up to 2 mm in size occur within proximity to the vein (Figure 5.7 F).

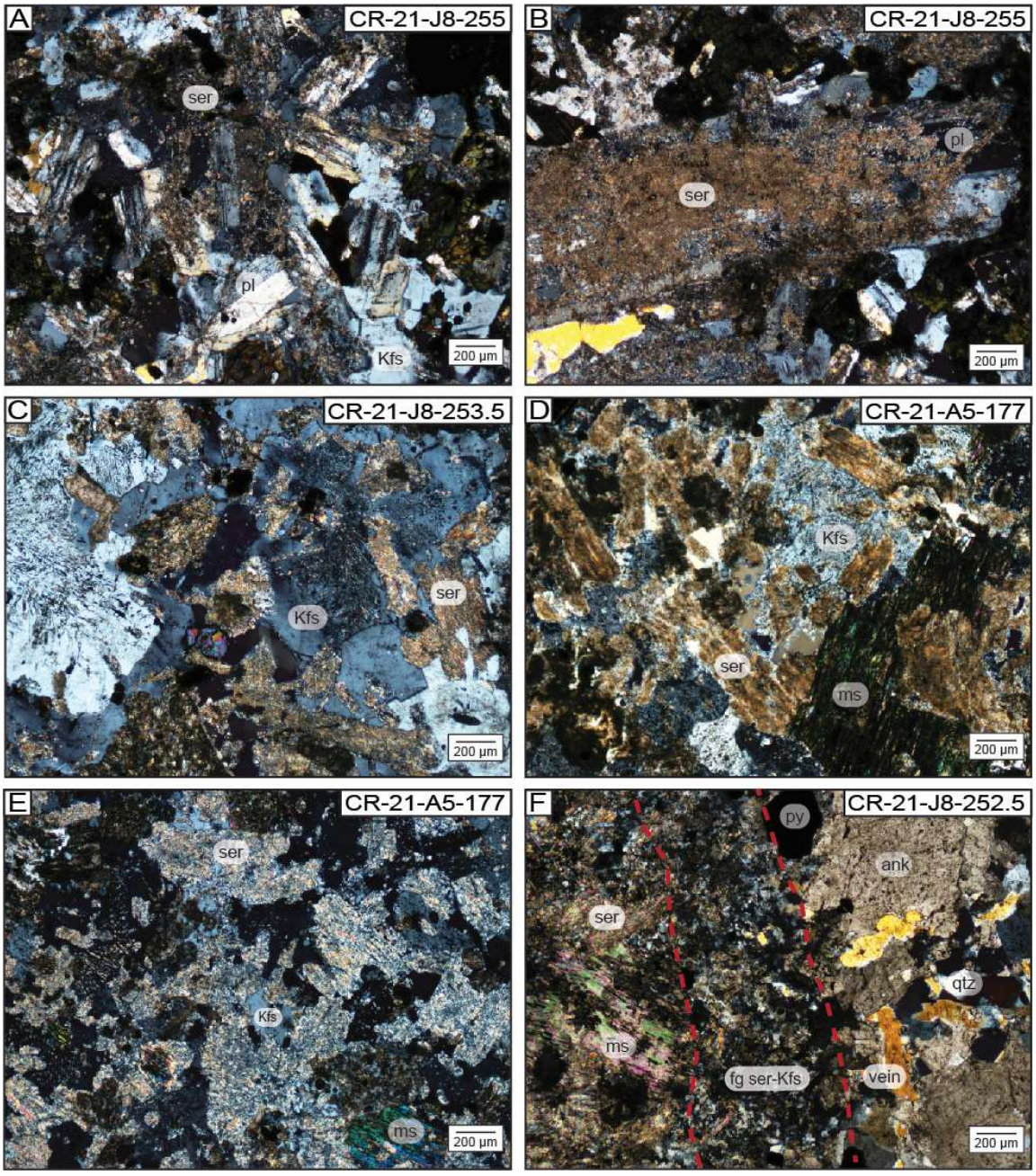

Figure 5.7 Cross-polarized light photomicrographs of sericite alteration with respect to intensity and distance from vein (A is distal, F is proximal): A) Distal plagioclase grains are still present with minimal sericite replacing micro fractures through plagioclase grains (from Crown Point); B) Most of a plagioclase grain is sericitized, but twinning is still visible (from Crown Point); C) Twinning is no longer visible, but the shape of the plagioclase grains is still present (from Crown Point); D) Even stronger intensity sericitization with a large muscovite grain encompassing sericitized plagioclase grains (from Apache-Potosi); E) The plagioclase crystal shape is hardly recognizable, and sericite is up to 60% of the field of view (from Apache-Potosi); F) Proximal halo of fine-grained sericitized K-feldspar directly next to an ankerite-quartz-pyrite vein; outside of this halo is course-grained sericite and muscovite that replaces 80% of the host rock (from Crown Point).

Minor silicification occurs replacing K-feldspar and preserves the sericitized plagioclase grains. All of the quartz in between different plagioclase grains go extinct at the same orientation. This quartz is clear and completely anhedral, filling in space between plagioclase grains.

Biotite and amphibole are altered to chlorite distally from the vein (Figure 5.8). Biotite and amphibole are not present closer to the vein as the have been completely replaced by potassium micas. But distally from the vein, biotite and amphibole are still present with some minor sericite and chlorite alteration.

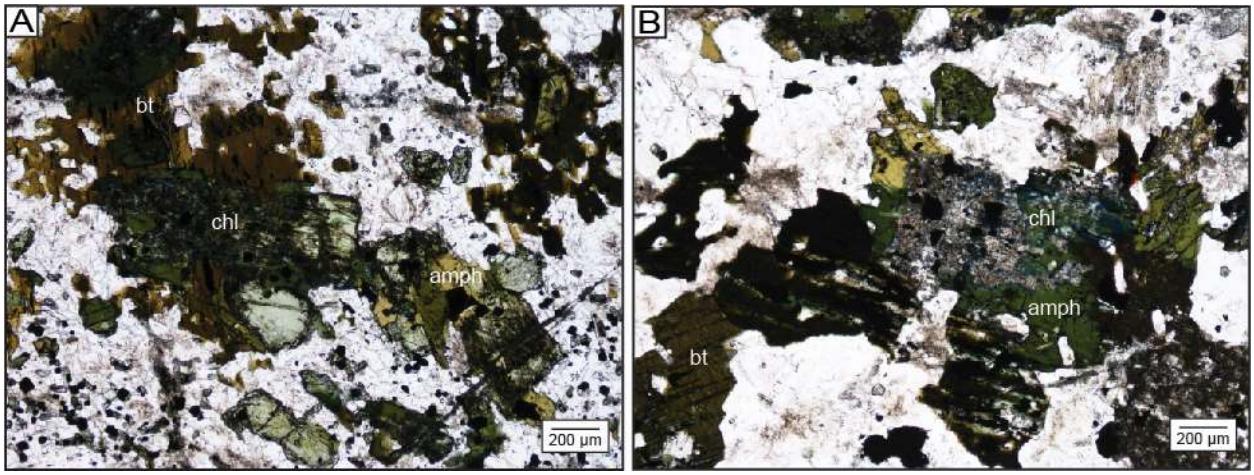

Figure 5.8 Plane polarized light photomicrographs of chlorite alteration of biotite and amphibole distal to the mineralized vein in sample CR-21-J8-255 (from Crown Point): A) Brown biotite and green to tan amphibole being replaced by fuzzy chlorite; B) Similarly, brown biotite and green to tan amphibole being replaced by blue fuzzy chlorite more pervasively than in A.

5.2.2 Vein Mineralogy

Early-stage quartz, referred to as Q1 (Figure 5.9), ranges from anhedral to euhedral grains ranging in size from 50 microns to 2 mm and forms tight interlocking grain boundaries, indicating a lack of open space. The grains exhibit undulose extinction and grain boundary migration also indicating deformation after formation. There are distinct zones of fine-grained Q1 and course grained Q1. Fine-grained Q1 grains are smaller than 1 mm occurring on vein margins, whereas course grained Q1 is larger than 1 mm and occurs central in the vein.

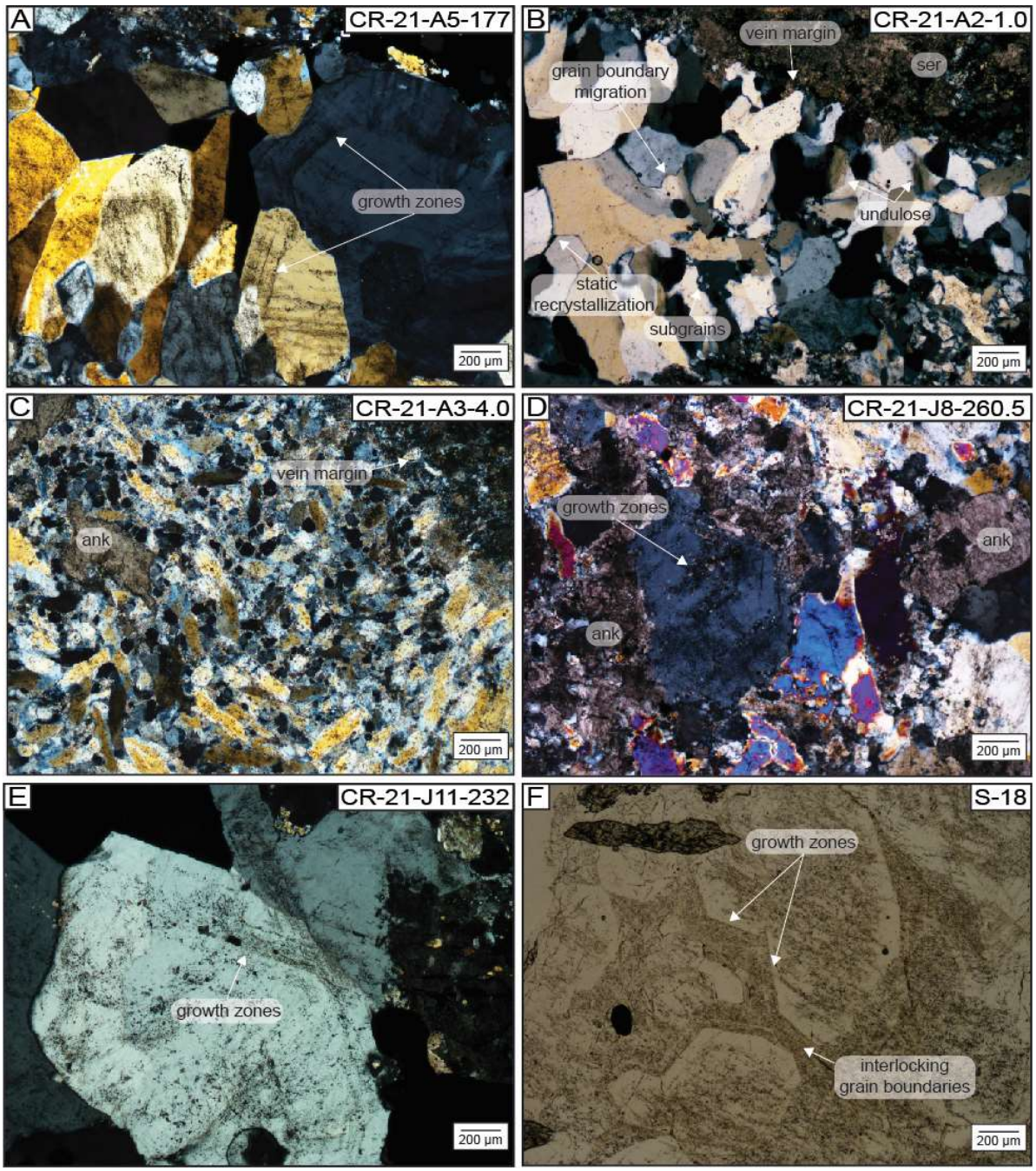

Figure 5.9 Photomicrographs of Q1 with different textures: A) Course-grained interlocking Q1 with fluid inclusions along growth zones (XPL; from Apache-Potosi); B) Deformed, medium-grained Q1 with undulose extinction and grain boundary migration (XPL; from Apache-Potosi); C) Deformed Q1 where the grains are oriented in three main directions with basal quartz showing as well as elongate grains at angles of approximately 120 degrees apart (XPL; from Apache-Potosi); D) Relict Q1 with fluid inclusions along growth zones, undulose extinction and intruding more deformed Q1 and ankerite overprinting the Q1 (XPL; from Crown Point); E) Course-grained Q1 with interlocking grain boundaries, fluid inclusions along growth zones, and grain boundary migration (XPL; from Hopewell); F) Course-grained, euhedral Q1 with fluid inclusions along growth zones with titanite (PPL; from a waste-rock pile).

Pyrite grains occur in the vein and less commonly disseminated throughout the host rock. Pyrite is subhedral to euhedral, commonly brecciated, and ranges in size from 100 μm to 2 mm. Pyrite occurs in or near the vein, typically along vein margins or crosscutting through quartz and ankerite bands. Sometimes pyrite forms euhedral crystals but is more commonly rounded on the edges in contact with other sulfides. Sometimes, when the pyrite is finer grained, it grows along gangue grain boundaries.

Silver-bearing gold grains occur in between fractures in pyrite and cut through the pyrite (Figure 5.10). It has a close spatial association with the base-metal sulfides sphalerite, galena, and chalcopyrite. Silver-bearing gold ranges in size from 5 μm to 50 μm. The Au:Ag atom percent ratios of Ag-bearing gold grains are typically around 60:40 based on EDS spectra but can occasionally vary, which is described in more detail in each following section.

Late-stage quartz, referred to as Q2, forms euhedral, clear, zoned grains into open space (Figure 5.11). They range in size from 100 μm up to a few millimeters. This quartz stage has base-metal sulfide inclusions and primary fluid inclusions along growth zones, which are discussed in more detail in the fluid inclusion section.

Chalcopyrite, galena, and sphalerite formed after pyrite in open space (Figure 5.12) with chalcopyrite having formed first followed by sphalerite, galena and stromeyerite, then Ag-bearing gold. Chalcopyrite, sphalerite, galena, and stromeyerite replace, surround, and crosscut earlier pyrite. Sometimes the base-metal sulfides occur as distinct bands in banded veins, and other times they occur in the central or the margins of the veins.

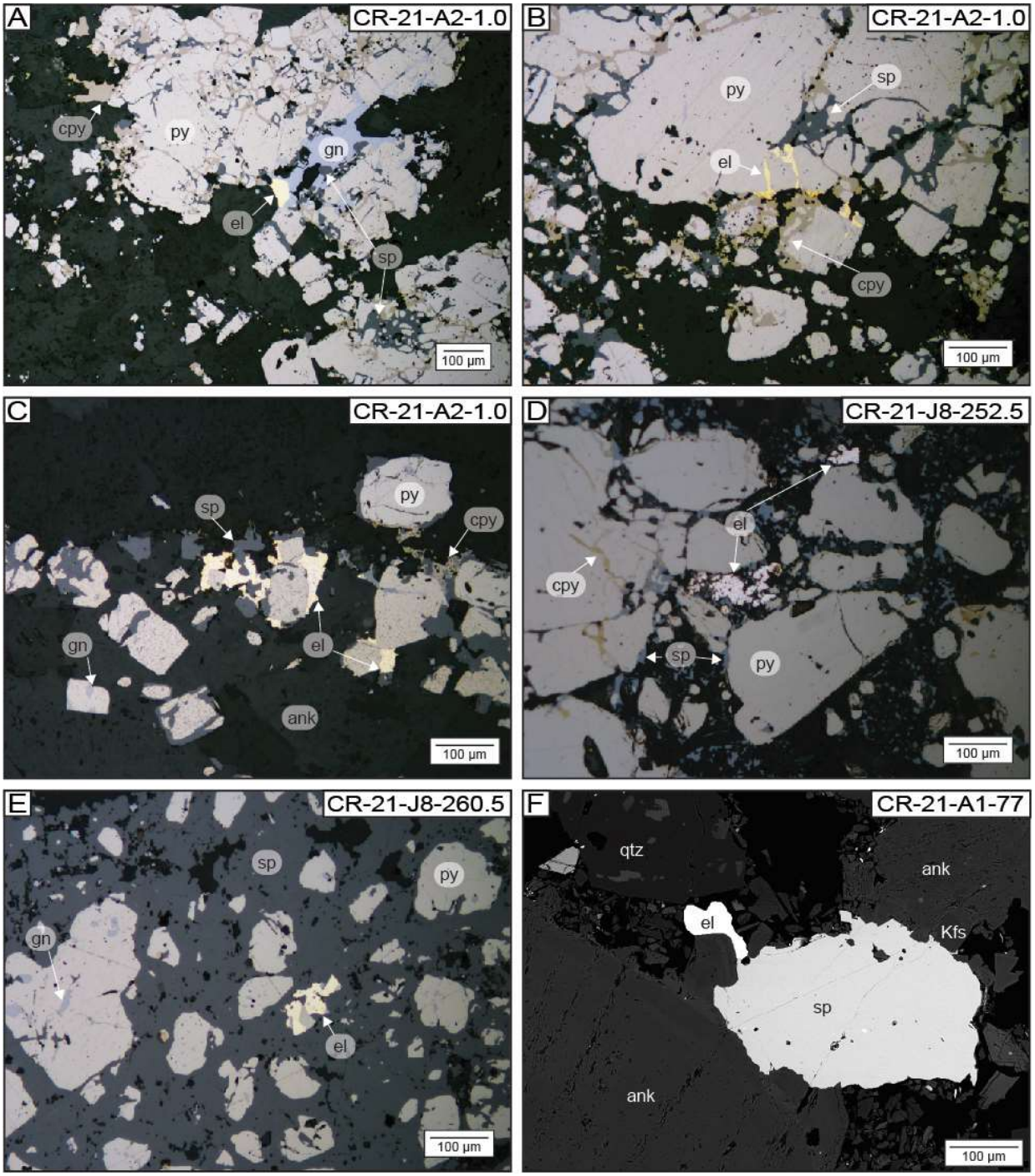

Figure 5.10 Photomicrographs of Ag-bearing gold grains in reflected light and FE-SEM BSE: A) Silver-bearing gold exhibiting a core with Au:Ag atom percent ratio of 58:32 and a rim of 72:28 associated with galena (from Apache-Potosi); B) Silver-bearing gold occurring through pyrite fractures and on pyrite rim similarly to sphalerite and chalcopyrite (from Apache-Potosi); C) Silver-bearing gold surrounding pyrite and sphalerite grains (from Apache-Potosi); D) Silver-bearing gold occurring in gangue minerals, likely ankerite (from Crown Point); E) Silver-bearing gold consuming pyrite grains (from Crown Point); F) Silver-bearing gold associated with sphalerite occurring in association with an ankerite grain (BSE image; from Apache-Potosi).

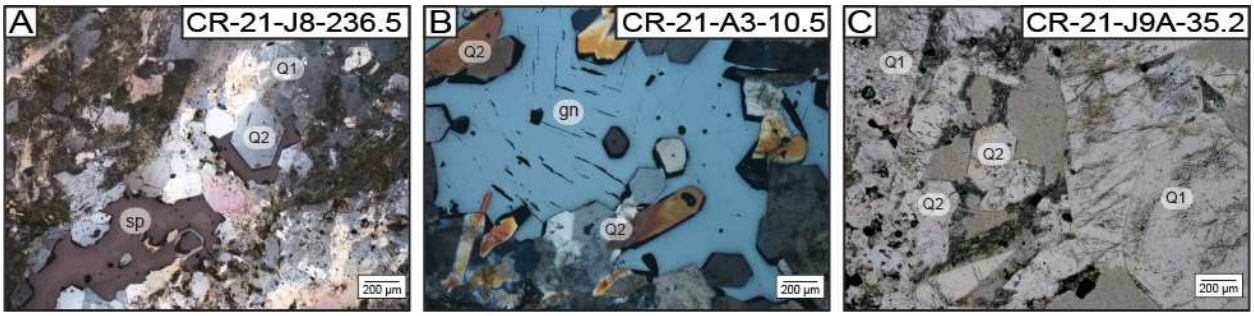

Figure 5.11 Photomicrographs of Q2 growing into open space: A) Euhedral Q2 growing into a vug from Q1 with sphalerite infilling the open space (XPL; from Crown Point); B) Euhedral Q2 with sphalerite inclusions and being later infilled by galena (XPL and reflected light; from Apache-Potosi); C) Clear Q2 growing into open space from Q1 grains, with ankerite growing on Q2 grain boundaries (PPL; from Hopewell).

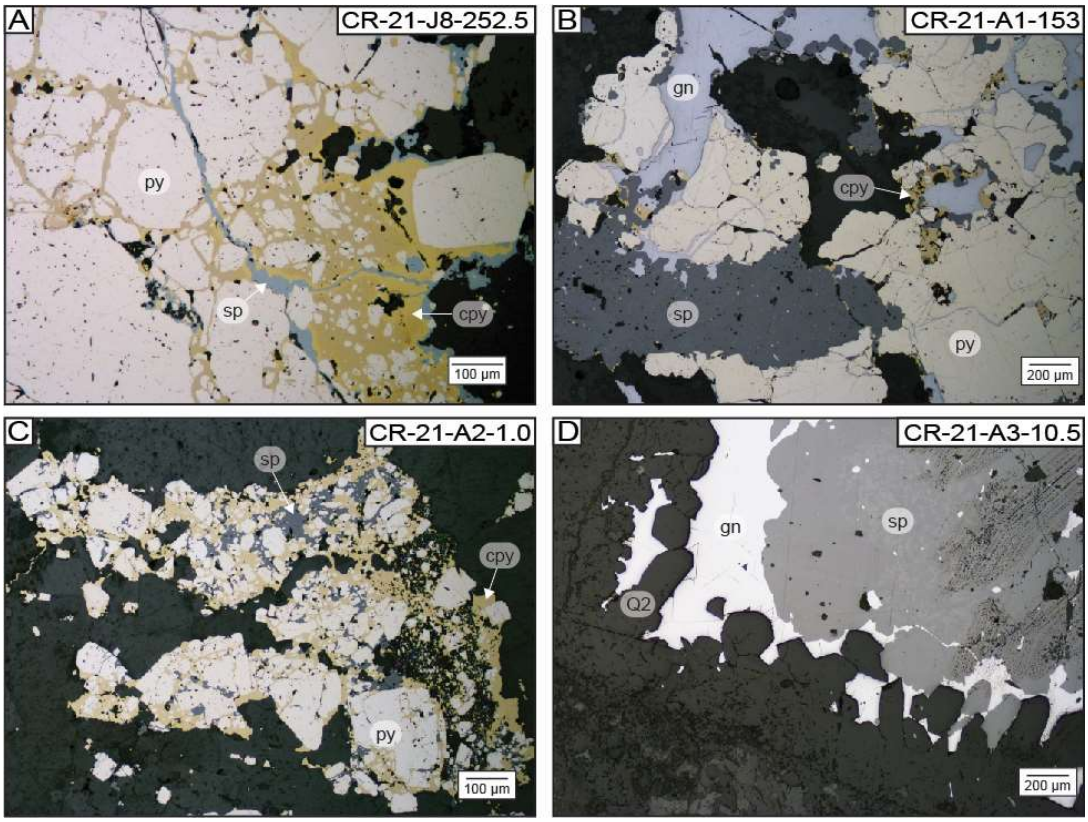

Figure 5.12 Reflected light photomicrographs of pyrite and base metals: A) Fractured and rounded pyrite grains with chalcopyrite consuming pyrite and sphalerite later crosscutting chalcopyrite (from Crown Point); B) Fractured pyrite grains being replaced by sphalerite, chalcopyrite, and galena and the sphalerite has chalcopyrite disease (from Apache-Potosi); C) Fractured pyrite being replaced by chalcopyrite which is then replaced by sphalerite (from Apache-Potosi); D) Euhedral Q2 growing into an open vug (from Apache-Potosi). Sphalerite with chalcopyrite disease is central to the vug and is replacing some Q1 grains. Galena is on the edges of the vug and has inclusions in sphalerite.

Stromeyerite, a silver copper sulfide (AgCuS), occurs throughout the deposit at all depths and is commonly associated with galena (Figure 5.13). Stromeyerite shows three distinctly different textures. First is stromeyerite occurring in equilibrium with galena (Figure 5.13 A). Another is stromeyerite filling vugs lined by iron oxides (Figure 5.13 B). A third is stromeyerite replacing galena (Figure 5.13 D). Often native silver, acanthite, and Ag-bearing gold occur in association with stromeyerite.

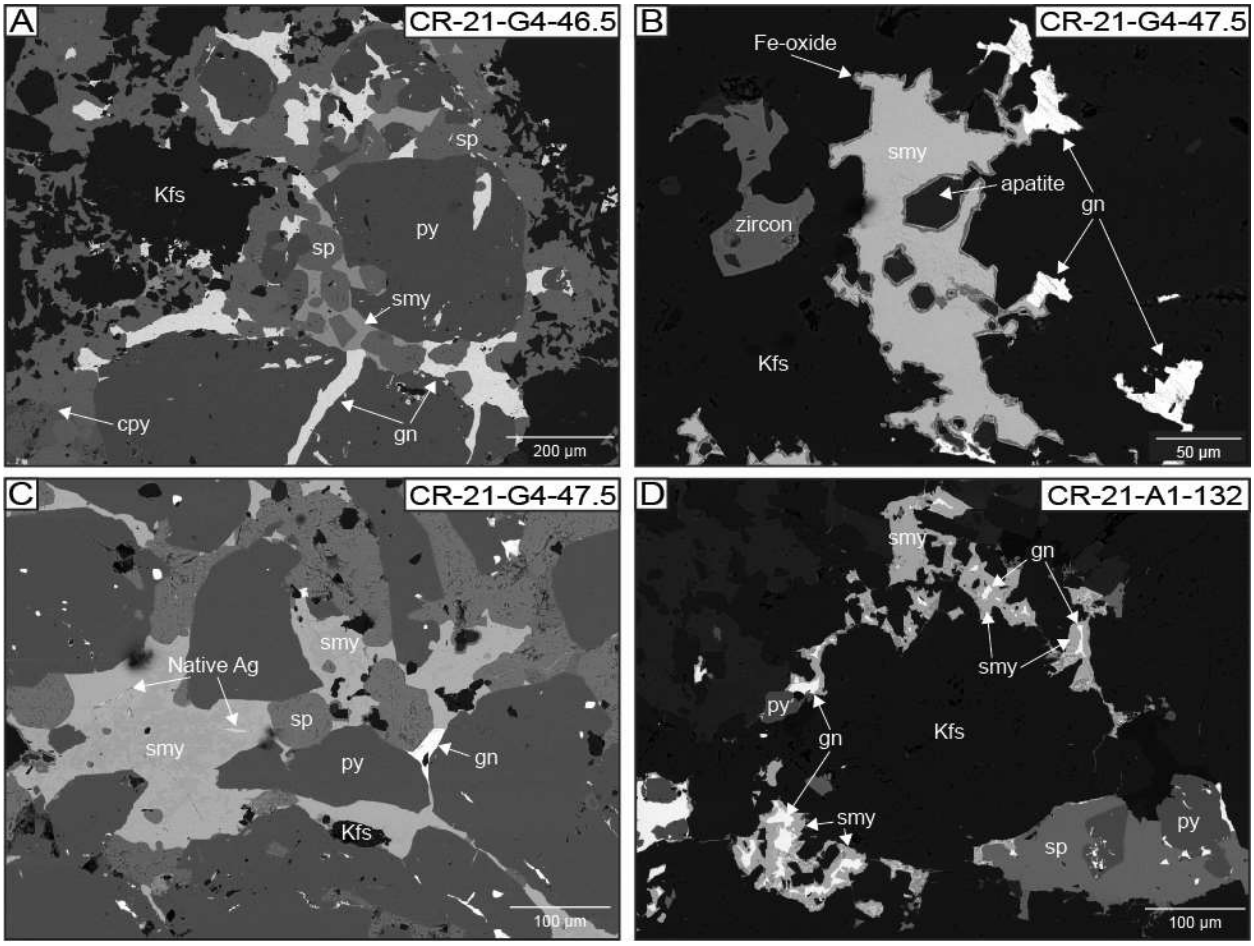

Figure 5.13 Backscattered electron images of stromeyerite occurring alongside sulfides: A) Stromeyerite infilling open space around pyrite and sphalerite grains, occurring contemporary with galena (from the stockwork zone); B) Stromeyerite contemporaneous with galena infilling a vug lined with Fe-oxide (from the stockwork zone); C) Stromeyerite filling open space with slivers of native Ag (from the stockwork zone); D) Stromeyerite surrounding galena both in vugs (from Apache-Potosi).

Clear to yellow-brown sphalerite occurs as open-space fill and is translucent in PPL (Figure 5.14 A). It typically has chalcopyrite disease where there are many small inclusions of chalcopyrite in the sphalerite, giving it a darker color (Figure 5.12 B and Figure 5.14 B). In a few instances, sphalerite has lamellae in XPL, and often sphalerite is subhedral. Sphalerite is consistently iron poor (Table 5.2) as indicated by semi-quantitative EDS spot analysis.

Table 5.2 Iron content in sphalerite

EDS Point Data in Atom %			
Spot	**Fe**	**Zn**	**S**
59	0.2	48.9	50.9
61	2.2	48.8	49.0
66	1.0	46.9	52.0
419	1.1	49.2	49.7
430	4.6	45.7	49.7
331	0.4	51.5	48.1
369	2.0	48.8	49.2
370	1.5	50.1	48.4
373	1.8	49.8	48.4
Average	**1.6**	**48.9**	**49.5**
Minimum	**0.2**	**45.7**	**48.1**
Maximum	**4.6**	**51.5**	**52.0**

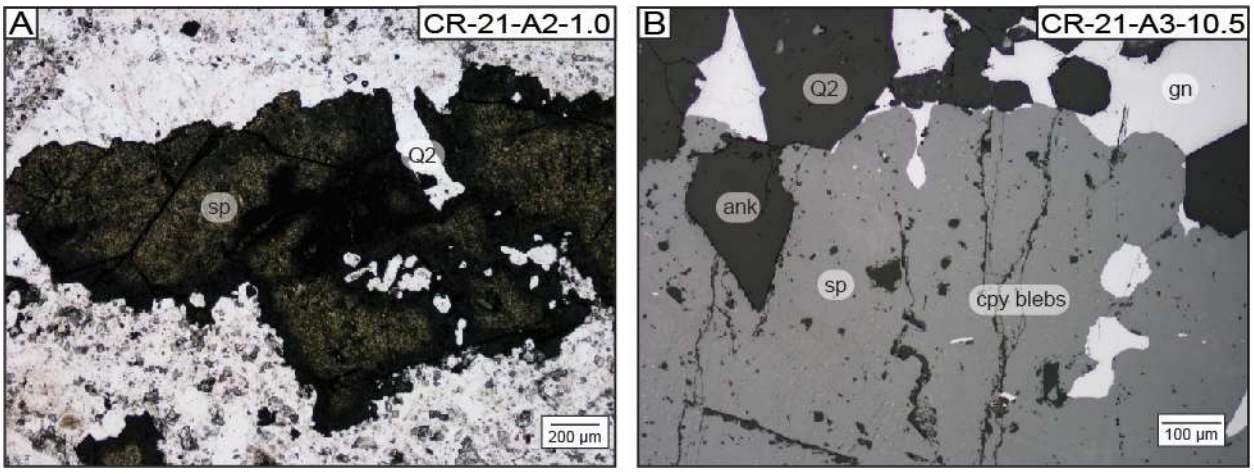

Figure 5.14 Photomicrographs of sphalerite: A) Translucent sphalerite filling an open vug (transmitted PPL; from Apache-Potosi); B) Sphalerite with chalcopyrite disease and later galena infilling a vug with Q2 and ankerite (reflected PPL; from Apache-Potosi).

The dominant carbonate species present in the veins is ankerite, but siderite, dolomite, rhodochrosite, and calcite are also present. Ankerite is anhedral to euhedral and ranges in size from 50 µm to 3 mm (Figure 5.15). Euhedral ankerite grains are often zoned and grow over Q1 quartz. Anhedral grains are interlocking and often form banded veins. Occasionally ankerite alteration occurs distal to the vein.

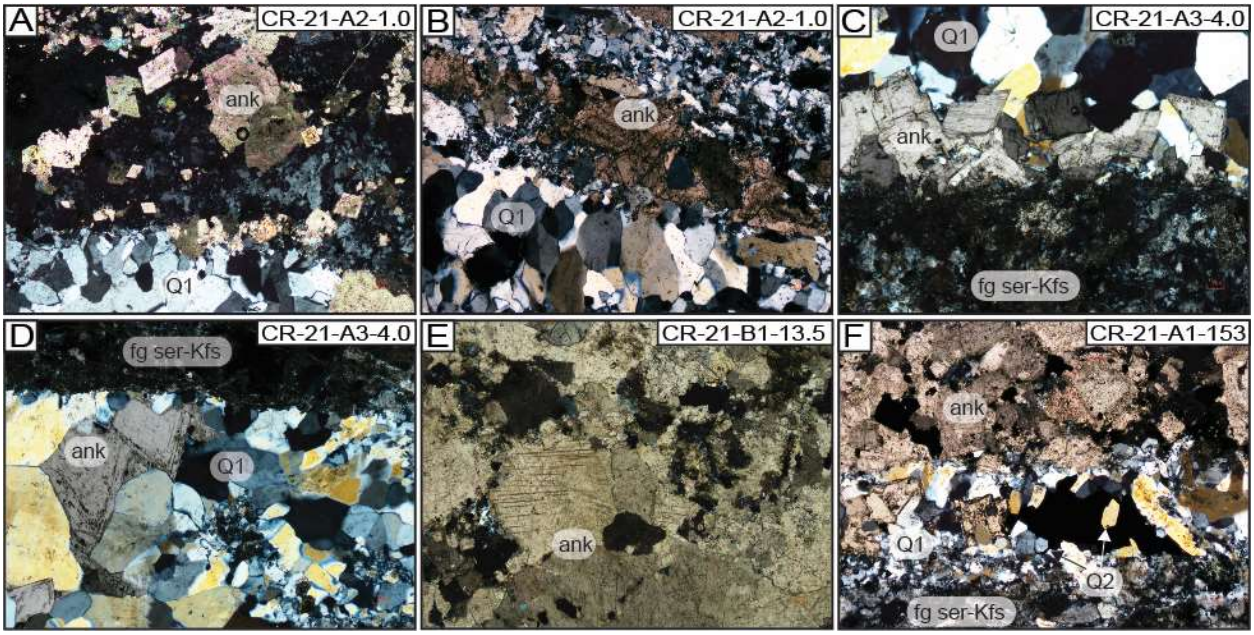

Figure 5.15 Photomicrographs of ankerite textures in veins (XPL; examples from Apache-Potosi): A) Euhedral ankerite grains; B) Subhedral to euhedral ankerite veins occurring between two Q1 bands; C) Euhedral ankerite growing on the rim of the vein into recrystallized Q1; D) Euhedral ankerite being intruded by Q1; E) Anhedral ankerite with cleavage visible; F) Anhedral ankerite band replacing Q1 and an open vug with euhedral Q2.

Based on observations from core logging, late barren carbonate veins crosscut all other vein types. These veins are thin, wavy veins that are typically no greater than a few millimeters wide. Carbonate grains are euhedral to subhedral and range in size from 50 µm to 4 mm. These veins have thin alteration halo consisting of sericite and carbonate minerals.

The deposit can exhibit high-grade silver values. Silver-bearing sulfosalts occur in veins throughout the district. These sulfosalts often appear as dendritic growths in fractures or along pyrite or chalcopyrite grain boundaries. Acanthite, native silver, and a wide range of silver sulfosalts occur associated with oxide minerals in fractures. The sulfosalts are typically euhedral, often showing dendritic or globular growth on grain boundaries or replacing galena (Figure 5.16). Euhedral ruby silvers, which are pyrargyrite, polybasite, and proustite exist in core.

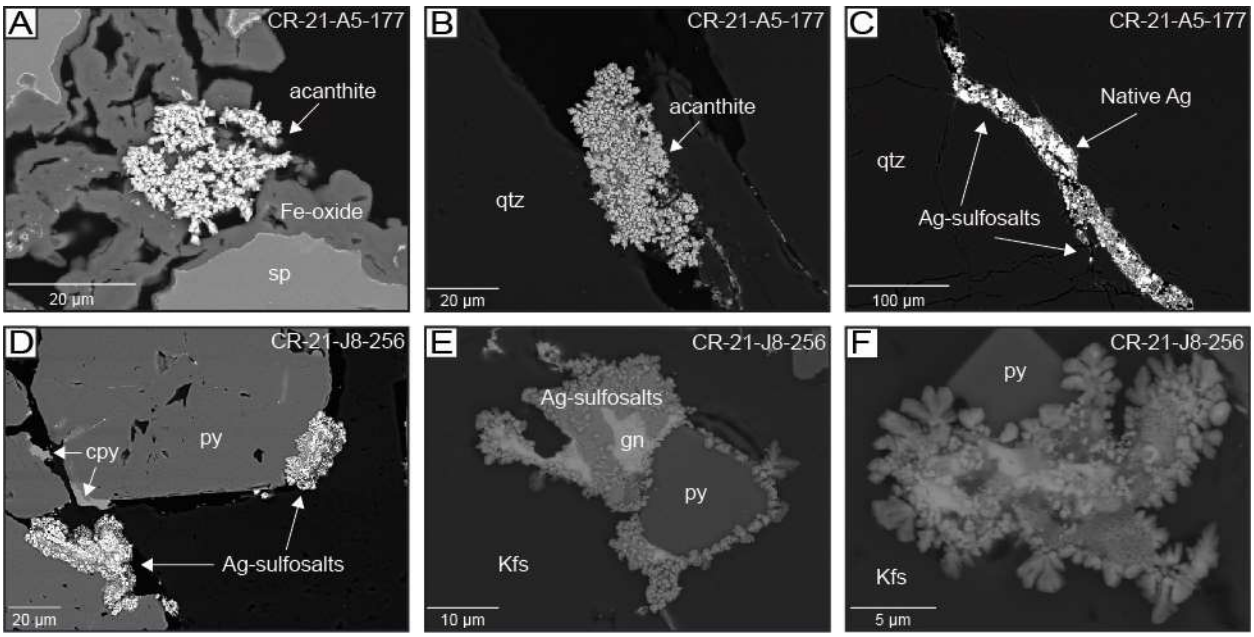

Figure 5.16 Backscattered electron images of silver sulfosalts: A through C show silver sulfosalts in the Apache-Potosi vein system; D through F show silver sulfosalts in the Crown Point vein system. A) Dendritic acanthite occurring surrounded by an iron-oxide rim around sphalerite; B) Acanthite occurring in a fracture through quartz; C) Native Ag and undifferentiated Ag-sulfosalts occurring in a fracture through quartz; D) Dendritic undifferentiated Ag-sulfosalts occurring at grain boundaries of pyrite; E) Undifferentiated dendritic and globular Ag-sulfosalts replacing pyrite and galena; F) Undifferentiated dendritic Ag-sulfosalts

5.2.3 Apache-Potosi (Cross)

The Apache-Potosi vein system (Figure 3.5) contained the best samples for this study in that they exhibited excellent alteration halos (Figure 5.6, Figure 5.7, Figure 5.17) and Ag-bearing gold occurrences (Figure 5.10). The alteration halos shown in the automated mineralogy images commonly show a prominent K-feldspar selvage proximal to the vein and distal sericite alteration (Figure 5.17). Multiple vein types were observed including ankerite veins, quartz-ankerite veins, veins containing sulfides, and veins containing barite (Figure 5.18). This subset of samples shows evidence of Q1 (Figure 5.9) and Q2 (Figure 5.11) as well as significant ankerite in the veins (Figure 5.15). Chalcopyrite, galena, and sphalerite are present in many samples and multiple samples have Ag-bearing gold grains with variable Au:Ag ratios (Figure 5.12, Figure 5.19). Silver sulfosalts, acanthite, stromeyerite, and native silver are present in samples even at depth (Figure 5.16).

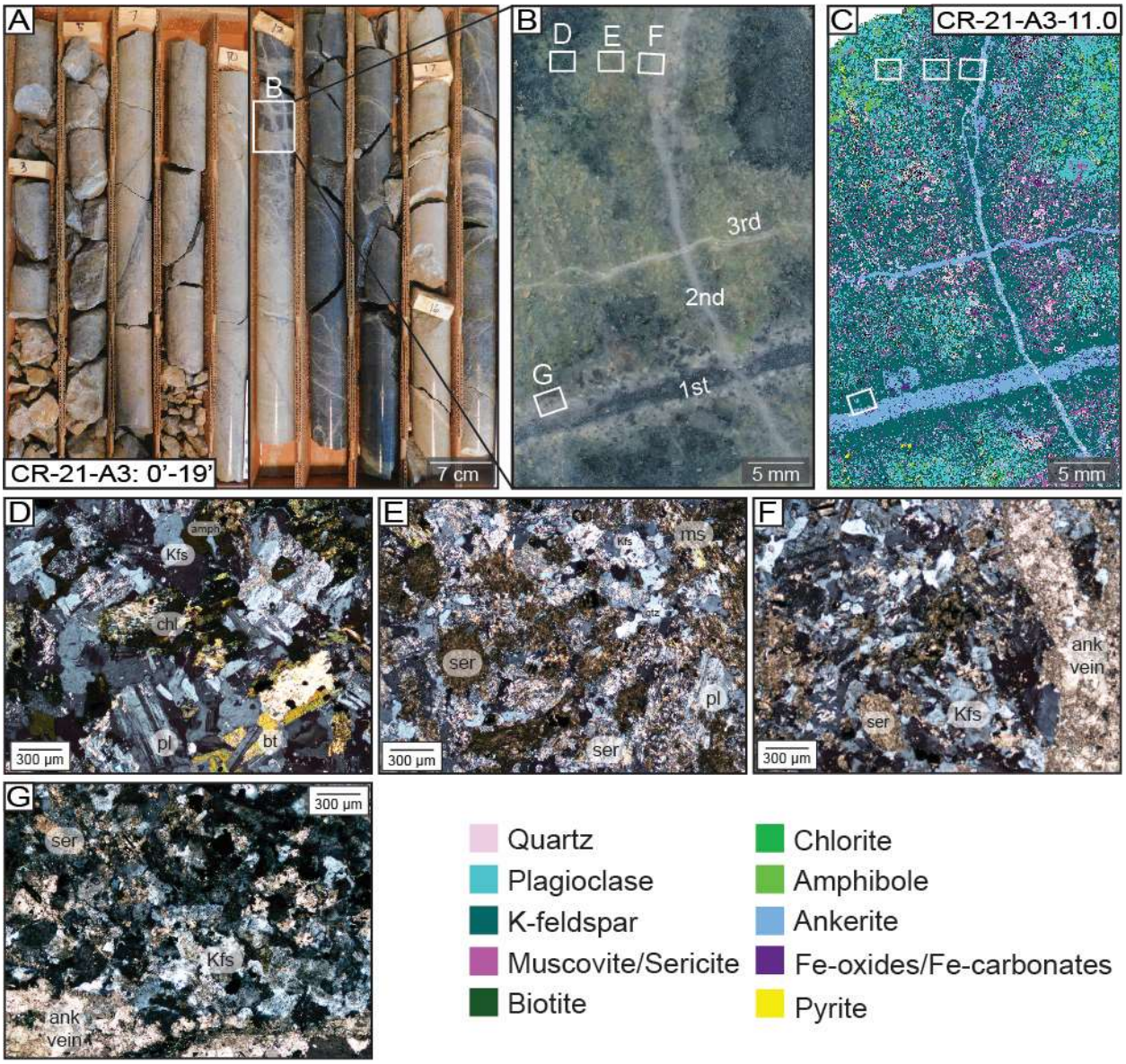

Figure 5.17 Alteration assemblage of sample CR-21-A3-11.0: A) Core photograph from 0' to 19' showing pervasively altered interval from 0' to 11' and a gradual change to fresh rock from 12' to 15' which is a sharp transition to pervasively K-feldspar and sericite altered interval and a white box indicating the location of sample CR-21-A3-11.0; B) Photograph of the billet for sample CR-21-A3-11.0 showing distinct alteration halos around three different vein stages showing crosscutting relationships and white boxes indicating the locations of microphotographs D through G; C) Automated mineralogy image of sample CR-21-A3-11.0 showing K-feldspar alteration halo proximal to the vein followed by sericite and chlorite distal to the vein; D) Distal chlorite alteration and minor sericite alteration with plagioclase grains still preserved; E) Strong sericite alteration with trace relict plagioclase and minor quartz and K-feldspar; F) Vein proximal K-feldspar alteration with limited sericitization; G) Sericitized K-feldspar alteration halo proximal to the ankerite vein.

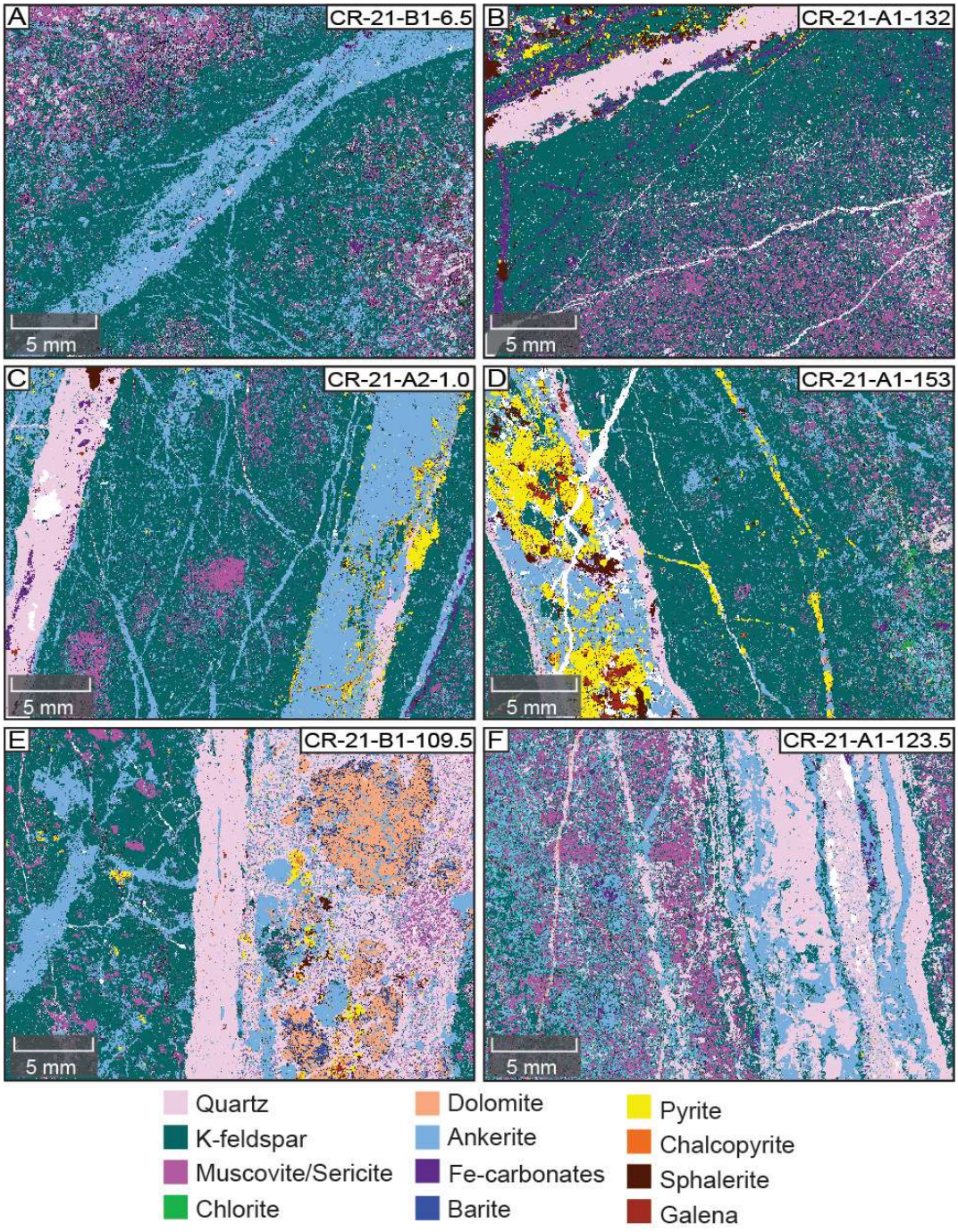

Figure 5.18 False-colored automated mineralogy images of Apache-Potosi vein samples: A) Barren ankerite vein with a wide alteration halo gradually transitioning into fresh host rock; B) Quartz-Fe carbonate-pyrite-base metal vein with an alteration halo and thin wavy quartz stringer veins; C) Quartz vein and quartz-ankerite vein both with pyrite and base metals and thin stockwork ankerite veins; D) Quartz vein cracked open and filled with ankerite, pyrite, base metals, with some K-feldspar brecciated clasts, stringers of sulfides and ankerite; E) Large banded quartz vein with barite, various carbonates including ankerite, siderite, and dolomite, and sulfides central in the vein and ankerite stringers in the altered host rock; F) Banded quartz-ankerite vein with sericite and carbonate host rock alteration.

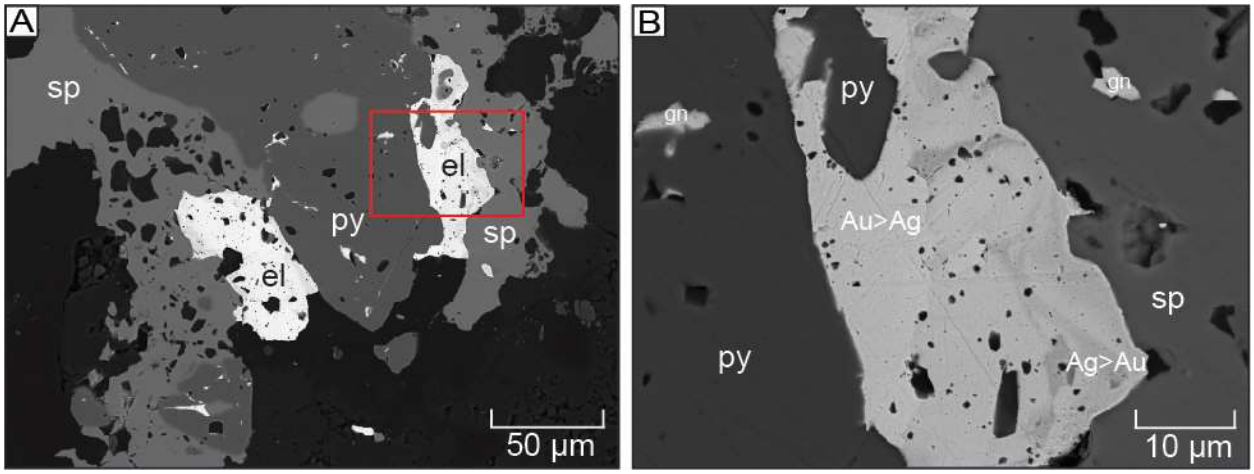

Figure 5.19 Backscattered electron images of Ag-bearing gold in sample CR-21-B1-3.5: A) Two Ag-bearing gold grains with sphalerite, pyrite, and galena; B) close-up of the red box indicated in A) Where the lighter portion of the grain has a higher Au:Ag ratio and the darker portion of the grain has a lower Au content.

Silver-bearing gold grains from the Apache-Potosi system have variable Au:Ag ratios. Sample CR-21-A2-1.0 (Figure 5.10 A) contains an Ag-bearing gold grain with Au:Ag atom percent ratios of 58:32 at the core and 72:28 on the outer part of the grain. Sample CR-21-B1-3.5 (Figure 5.19) has an average (N=19) Au:Ag compositional ratio of 41:59, showing that it is more silver rich than gold rich (Table 5.3). There is significant variation in the Au:Ag composition across Ag-bearing gold grains. The darker areas in the BSE image (Figure 5.19) are more silver-rich than the lighter BSE portions of the grain, which are more gold-rich.

Table 5.3 Au and Ag atom percent of Ag-bearing gold in sample CR-21-B1-3.5 collected from semi-quantitative EDS spot analysis.

Spot	Au	Ag
290	55.5	44.5
297	57.2	42.8
292	29.0	67.8
289	58.1	42.0
300	57.4	42.6
301	49.9	50.1
302	13.9	86.1
303	10.3	89.7
304	9.9	90.1
305	20.2	79.8
306	40.5	59.6
307	31.4	68.7
323	15.9	84.1
324	44.0	56.0
342	56.4	43.6
348	55.2	44.8
352	54.7	45.3
353	55.7	44.3
359	64.6	35.4
Average	**41.0**	**58.8**
Minimum	**9.9**	**35.4**
Maximum	**64.6**	**90.1**

5.2.4 Stockwork Zone (Cross)

The stockwork zone at the Cross (Figure 3.5) contains abundant stockwork and brecciated veins with high grade ore. Some veins have well-defined vein walls with clear alteration halos similar to those at Apache-Potosi, but other veins are brecciated, irregular, and show pervasive or blocky sulfide mineralization (Figure 5.20). The dominant ore minerals are pyrite, galena, sphalerite, chalcopyrite, and stromeyerite. Native silver, silver sulfosalts, stromeyerite, and acanthite are very common in the stockwork zone (Figure 5.13). There is an abundance of copper minerals in the stockwork zone, including what was historically called the

Copper Seam, which contains abundant chalcopyrite, azurite, malachite, and other copper minerals.

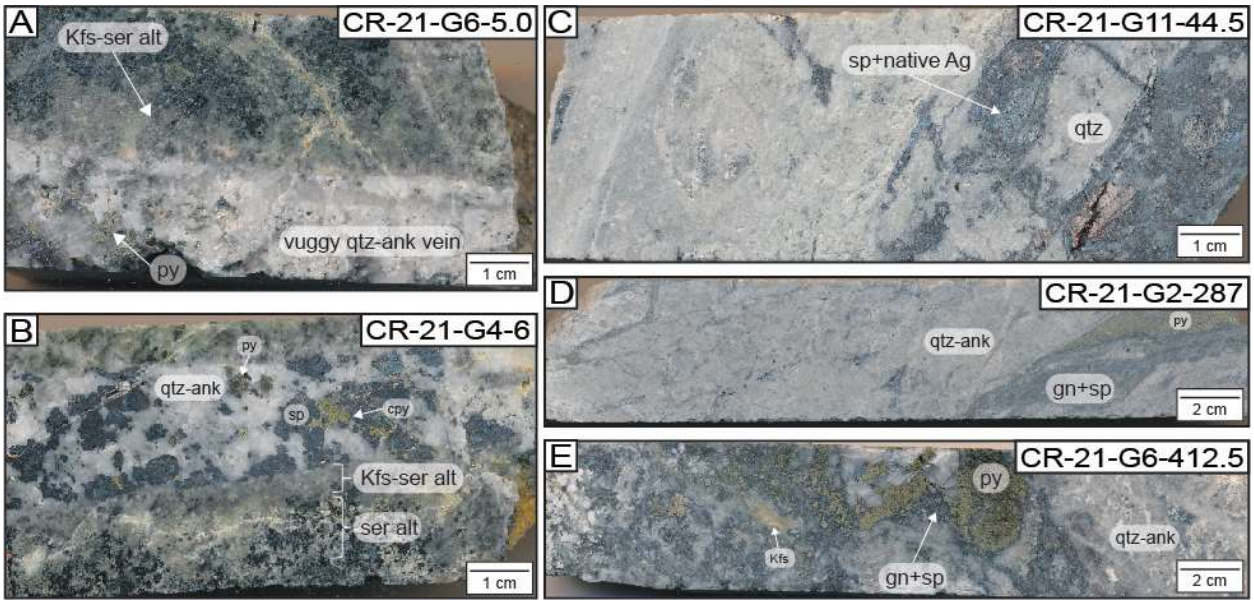

Figure 5.20 Hand sample photographs of samples from the stockwork zone: A) Vuggy quartz-ankerite-sulfide vein with a distinct vein wall and clear K-feldspar and sericite alteration halo; B) Dominantly ankerite with some quartz and course-grained sphalerite and chalcopyrite vein with a definitive vein wall and alteration assemblage; C) A portion of the sample shows banded texture, but the sulfides occur in the brecciated and irregular zone consisting of sphalerite with crosscutting native silver, stromeyerite, and chalcopyrite; D) Irregular stockwork veins consisting of pyrite and base-metal sulfides; E) Large pyrite blebs with base-metal sulfide infill and irregular quartz-ankerite vein.

Sample CR-21-G4-6 (Figure 5.21 A) contains a well-defined vein consisting mostly of ankerite, followed by pyrite, sphalerite, galena, chalcopyrite, and quartz. Thin quartz veins crosscut through the large sphalerite veins. K-feldspar clasts are also present in the vein. The alteration halo is relatively thin and contains K-feldspar, sericite, and chlorite. Sample CR-21-G4-46.5 (Figure 5.21 B) is from a brecciated zone with ankerite, pyrite, and base metal sulfide infill. Rounded pyrite grains are brecciated and are later infilled by galena, sphalerite, chalcopyrite, and stromeyerite. The large clasts are K-feldspar altered. Sample CR-21-G6-5 (Figure 5.21 C) is an ankerite vein that has been brecciated and infilled by quartz, indicating multiple evolutions of the system. Sample CR-21-G14-3.6 (Figure 5.21 D) shows a brecciated texture with large, rounded K-feldspar-altered clasts and a matrix of pyrite, ankerite, and base-metal sulfides.

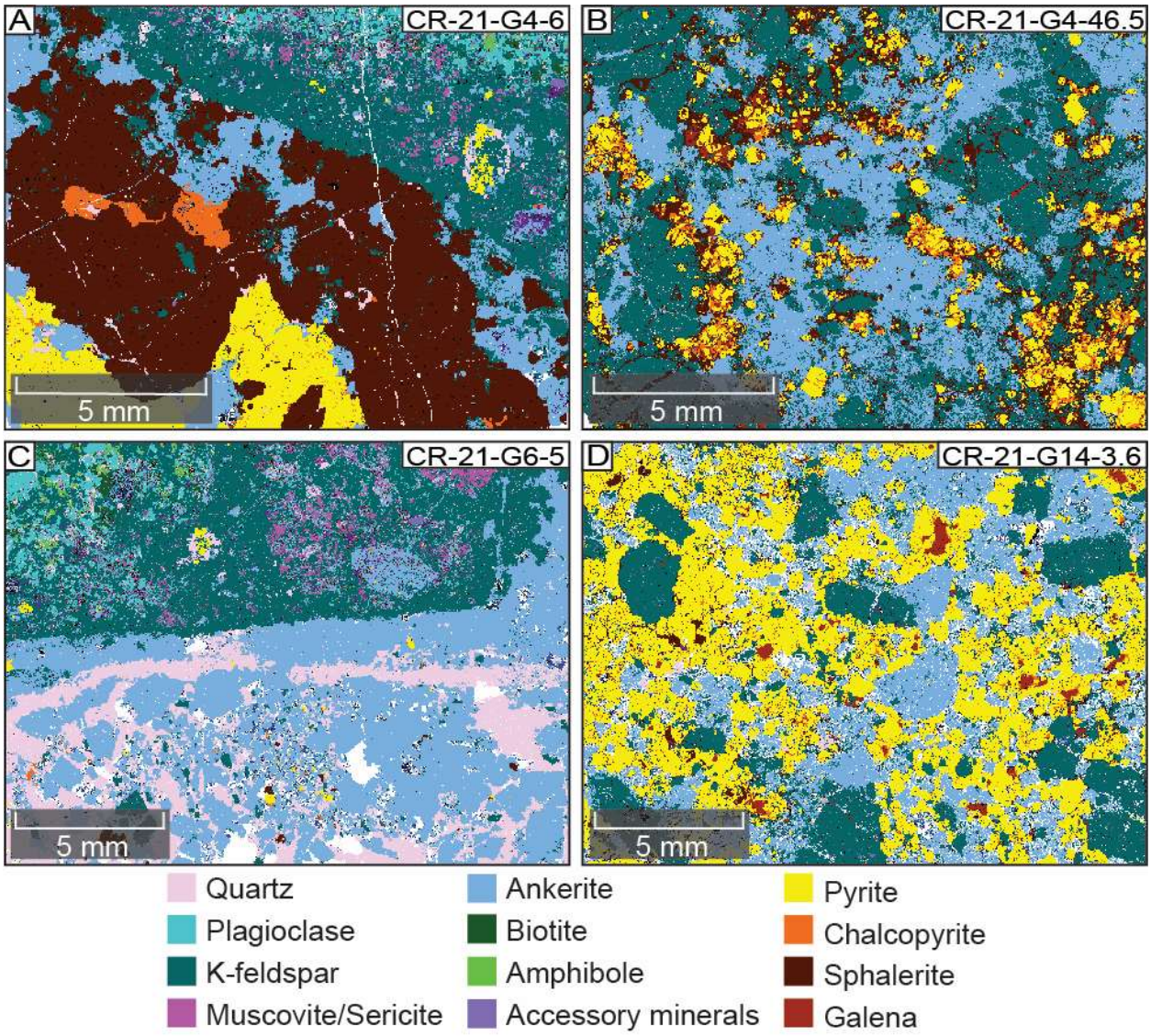

Figure 5.21 False-colored automated mineralogy images of samples from the stockwork zone (Cross): A) Ankerite-sphalerite-pyrite-chalcopyrite vein with K-feldspar clasts in the vein and cross-cutting quartz through the sphalerite grains and a K-feldspar-sericite-chlorite alteration halo; B) K-feldspar clasts with ankerite matrix and pyrite throughout surrounded by base metals; C) Brecciated vein with ankerite and K-feldspar clasts in a quartz matrix with K-feldspar-sericite-chlorite alteration; D) K-feldspar altered clasts in a matrix of ankerite-pyrite-base metals.

Two Ag-bearing gold grains were found in the stockwork zone with Au:Ag compositional ratios between 60:40 and 67:33, of which the latter is one of the higher gold contents found in this study. Both Ag-bearing gold grains are closely associated with stromeyerite (Figure 5.22). Native Ag commonly occurs as thin slivers crossing through stromeyerite (Figure 5.22 B), but it also occurs with close spatial association with galena. Thin

native Ag, stromeyerite, chalcopyrite veins crosscut through and terminate at the boundaries of a large sphalerite grain (Figure 5.22 D).

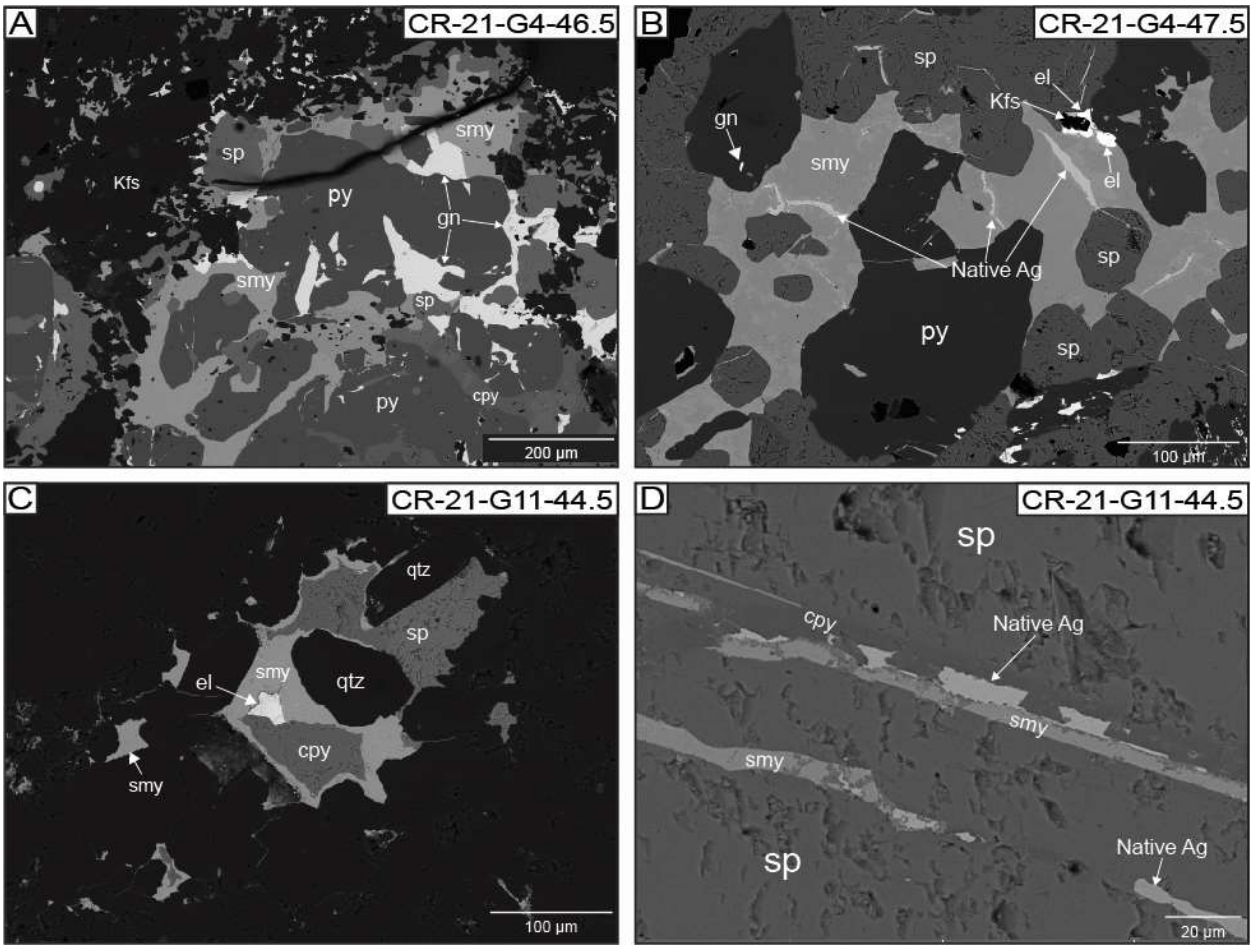

Figure 5.22 Backscattered electron images of ore minerals in the stockwork zone: A) Sphalerite and chalcopyrite filling in open space around pyrite followed by galena and stromeyerite filling open space and replacing pyrite; B) Stromeyerite filling an open vug with native Ag slivers through stromeyerite and an occurrence of Ag-bearing gold with a Au:Ag compositional ratio of 67:33; C) Vug-filling sphalerite, chalcopyrite, and Ag-bearing gold being replaced by stromeyerite; D) Veins of stromeyerite, native Ag, and chalcopyrite crosscutting through a large sphalerite grain.

5.2.5 Hopewell (Cross)

The Hopewell subset (drillhole CR-21-J9A, Figure 3.5) contained veins with both quartz and ankerite with variable ratios of quartz to ankerite. Veins are typically brecciated or banded, and the host rock shows pervasive destructive sericite alteration. The sulfide mineralogy is consistent with other areas, consisting of pyrite, sphalerite, chalcopyrite, and galena. Silver-

bearing gold is present in one sample (CR-21-J9A-224) and no silver-bearing minerals were observed.

Sample CR-21-J9A-224 is a unique sample because it contains Ag-bearing gold occurring in a thin wavy sulfide vein hosted in a quartz-K-feldspar pegmatite (Figure 5.23). Pegmatite intervals are common, especially in the Idaho Springs gneiss, which is the surrounding country rock of the Hopewell. The sulfide mineralization occurs along grain boundaries between large K-feldspar and quartz grains, which occasionally exhibit graphic texture.

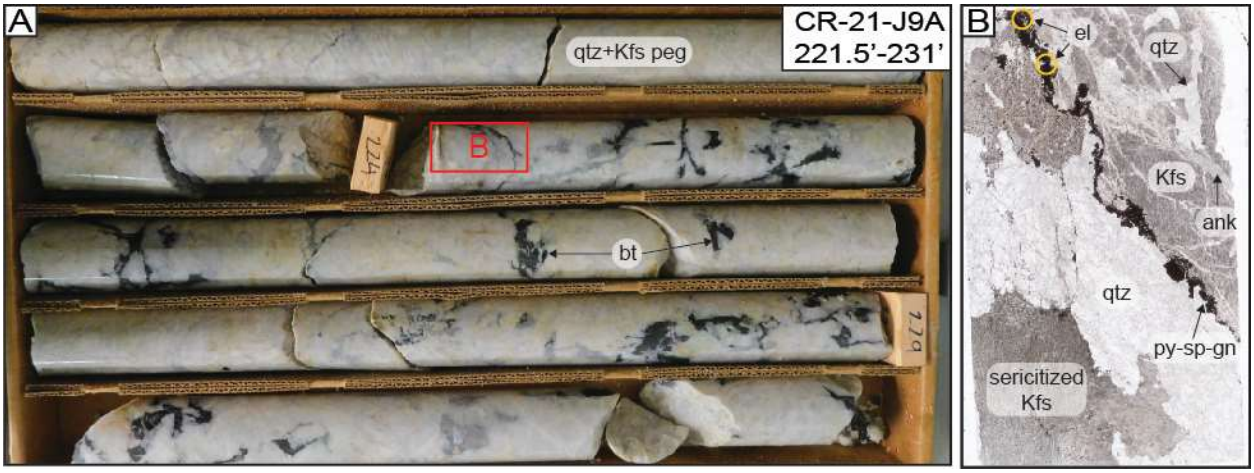

Figure 5.23 Silver-bearing gold occurrence in a pegmatite: A) Core photograph of pegmatite interval in hole CR-21-J9A-224 from 221.5' to 231' with very course-grained quartz and K-feldspar, occasionally with graphic texture, and course-grained biotite clots with location of sample CR-21-J9A-224 marked by the red box; B) Scan of thick section CR-21-J9A-224 showing a pyrite-sphalerite-galena vein containing Ag-bearing gold occurring along grain boundaries and an ankerite vein cross cutting the quartz and K-feldspar.

Silver-bearing gold grains, as indicated by the yellow circles in Figure 5.23 B, were imaged on the SEM-BSE (Figure 5.24), showing it occurs after pyrite as indicated by Ag-bearing gold filling in fractures of pyrite grains, along pyrite grain boundaries, and as blebs within pyrite. Sphalerite, galena, and chalcopyrite also deposited after pyrite formation.

The Au:Ag compositional ratio in sample CR-21-J9A-224 are very consistent. The average (N=7) Au:Ag ratio in these Ag-bearing gold grains imaged in Figure 5.24 is 62:38. The Ag-bearing gold grains are consistently more gold-rich, as outlined in Table 5.4 below. This differs from other areas such as the Apache-Potosi system which show large variability in Au:Ag ratios (Table 5.3).

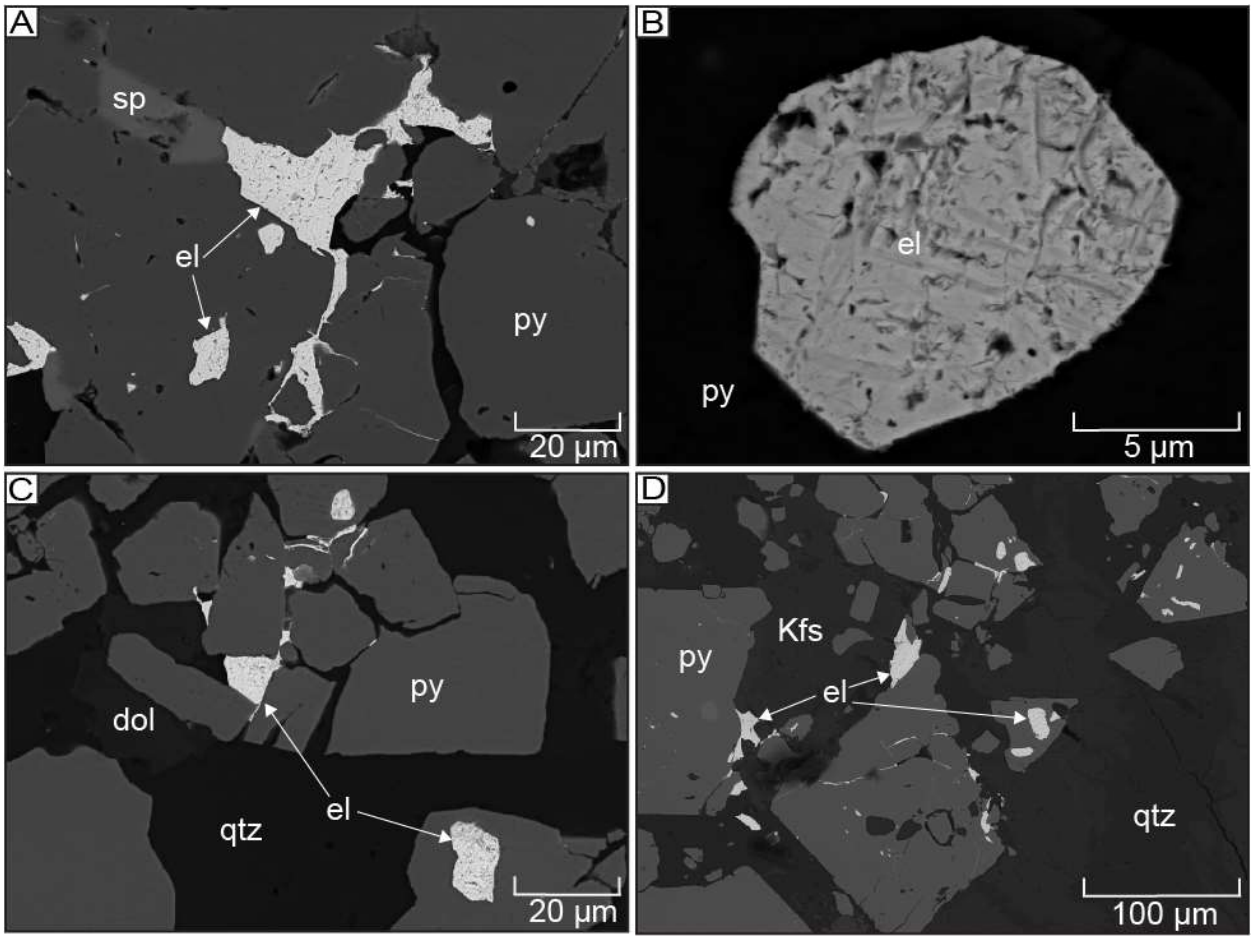

Figure 5.24 Backscattered electron images of Ag-bearing gold in sample CR-21-J9A-224: A) Silver-bearing gold occurring with sphalerite through pyrite fractures and in pyrite; B) Silver-bearing gold grain in pyrite; C) Silver-bearing gold grains in fractures and surrounding pyrite and in pyrite; D) Silver-bearing gold occurring on pyrite grain boundaries and in pyrite.

Table 5.4 Au and Ag atom percent in Ag-bearing gold grains in sample CR-21-J9A-224 from SEM-EDS semi-quantification.

Spot	Au	Ag
429	62.6	37.4
432	62.8	37.2
439	62.4	37.6
440	62.1	37.9
461	61.3	38.7
462	60.3	39.7
465	61.0	39.0
Average	**61.8**	**38.2**
Minimum	**60.3**	**37.2**
Maximum	**62.8**	**39.7**

5.2.6 Crown Point (Cross)

The Crown Point samples (drill hole CR-21-J8, Figure 3.5) are from veins hosted in monzonite but are surrounded by strongly oxidized zones (Figure 5.25). The highest-grade zones are the strongly oxidized intervals and low-grade zones are less oxidized intervals (Figure 5.25). These samples contained both quartz and ankerite veins with variable quartz to ankerite ratios and textures including stockwork veins (Figure 5.25 B), parallel veins of different compositions (Figure 5.25 C), crosscut and offset veins (Figure 5.25 D), thin barren ankerite veins (Figure 5.25 E), large quartz-ankerite-pyrite banded veins (Figure 5.25 F), and brecciated veins (Figure 5.25 G). Silver-bearing gold was identified in samples CR-21-J8-252.5 (Figure 5.10 D) and CR-21-J8-260.5 (Figure 5.10 E) from Crown Point as well as silver minerals including stromeyerite and native silver (Figure 5.26), and silver sulfosalts (Figure 5.16 D, E, and F).

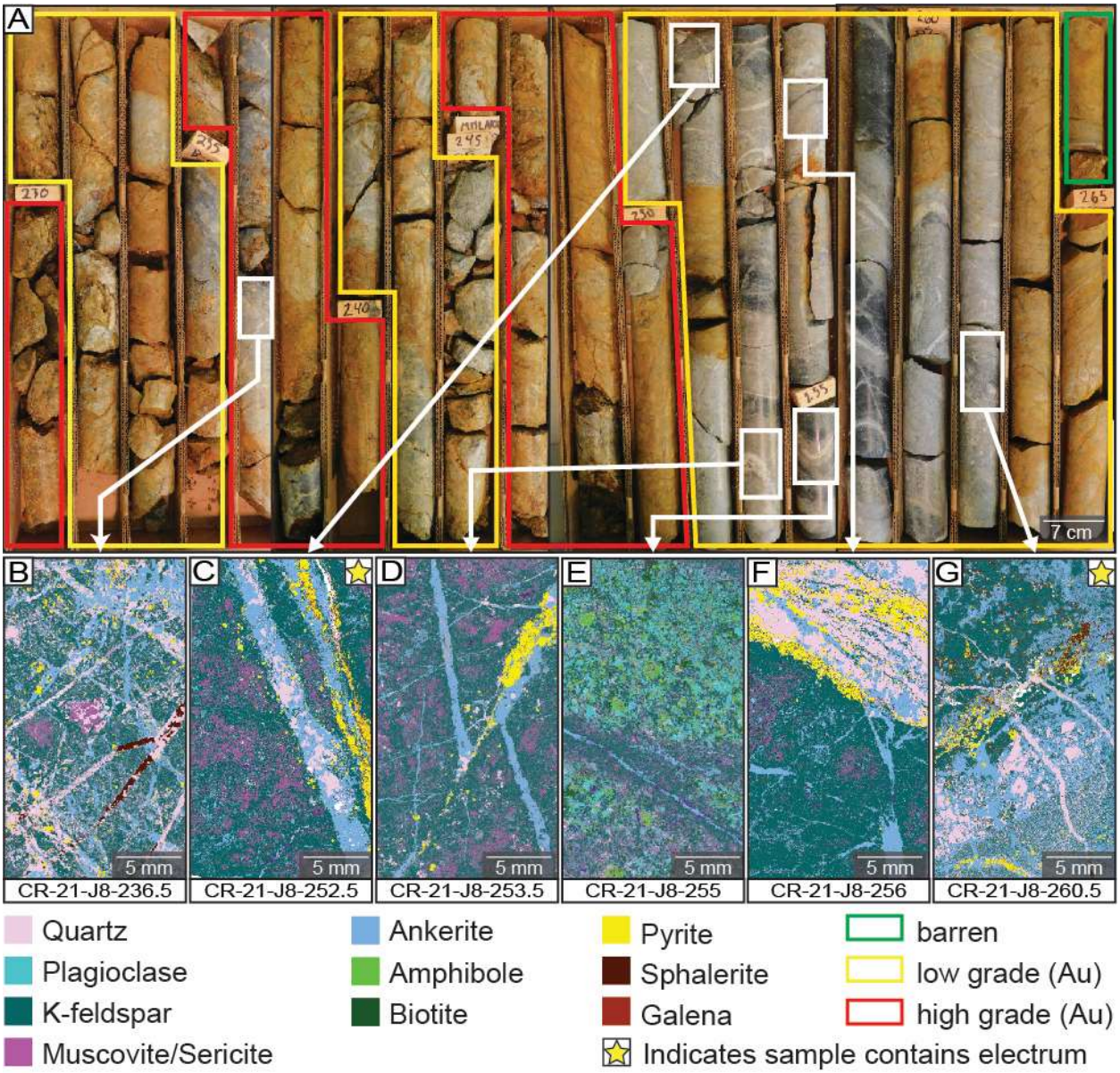

Figure 5.25 Core photographs of drill hole CR-21-J8 with sample locations marked by white boxes corresponding to false-colored automated mineralogy images of each sample: A) Core photographs of drill hole CR-21-J8 from 229 feet to 266 feet with zones of barren, low grade, and high grade marked by green, yellow, and red boxes respectively; B) AM image of CR-21-J8-236.5 showing stockwork vein textures including quartz veins with sphalerite filling in vugs and late ankerite stringers; C) AM image of sample CR-21-J8-252.5 showing two parallel veins with K-feldspar and sericite alteration; D) AM image of sample CR-21-J8-253.5 showing multiple sets of veins showing crosscutting relationships and offsets; E) AM image of CR-21-J8-255 showing a barren late ankerite vein with K-feldspar, sericite, and chlorite alteration; F) AM image of CR-21-J8-256 showing banded quartz-ankerite-pyrite vein with late ankerite stringers and K-feldspar and sericite alteration; G) AM image of CR-21-J8-260.5 showing brecciated and overprinted veins with complex cross-cutting relationships and K-feldspar alteration.

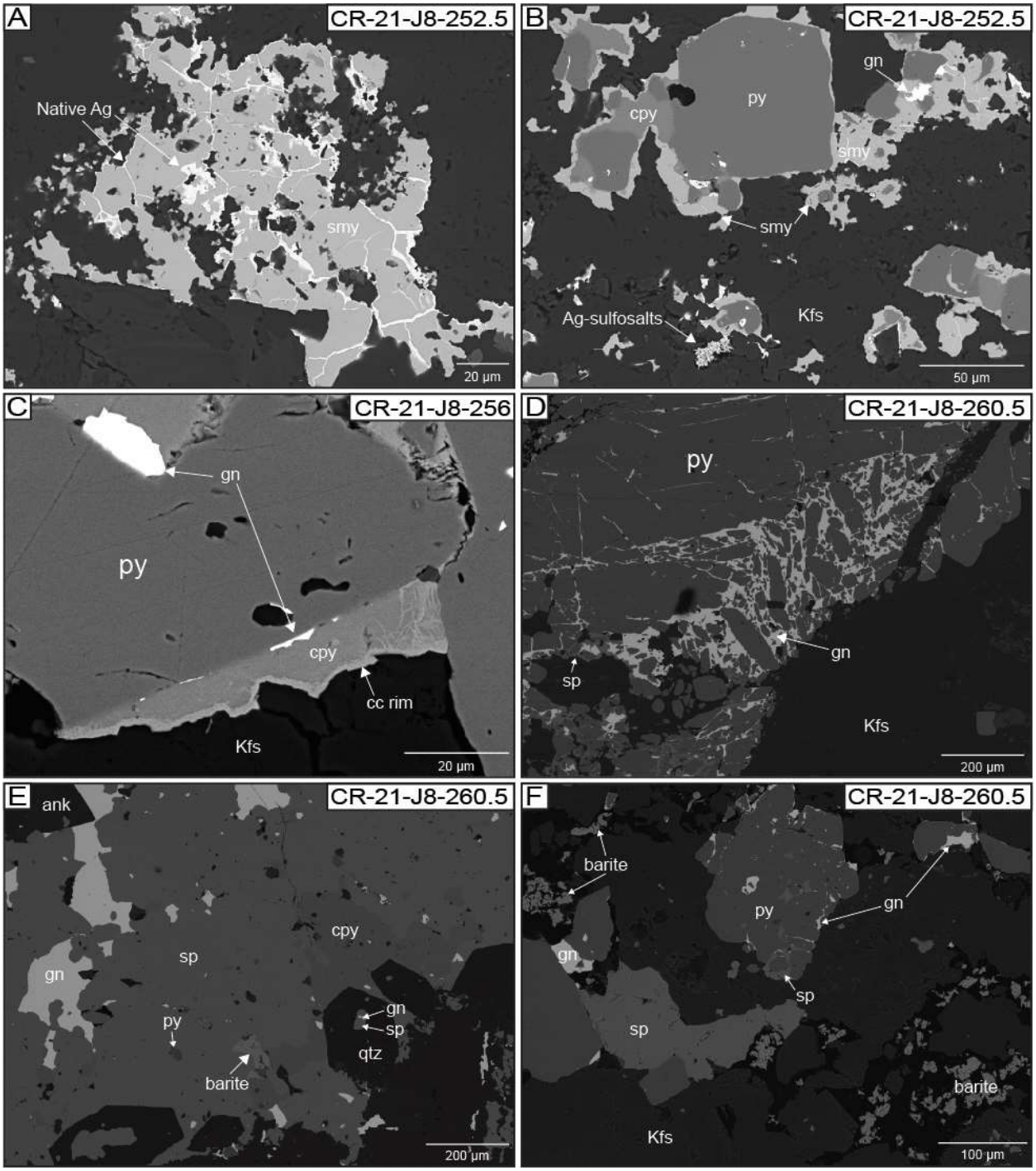

Figure 5.26 Backscattered electron images of ore mineralogy and base metals at Crown Point in drill hole CR-21-J8 progressively downhole: A) Stromeyerite filling in a vug and being crosscut by native Ag veinlets; B) Stromeyerite contemporaneous with galena replacing chalcopyrite and pyrite with nearby Ag-sulfosalts in open space; C) Chalcocite rims on chalcopyrite replacing pyrite with later galena growing on grain boundaries of pyrite ; D) Brecciated pyrite being infilled by galena and sphalerite; E) Sphalerite replacing chalcopyrite and pyrite with later galena and galena and sphalerite inclusions in quartz; F) Sphalerite and galena replacing pyrite and nearby barite filling in open space.

5.2.7 Cross at Depth

One sample, CR-98-108-1782, from significant depths (1782 feet downhole) at the Cross was analyzed. This sample only contains quartz gangue in the vein. It does not contain any chalcopyrite, Ag-bearing gold, or silver minerals, but it did show pyrite, galena, and sphalerite, and shows stockwork-like brecciated vein texture.

5.2.8 The Caribou Deposit (Shallow)

Most of the waste rock samples come from the workings around the Caribou (Figure 4.2), and therefor they provide a glimpse of the mineralogy at the Caribou since underground workings were not accessible at the time of this study. The following sections report the findings from this work.

The dominant minerals in waste rock samples, which are hosted by weathered and oxidized Caribou monzonite, from the Caribou deposit is quartz with minor biotite, chlorite, sericite/illite/smectite, barite, apatite, carbonates, amphiboles, iron oxides/hydroxides, and titanium minerals. The dominant sulfides identified are pyrite, galena, sphalerite, and Ag-bearing minerals including stromeyerite and acanthite. Secondary copper minerals such as chalcocite, malachite, and azurite were identified. Sphalerite and galena often formed in open space around euhedral quartz crystals. Based on SEM-EDS analysis, sphalerite from these waste rock pile samples was iron-poor, giving it the translucent appearance, similar to sphalerite at the Cross. The waste rock pile samples contain abundant silver-bearing minerals including sulfosalts, native silver, and silver-bearing chalcocite. No Ag-bearing gold was found in this subset of samples. The intergrowth texture is unique. Often the silver-bearing minerals are associated with barite and secondary copper minerals. The sulfides often have a Cu- or Pb- oxide rim around them.

Sample S-00 and S-5 are both from the same waste rock pile located surrounding an unknown shaft indicated in Figure 4.2. Sample S-00 is dominantly quartz that varies from large euhedral crystals with growth zones defined by primary fluid inclusion assemblages to small grained recrystallized quartz. There is trace pyrite that is subhedral with fractures filled by sphalerite. The sulfides occur in open space between large euhedral quartz crystals. Malachite and azurite occur along fractures and open space between large quartz crystals and malachite occurs as acicular radial aggregates (Figure 5.27). Sample S-5 consists dominantly of fine-grained quartz with later euhedral quartz veins and abundant iron oxides.

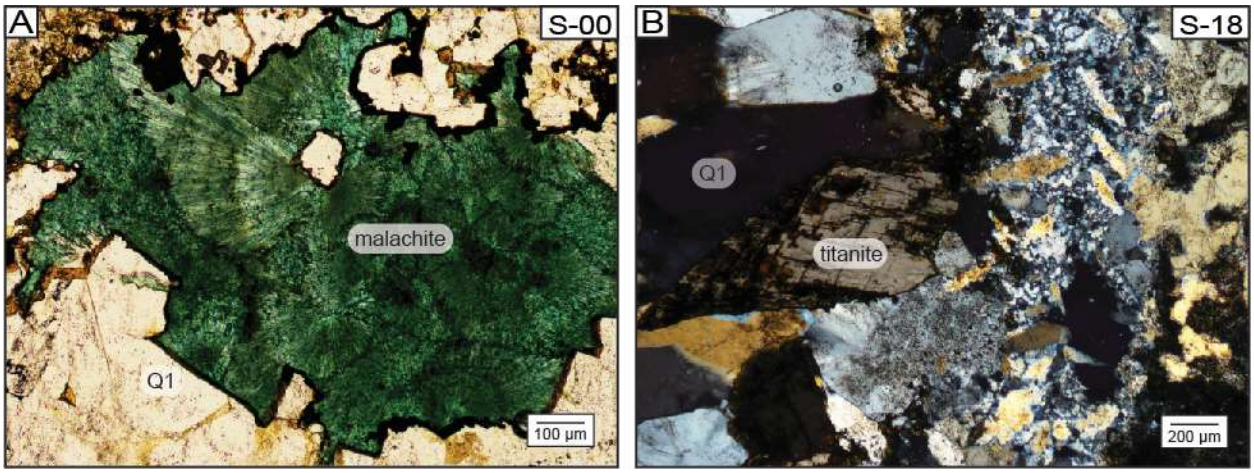

Figure 5.27 Photomicrographs of sample S-00 and S-18 from waste rock piles: A) Radial aggregates of malachite; B) Euhedral titanite growing into Q1 from a vein boundary of a deformed quartz generation.

Sample S-10, S-13, and NS-1 are from the Native Silver waste rock pile (Figure 4.2). Sample S-10 has a large quartz vein that contains trace pyrite, minor galena, and sphalerite. The vein has a sharp contact with the strongly sericitized and oxidized host rock. Sample S-13 contains a large vein composed of dominantly quartz and minor ankerite. The quartz varies from fine-grained to course-grained depicting numerous generations of quartz and subsequent recrystallization. Sulfides occur in vugs in euhedral quartz cavities. Galena is the major sulfide, along with sphalerite, stromeyerite, chalcopyrite, and chalcocite. Famatinite and enargite were identified under the SEM, and stromeyerite, galena and chalcocite display a beautiful symplectite texture (Figure 5.28). The host rock is composed of dominantly quartz, plagioclase, and K-feldspar, although the rock strongly is oxidized and sericitized, and there is minor apatite, barite, and titanite.

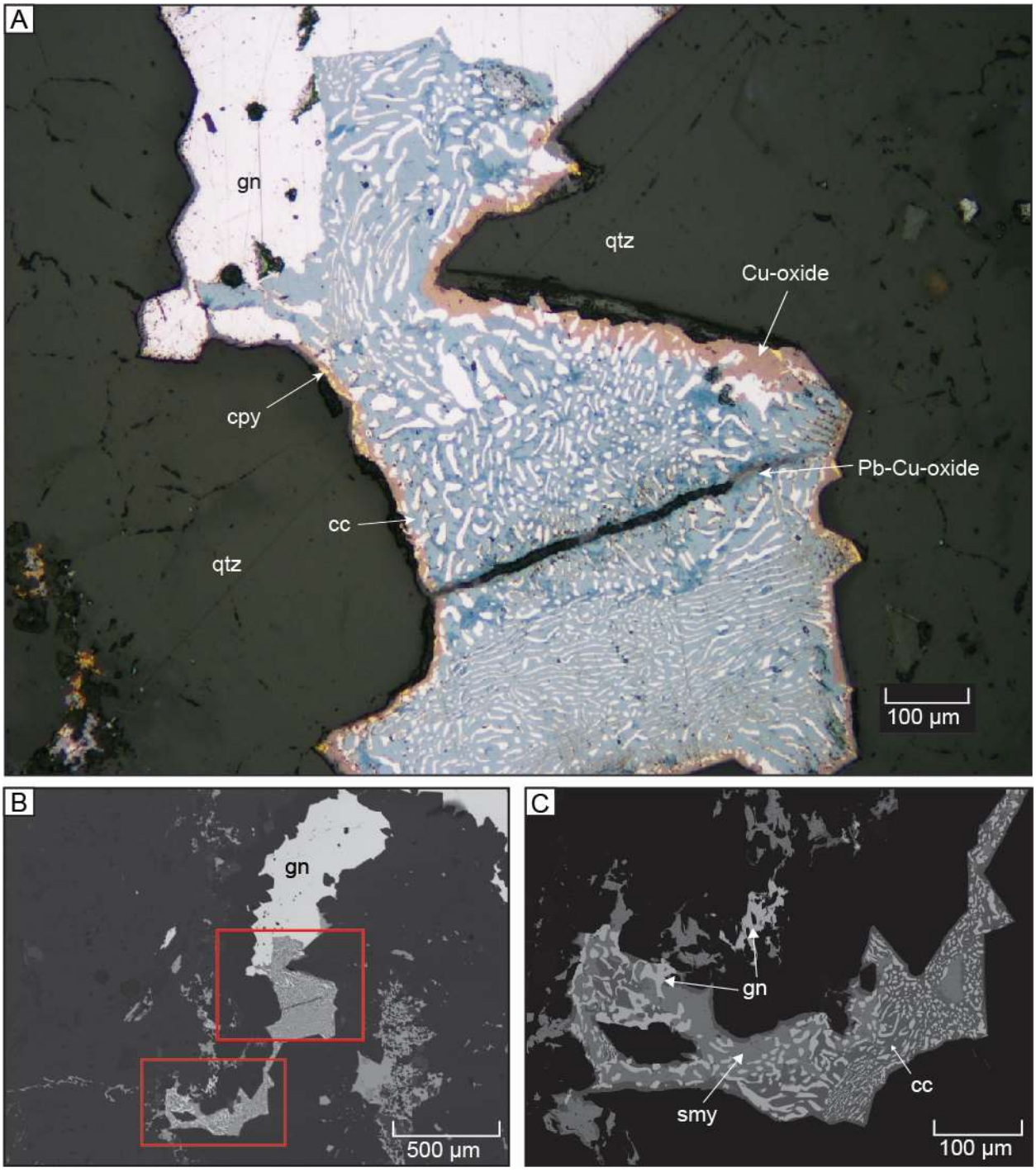

Figure 5.28 Reflected light photomicrograph and backscattered electron images of sample S-13 mineralization: A) Photomicrograph showing galena, symplectite intergrowth texture of galena and chalcocite with remnant chalcopyrite and Pb- and Cu-Pb-oxides; B) Backscattered electron image indicating the locations of A and C; C) Chalcocite-stromeyerite with galena (with 4 atom % As) symplectite with a tenorite rim surrounding the lining of the vug.

Sample S-18 and S-19 are from the 7-30 E extension waste rock pile (Figure 4.2). Sample S-18 contains brecciated and oxidized vein material. The host rock is medium to fine-grained quartz and K-feldspar with minor muscovite showing strong sericitization. The vein is host to coarse-grained subhedral zoned quartz with various degrees of recrystallization and deformation including subgrains, undulose extinction and deformation bands. Titanite occurs along the oxidized fractures and edges (Figure 5.27). It is often euhedral to subhedral and grows inwards from the vein walls. In reflected light, pyrite occurs as small anhedral grains with galena commonly along the outside of the pyrite grains. The sulfides occur on the edges of quartz and titanite along grain boundaries and sometimes filling open space. Sample S-19 dominantly consists of quartz of various sizes showing both undeformed and strongly deformed quartz. The sample is brecciated with strongly sericite-altered clasts and quartz matrix. Minor pyrite and galena are present.

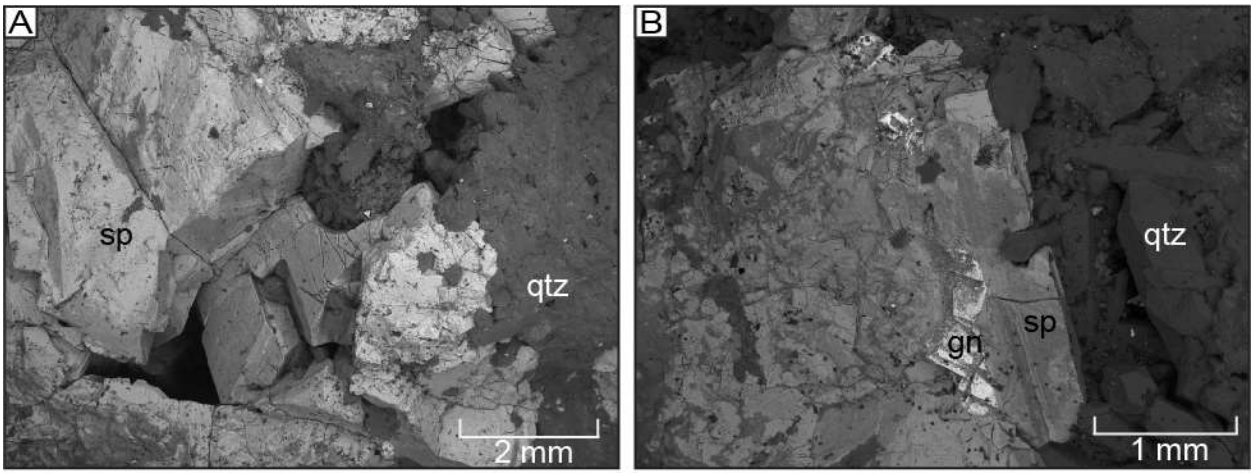

Figure 5.29 Backscattered electron images of sample SI-13 (San Isabel waste rock pile) showing quartz, sphalerite, and galena textures: A) Zoned iron-poor sphalerite and galena in a euhedral quartz vug; B) Euhedral to subhedral sphalerite associated with euhedral quartz vugs.

Sample SWP, from the Southwest Pandora deposit on Pomeroy Mountain (Figure 4.2) contains acanthite, native silver, tenorite, and cuprite (Figure 5.30). Often, native silver grains occur surrounded by secondary copper mineralization, showing a zoning of native silver at the core to stromeyerite, and then chalcocite rims (Figure 5.30 A). There's also an association of silver mineralization with barite (Figure 5.30). Samples from core of the Pomeroy Mountain Park Hill Breccia contain polybasite and pyrargyrite. Sample SWP contained the highest volume percent of precious metals out of all the waste rock pile samples. It also had the most secondary

copper mineralization mostly in the form of chalcocite (Figure 5.30). The Cu-oxides contain around 2 atom percent silver and occurs largely in fractures.

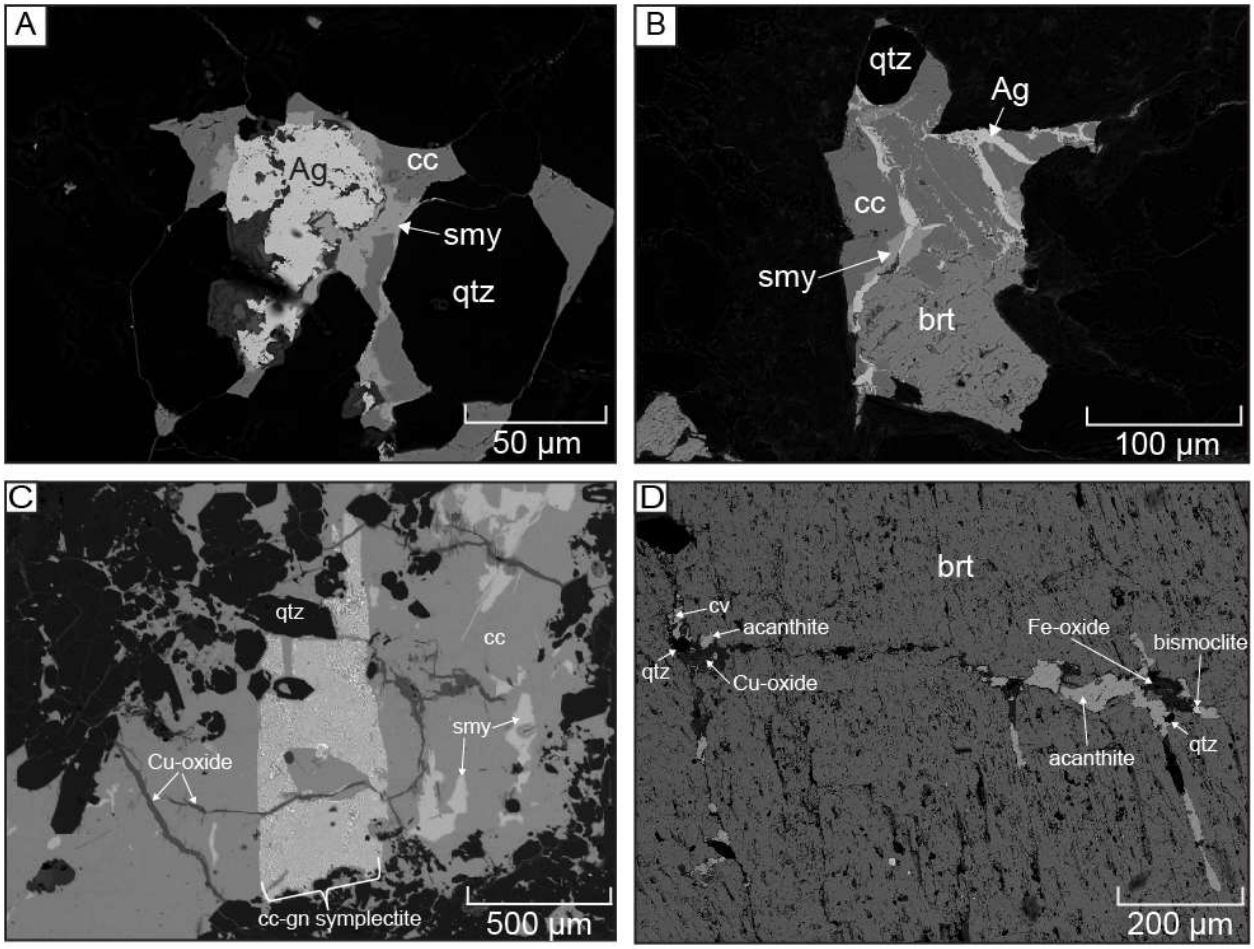

Figure 5.30 Backscattered electron images of sample SWP: A) Native silver surrounded by stromeyerite followed by chalcocite all filling in a vug with Q2; B) Chalcocite, barite, stromeyerite, and crosscutting native silver in a vug with euhedral Q2; C) Sulfides filling in a euhedral quartz vug consisting of a large zone of chalcocite-galena symplectite texture surrounded by chalcocite with irregular stromeyerite and Cu-oxide filled fractures; D) Acanthite, covellite, euhedral quartz, bismoclite, and Cu- and Fe- oxides in fractures through a large barite grain.

Figure 5.31 shows automated mineralogy images of samples from other various waste-rock piles. Sample 651 (Figure 5.31 A) has a pyrite vein displaying K-feldspar and sericite alteration. There are ankerite stringers and alteration around the main pyrite vein. Sample 659 (Figure 5.31 B) shows a quartz vein with K-feldspar-altered breccia clasts in the vein as well as brecciated pyrite with base metal sulfides infilling around the pyrite. This has a typical K-feldspar and sericite alteration halo as well as some chlorite. Sample 667 (Figure 5.31 C) has

quartz and ankerite veins with the typical brecciated pyrite and later infilling base metal assemblage. Sample NS-1 from the Native Silver waste-rock pile (Figure 5.31 D) shows a large quartz -pyrite vein that has been crosscut by later ankerite veins.

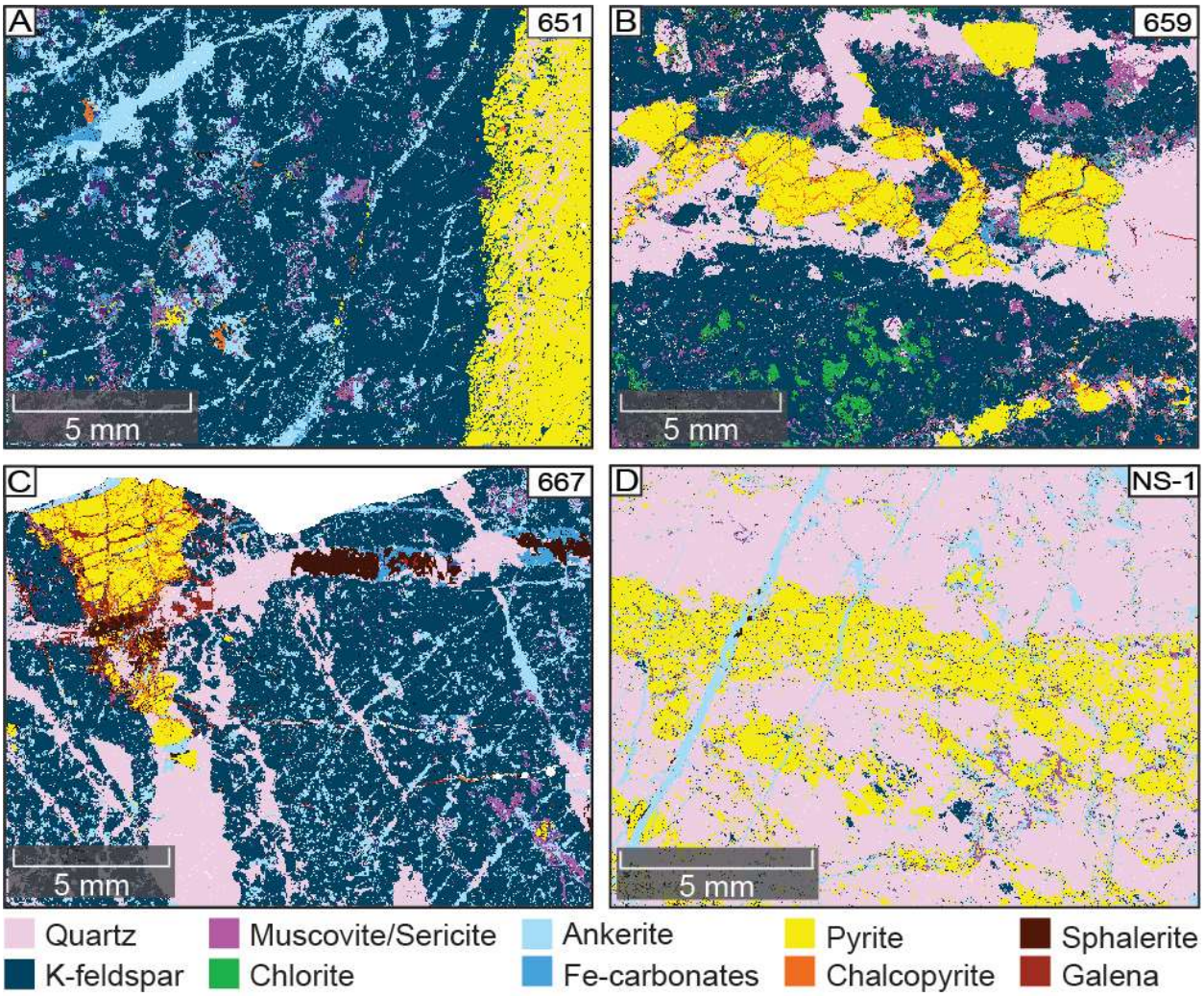

Figure 5.31 False-colored automated mineralogy images of waste rock samples: A) Large pyrite vein with some quartz, a wide K-feldspar halo, sericitization, and ankerite stringers; B) Quartz-pyrite-base metal vein where base-metal sulfides infill fractures through quartz and pyrite with K-feldspar, chlorite, and sericite alteration; C) A quartz-iron carbonate-sphalerite-galena vein crosscutting through a quartz-ankerite-pyrite-base metal vein with multiple quartz-ankerite and base-metal stringers in K-feldspar and sericite altered host rock; D) Large quartz-pyrite vein with crosscutting ankerite stringers.

5.2.9 The Caribou Deposit (Deep)

Veins at depth at the Caribou are very similar to those at the Cross. They contain both ankerite and quartz gangue mineralogy with evidence of multiple events. Base metals and silver-bearing minerals occur later than pyrite and fill in fractures through the brecciated pyrite. Alteration consists of K-feldspar, sericite, and ankerite alteration. Figure 5.32 shows automated mineralogy images of samples from core at the Caribou. Sample SN01-1013 (Figure 5.32 A) is a sample from the No Name vein and contains the typical textures of brecciated pyrite. Acanthite and stromeyerite were found weaving through the pyrite grains. Sample CR-97-104-1346.5 (Figure 5.32 B) shows typical quartz-ankerite stockwork veining with K-feldspar and sericite alteration. Sample CR-95-110-1584 (Figure 5.32 C) shows a unique texture where the main pyrite vein is crosscut and offset by a later sulfide and iron-carbonate vein. Later sphalerite, galena, and chalcopyrite crosscut through the original pyrite vein and have en-echelon splays. Just 8 feet downhole, sample CR-95-110-1592 (Figure 5.32 D) shows multiple vein assemblages with cross-cutting relationships and offsets. Sample CR-97-103-1815 (Figure 5.32 E) shows a vein dominated by ankerite with some barite, silicification, K-feldspar alteration, and sericitization. The precious metal in this sample is hessite, which was a peculiar instance of a silver-telluride. Farther down hole, sample CR-97-103-1936 (Figure 5.32 F) shows a quartz vein with sphalerite, galena, and chalcopyrite that has been displaced by minor normal faults. On the larger scale, this vein has been offset multiple times by horst and graben style faulting. The fault line itself shows a K-feldspar alteration selvage indicating fluid interaction through the faults after the formation of the base-metal vein.

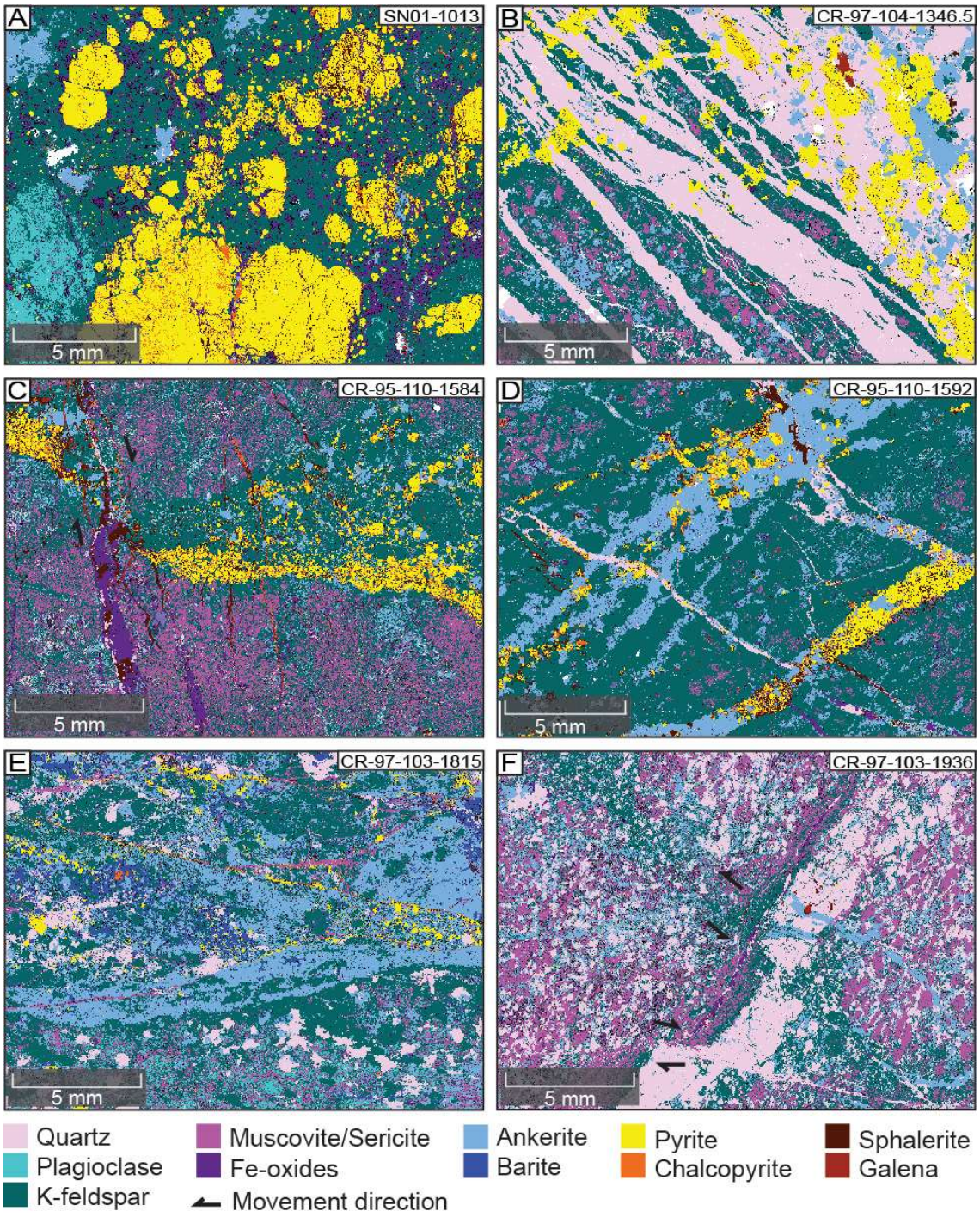

Figure 5.32 False-colored automated mineralogy images of samples from historical core deep below the workings of the Caribou: A) Brecciated pyrite with base-metal sulfide infill and K-feldspar alteration; B) Quartz stringer veins and ankerite-quartz vein with pyrite and base metals and K-feldspar, sericite, and ankerite alteration; C) Pyrite and base-metal sulfide vein being crosscut and offset by a base-metal and iron carbonate vein; D) Multiple vein assemblages with complex crosscutting relationships; E) Dominantly ankerite vein with barite, minor silicification, pyrite, and trace hessite; F) Quartz and base-metal vein offset by horst-and-graben style fractures with K-feldspar halos.

5.3 Cathodoluminescence Microscopy

Early and late-stage quartz shows the same blue CL response. There is clearly defined zoning apparent in both quartz generations. Both Q1 and Q2 quartz exhibit a long-lived dark blue CL response with core-rim zoning. Sphalerite exhibited variable orange CL response. Figure 5.33 A shows a thin subtle pink-orange halo around the Q2-sphalerite assemblage whereas Figure 5.33 B shows only blue quartz, sphalerite, and some light-yellow speckles. Figure 5.33 C and Figure 5.33 D show a wide light pink halo around the vein with blue-purple grains and yellow speckles. The green in all the images is epoxy.

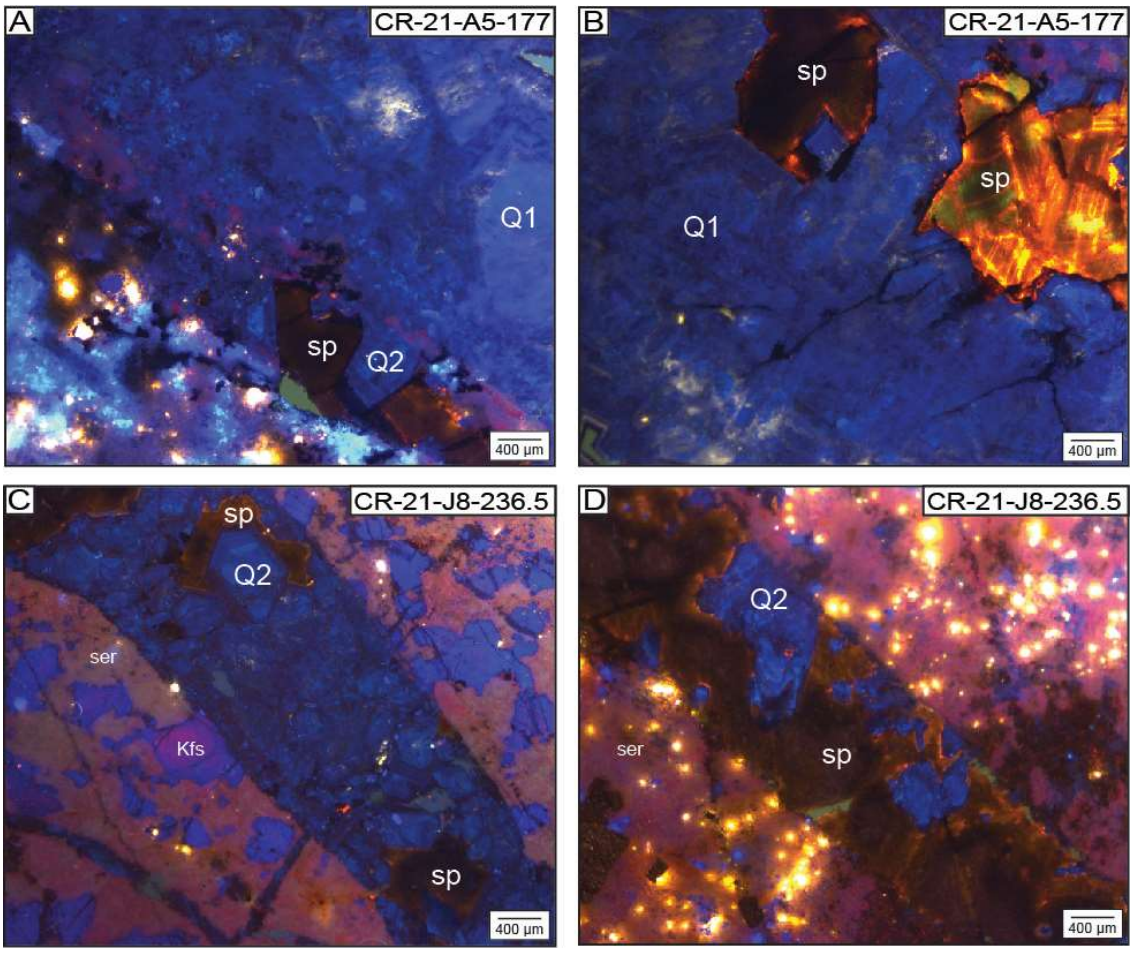

Figure 5.33 Cathodoluminescence photos with two quartz stages: A) Blue CL response of Q1 and Q2 with a weak pink selvage, bright yellow speckles, and brown-orange sphalerite CL response; B) Blue Q1 with a dark brown sphalerite vug and brighter orange-yellow sphalerite vug; C) Blue zoned Q2 growing into a sphalerite-filled bug with a broad light pink-orange alteration halo with blue-purple irregular grains in the wall rock; D) Partially replaced blue Q2 crystals growing into a sphalerite-filled vein with a broad light-pink halo with many bright yellow speckles.

K-feldspar shows a bright light blue CL response. Plagioclase exhibits a brownish CL response. Apatite shows a light orange-yellow CL response. Other speckles of deep orange are scattered throughout these samples. The ankerite does not show any CL response.

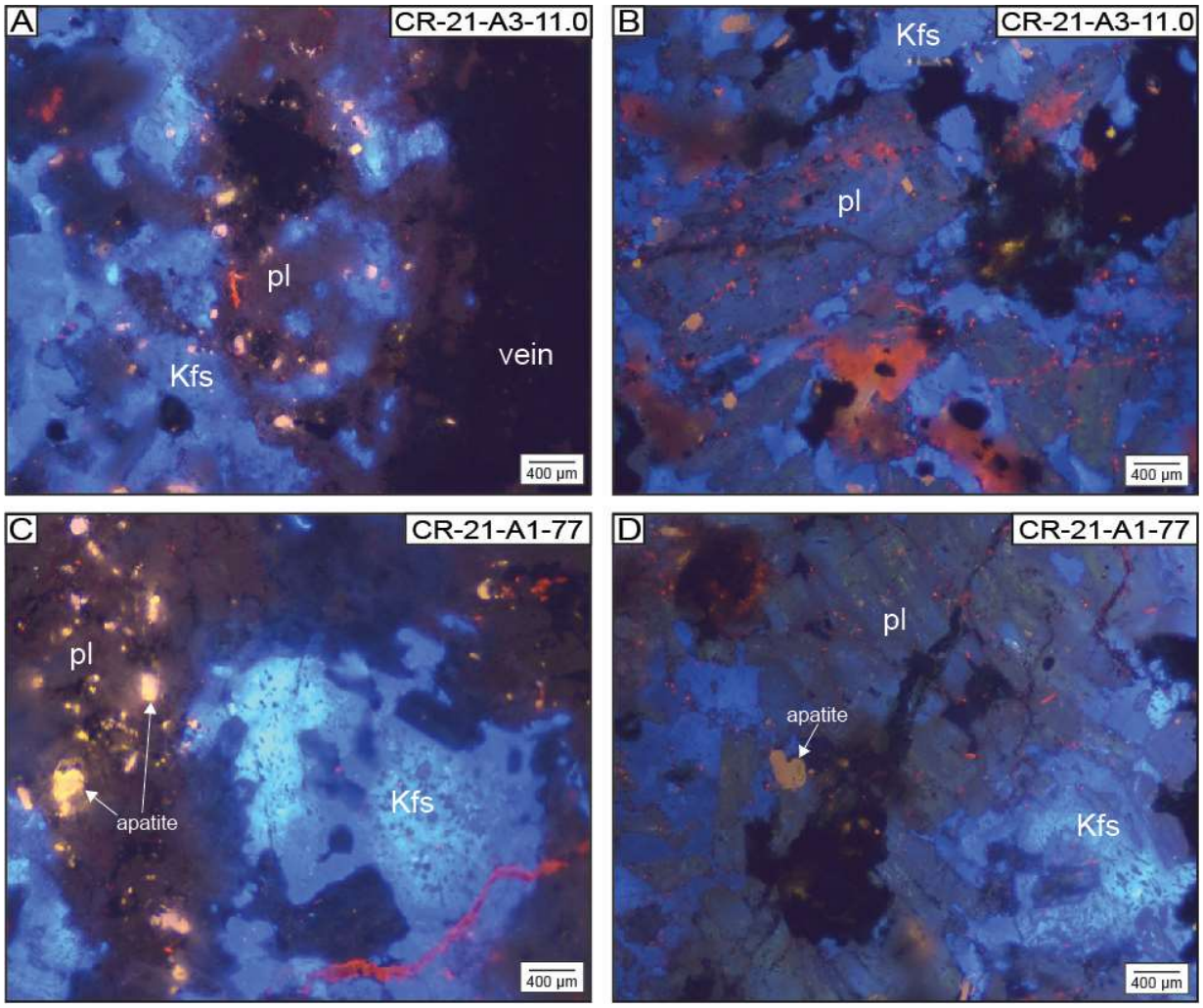

Figure 5.34 Cathodoluminescence images of K-feldspar alteration halos: A) Hydrothermal blue K-feldspar and sericitized plagioclase directly next to a vein; B) Hydrothermal deep blue K-feldspar with partically sericitized plagiocase grains in the distal vein halo; C) Hydrothermal blue K-feldspar and sericitized plagioclase in the halo next to the vein; D) Hydrothermal K-feldspar and weakly sericitized plagioclase grains distal from the vein.

5.4 Fluid Inclusion Petrography

Fluid inclusion petrography identified two quartz generations. The first quartz generation (Q1) is defined by intergrown subhedral grains. These quartz grains contain fluid inclusions with a double meniscus indicating the presence of high CO_2 concentrations. These inclusions are

irregularly shaped and exibit inconsistent liquid to vapor ratios, indicating that they had undergone post entrapment modifications. The second quartz stage (Q2) exhibits euhedral, clear, zoned crystals growing into open space with rare primary fluid inclusions that have not been affected by post-entrapment modification. These fluid inclusions do not show double bubbles. This quartz stage often had sphalerite inclusions within crystal growth zones associated with fluid inclusions. From petrographic analysis of the fluid inclusions, the fluid inclusion assemblages measured are primary fluid inclusions within Q2 and are associated with base-metal ore forming fluid.

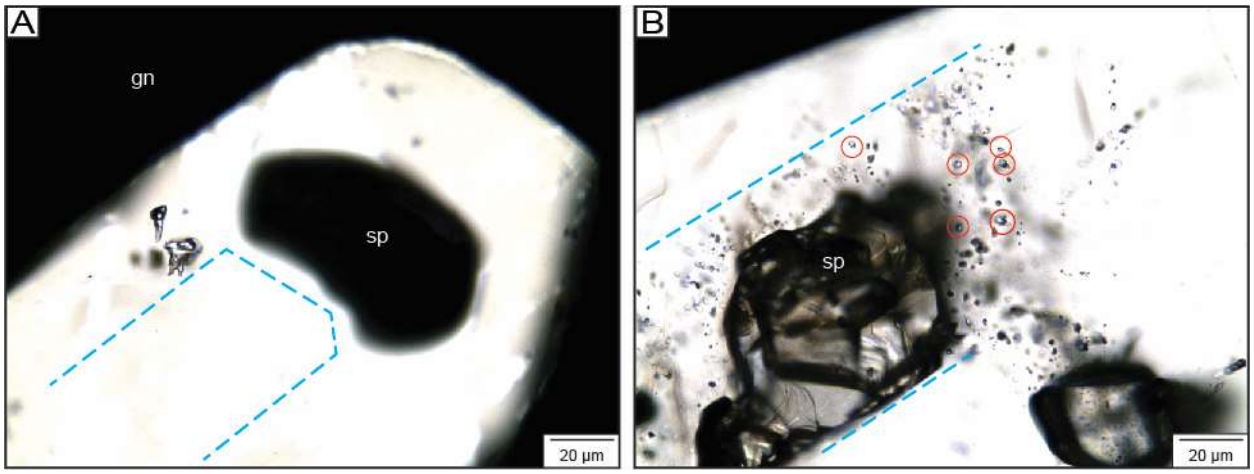

Figure 5.35 CR-21-A3-10.5 fluid inclusion assemblages: A) Euhedral Q2 grain with a sphalerite and two fluid inclusions along a growth zone (blue dashed line); B) Euhedral Q2 grain with sphalerite and many fluid inclusions along the same primary growth zone (blue dashed line) and the fluid inclusions large enough to be measured are circled in red.

One Q2 quartz FIA included two fluid inclusions that were large enough for microthermometry (Figure 5.35 A). The homogenization temperature recorded was 249.6°C, which is the minimum temperature of formation. Upon freezing, one fluid inclusion had a last ice melting at a range from -5°C to -5.5°C and the other fluid inclusion ranged from -5.5°C to -6°C. There was no evidence of clathrate formation upon freezing.

The second Q2 grain contained many primary fluid inclusions, but five were large enough for microthermometry (Figure 5.35 B). The homogenization temperatures recorded were 210°C to 215°C on one inclusion and 220°C to 225°C on four inclusions. The temperature of last ice melting for this FIA was -10°C to -9°C observed on three inclusions. No evidence for clathrate formation was found.

The slightly irregular shape of the fluid inclusions indicates formation temperatures likely exceed the measured temperatures and require a pressure correction. A 30°C pressure correction was made. Based on the second FIA, the temperature of entrapment is estimated to be 240°C-250°C.

Salt crystals were not present, so cycling was used to determine the temperature of ice melting. Because it was not possible to determine a eutectic temperature, which would provide the salt species present, it is assumed that the fluid inclusion form part of the H_2O-NaCl system. Based on this assumption and the temperature of ice melting, the salinity of the fluid ranged from 7.9 to 13.9 wt. % NaCl equivalent based on the two fluid inclusion assemblages measured.

CHAPTER 6: DISCUSSION

Through a detailed characterization of alteration and vein mineral assemblages, this study aims to improve our understanding of the ore mineralogy and zonation, characterize host rocks, related alteration assemblages, and develop a conceptual model for the Caribou-Cross deposit. To achieve this goal, homogenous igneous textures from the Caribou monzonite were investigated as well as vein assemblages and alteration assemblages across the Grand Island district.

6.1 Igneous Characterization and Evolution

The Caribou monzonite stock, dated at approximately 62.6 Ma (Marvin et al. 1974), is a composite intrusive in the Grand Island district and is a primary host rock. This study identified five sub-lithology groups occurring within the Caribou monzonite: magnetite dunite, monzonite and quartz monzonite, amphibolite, magnetite amphibolite, and lamprophyre (Figure 5.1). The following section discusses the interpretation and implications of these sub-lithology groups. Although the magnetite dunite and genesis of the Caribou stock is not the primary focus of this study, it provides insight on the intrusion itself and may help deduct base- and precious- metal ore forming processes. It is also important to note that different host rocks react differently with hydrothermal fluids and produce different alteration and mineralogical signatures.

Assay data from the 2021 drill program were plotted on an AFM diagram in ioGas with different logged lithologies plotted in different colors (Figure 6.1). The igneous suite follows the alkaline trend with the mafic compositions (gabbro, diorite, diabase) plotting at more primitive compositions and the monzonite showing a more evolved geochemical signature. At the time of core logging, host rock nomenclature was solely based on optical inspection leading to some overlap in depicted host rock lithologies in Figure 6.1.

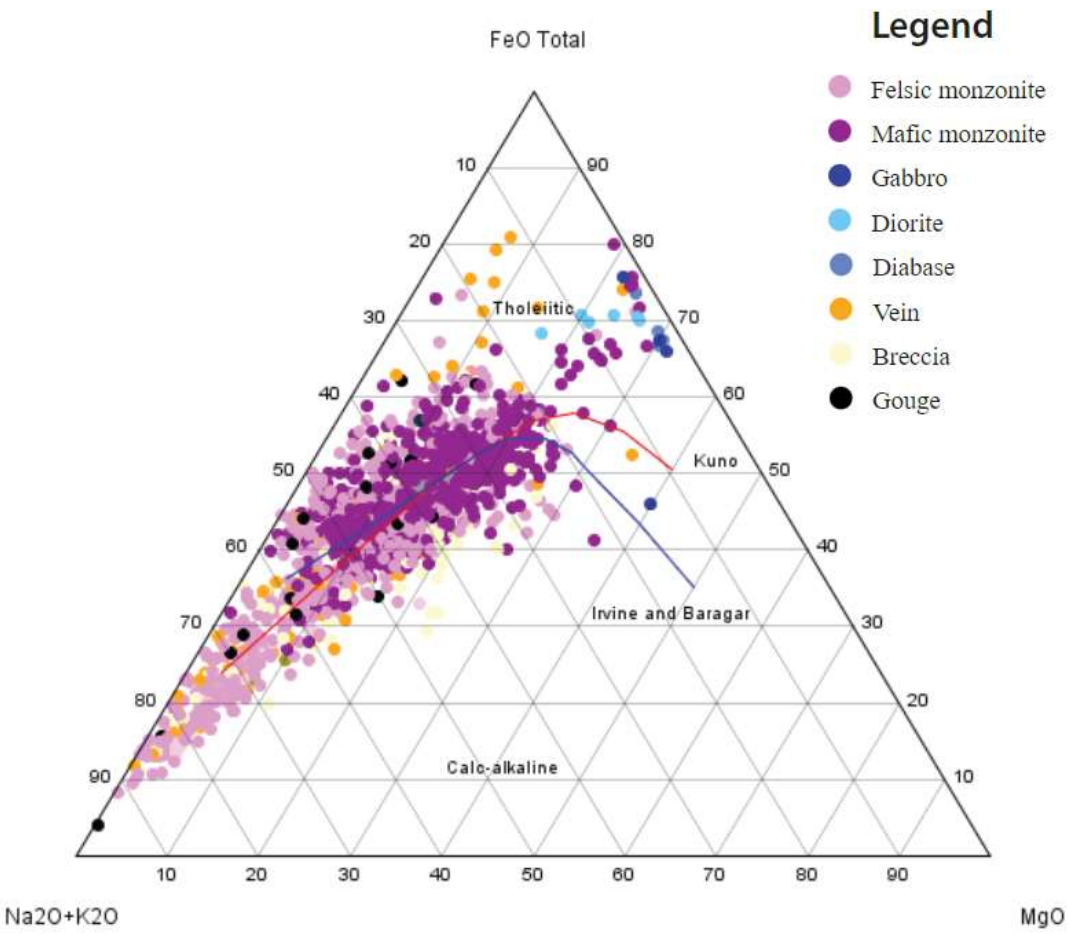

Figure 6.1 AFM diagram plotted in ioGas of all assay data, excluding assays logged as gneiss, in weight percent. Trend lines on the diagram are after Irvine and Barager (1971) in blue and Kuno (1968) in red. Felsic monzonite (leucocratic) and mafic monzonite (melanocratic) are based on core logging during 2021.

The magnetite dunite (group 1, Figure 5.2 A and B) was investigated in the past as an iron ore resource, recently as a potential REE resource and as a host rock to hydrothermal veins. Unravelling the history and significance of the "iron dike" contributes to the evolution of the geologic history at Caribou hill. The cumulate texture of phaneritic olivine phenocrysts suggests that olivine crystallized first, followed by hematite phenocrysts. The edges of samples collected in exposed trenches on the surface of Caribou hill show alteration or weathering to possibly amphibole and serpentine. The general shape of the body is not dike-like, and more of an irregular mass within the monzonite.

Monzonite and quartz monzonite (group 2, Figure 5.3) is somewhat consistent across the district. Grain size is typically phaneritic indicating it crystallized deep in the crust; however, grain size does change throughout the stock, including some portions with porphyritic texture.

Course-grained black hornblende and green silicates form in aggregates, which indicates some heterogeneity and mineral clustering indicates slow cooling rate. Plagioclase generally has a tabular euhedral shape, indicating that it formed first within the monzonite; however, plagioclase composition varies from end member anorthite (Ca) to andesine (Ca-Na). Changes in igneous textures indicate a complex history with varying cooling and ascent rates causing variable grain sizes.

Amphibolite (group 3, Figure 5.2 C and D) and magnetite amphibolite (group 4, Figure 5.2 E and F) are distinct rock types in the district, and the amphibole was confidently discerned from pyroxene in hand sample. Group 4 magnetite amphibolite had larger lenses of magnetite, indicating some separation of the magnetite and likely the magnetite crystallized later than the silicates present in this sample (amphibole). Gable (1969) recorded pyroxenite rock type, which was not identified in the field or in any core. It is unknown how a potential pyroxenite occurs in the district and how it may interact with other rock types such as amphibolite. It is also worth noting that sometimes amphibolite rock name is interpreted as being a metamorphic rock, but in this case, it is purely based on mineralogy. Due to varying amounts of plagioclase, this could possibly be classified as anorthosite.

Group 5 (Figure 5.2 G and H) was given the name lamprophyre due to the presence of course-grained biotite with amphibole. Lamprophyre is a heterogeneous term that is still somewhat debated and poorly understood but typically has these common characteristics: occurs late in igneous activity, explosive emplacement is common, occurs as dikes, plugs, sills, vents, and lava flows, commonly porphyritic showing panidiomorphic texture consisting of hydrous mineralogy (biotite and/or amphibole) and lacking felsic phenocrysts, and are chemically intermediate to ultrabasic with high alkali contents (Rock, 1977). There are many subtypes of lamprophyre and often imply genetic connotations (Rock, 1977), but for the purposes of this report, simply the mineralogy and textures were observed from core since it does not outcrop.

Addressing the system based on the assumption that the igneous bodies are genetically related and assuming an alkaline/tholeiitic evolutionary path as indicated in Figure 6.1, the oxidizing character of the primitive melt caused magnetite dunite (group 1) to crystallize. Crystallization and removal of olivine and magnetite decreases iron and magnesium in the remaining melt, creating an increase in relative silica concentration. Following Bowens reaction series, hornblende and biotite then crystallized from the melt, inhibiting further iron enrichment,

and creating an increase in silica concentration in the remaining melt, leading to the crystallization of amphibolite (group 3) with hornblende-amphibole, plagioclase, and minor magnetite and titanium minerals. Subsequently, significant biotite crystallized, forming the lamprophyre (group 5) which further evolved the magma to the conditions forming the main rock unit in the sequence, the monzonite (group 2), consisting of K-feldspar and plagioclase. As the melt continued to increase in silica saturation, it evolved to quartz monzonite. The system was generally silica poor throughout the process, and never reached silica concentrations to evolve into a granitic composition. The system evolved from a gabbro/diorite to monzonite and quartz monzonite as the melt became gradually more enriched in silica (Figure 6.2).

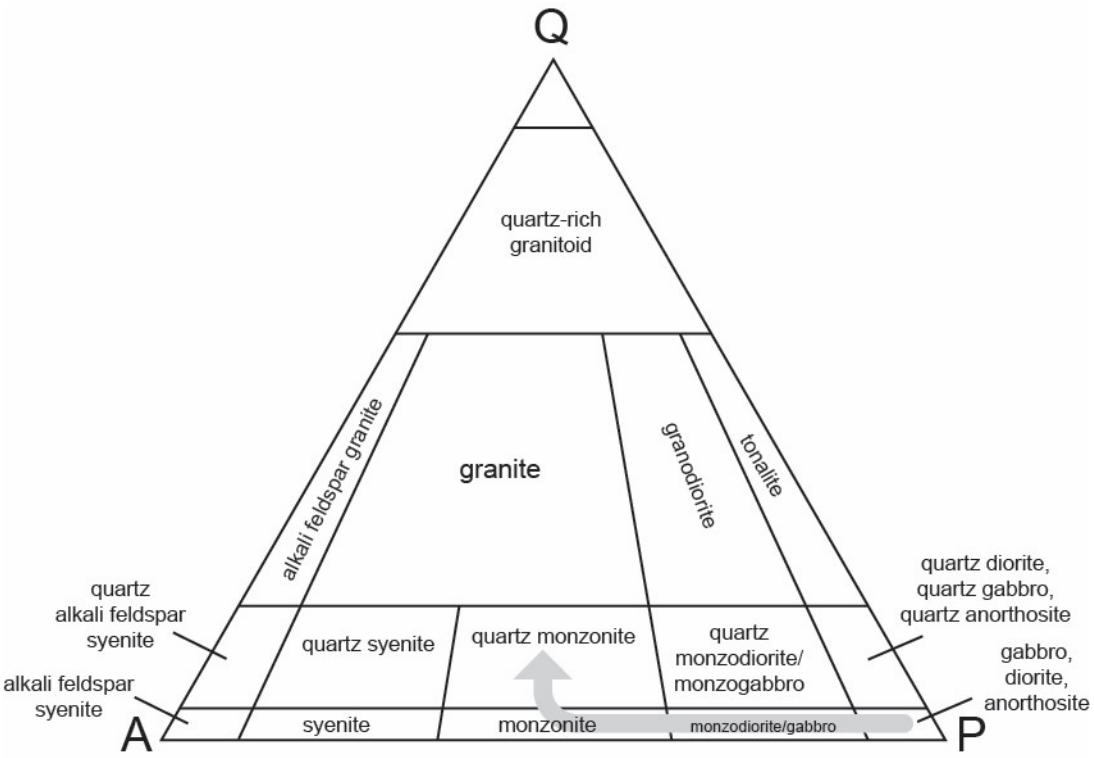

Figure 6.2 QAP diagram with the alkaline crystallization path indicated by the grey arrow, as seen in the Caribou-Cross area.

The density differences, thermal gradients, rate of cooling, and magma ascent affect the evolution of any magma body. Although this is rather speculative, these factors are proposed to be the reason the magnetite dunite does not form the morphology of a proper dike or a layered mafic intrusion. It was dense enough to separate out from the parent magma, but other factors outlined above are the reason this body has an irregular shape.

The story of the evolution of the Caribou stock and how the mafic bodies originated was theorized by many geologists. Smith (1938) rejected the former conclusions of magmatic differentiation (Bastin and Hill, 1917) or assimilation of the surrounding Precambrian rocks (Reynolds, 1935; Lovering and Goddard, 1938), and instead found evidence that the composite stock formed from separate intrusions of magmas followed by metasomatic alteration of the primary intrusions. Lovering and Goddard (1950) refined their theory and conclude that the mafic rocks are present due to reaction between the monzonite magma and calcareous beds in the Idaho Springs gneiss.

The interpretation from this study supports the work by Bastin and Hill (1917), suggesting magmatic differentiation, and rejects the theories by Smith (1938) as well as Lovering and Goddard (1950). From core logging observations, there are occasionally small xenoliths (no more than a few centimeters in diameter) that are in nearly all rock types. It may be likely that these represent small xenoliths from the surrounding country rock incorporated during ascent and emplacement.

6.2 Waste Rock Samples

While abundant in-situ sample material was collected to characterize host rocks, alteration, and vein assemblages of the Cross deposit, the Caribou deposit was not accessible for in-situ sampling at the time of this study. To overcome this lack of available sample material, historic waste rock pile samples from the Caribou deposit were sampled to get insights into the mineralogy of the Caribou deposit and to correlate findings from those of the Cross deposit. The following section will introduce a paragenetic sequence of hypogene and supergene minerals for samples from the Caribou deposit and try to reconstruct their original sample location to help improve our understanding of ore forming processes responsible for the mineralization of the Caribou-Cross system.

The waste-rock pile samples showed very similar mineralogy, textures, and paragenesis as samples from the rest of the study. The gangue mineral assemblage of quartz and ankerite is consistent with the Cross, as well as the sulfide assemblage consisting of pyrite, galena, sphalerite, chalcopyrite, and precious metal phases. The main differences identified are that the waste-rock samples do not contain any Ag-bearing gold, but they do exhibit malachite, azurite, enargite, famatinite, bismoclite, alisonite, and chalcocite-galena symplectite texture. Silver-

bearing minerals are often associated with barite. Silver-bearing minerals are also associated with copper minerals such as chalcocite and stromeyerite, suggesting that secondary processes have affected the deposit to some extent.

The symplectite texture with galena, stromeyerite, and chalcocite shown in Figure 5.29 and Figure 5.30 was also only found in samples from the waste-rock piles. Galena associated with stromeyerite was found at depths in the Cross deposit, but nothing similar to the chalcocite-stromeyerite-galena intergrowth texture. These intergrowth textures can form from either exsolution reactions or from replacement (Winter, 2014). The rim of these grains contains Pb-Cu-oxides and remnant chalcopyrite. Kouzmanov (2004) investigated this texture present at the Radka copper-gold epithermal deposit in Bulgaria and proposed that galena-chalcocite intergrowth texture formed by betekhtinite ($Pb_2(Cu, Fe)_{22-24}S_{15}$) breakdown into two separate phases during increasing temperature of late-stage ore formation. Betekhtinite formed from metasomatic replacement of bornite in the Radka deposit (Kouzmanov, 2004). Brodin (1960) interpreted the same textures of these minerals present at the Ken-Shanik (Russia) and Vrancic (Check Republic) deposits to be formed diffusion replacement of chalcocite by galena. Often the galena had small amounts of As or Cu. Many undifferentiated Ag-Cu-Pb-sulfides were present as different rims around galena, stromeyerite, chalcopyrite, and chalcocite. The symplectite has Cu-oxide and Pb-Cu-oxide rims around the entire grain, which further suggests that the chalcocite may be supergene. In sample SWP, the symplectite texture was terminated at what seems to previously have been a mineral grain boundary, indicating replacement.

The Grand Island district is located in a high alpine environment where physical weathering rather than chemical weathering prevails. Rocks on waste-rock piles and along major fractures in the rock are oxidized, but while chemical weathering is not pronounced as evidenced by the general lack of soil. Typically, in a supergene environment, oxidation occurs above the water table and secondary enrichment accumulates below the water table. During this process, sulfides become sulfates and oxides/hydroxides above the water table and secondary sulfides are formed through replacement of other sulfides. The pyrite breaks down, leaves iron oxide, and produces an acidic solution which can carry and redeposit metals (Wang et al., 2022). When the solution crosses below the water table, the solution is buffered, and metals are precipitated (Wang et al., 2022). Supergene gold typically means fine-grained nano gold inclusions or gold in sulfide crystal structure becomes liberated during surface oxidation (Wang et al., 2022). Gold is

immobile in surface waters, so the supergene process creates micro free gold in oxides. Determining the effect of supergene enrichment and oxidation processes would involve a more in-depth study, however, this is discussed as it relates to my observations below.

Nearly all samples in the district, particularly the waste-rock pile samples, exhibit oxidation often with accompanying silver and copper minerals, even in what is seemingly unoxidized core. There is a mix of hypogene and supergene textures, even at depths. Post mineralization faulting allows for groundwater fluid flow to significant depths. Often silver minerals such as Ag-sulfosalts, acanthite, and native Ag occur associated with either barite or in oxidized fractures with Cu-, Pb-, and Fe-oxides. Often acanthite and stromeyerite form rims around pyrite and sulfides are rimmed by various oxides. Although this is not a typical supergene profile where there's a typical oxidized zone above the water table and an enrichment zone just below or at the water table, it is believed that groundwaters have created a fracture-controlled supergene and oxidized environment to some extent. In the alpine environment, it is generally dry, but groundwater is pouring out of the mine constantly, and in the spring, groundwater that percolated down from snowmelt floods the mine. This is not a typical supergene blanket, but rather primary sulfide veins where intersected by post-mineralization faults show considerable oxidation and minor secondary sulfides.

Microscopy and SEM analysis has provided insight as to what minerals are present, mineralogical associations, and textural relationships. There is native silver, acanthite, stromeyerite and other silver-bearing sulfosalts in the waste rock pile samples, as well as pyrite, galena, sphalerite, and chalcopyrite. Supergene enrichment has somewhat enhanced the silver grades of these samples, but this cannot be an indication of depth. Base metals and precious metals do not always associate with pyrite but are often associated with chalcopyrite and barite. There were many samples that contained abundant pyrite but did not contain base or precious metals. Alteration was consistent across the samples, being primarily K-feldspar and sericite, so alteration differences were not observed in relation to mineralization.

It was the aim of this study to reconstruct the origin of the waste rock sample; however, due to their secondary overprint at surface and due to the fact that waste rock piles have been reworked and changed in the last 100 years, it was not possible to deduce the original sampling location in the underground workings. Because the exact locations with regards to depth cannot be determined from the waste-rock pile grab samples, it is difficult to determine any type of

primary zoning pattern between these samples, other than a general comparison of them to samples from the Cross. A few notable anomalies are described here. Based on automated mineralogy data, sample 667 contained the highest mineral modal abundance of galena and sphalerite, whereas sample 659 had anomalous amounts of chalcopyrite and bornite. Both samples had minor precious metal contents, which were associated with their respective primary sulfides. Based on assay data, sample SWP had the highest silver grade, followed by sample 651. The data from automated mineralogy and assay data is not representative of the waste-rock pile as a whole since they are grab samples that were selected specifically on the basis of having visible sulfides but do provide a glimpse into the mineralogy.

6.3 Ore Forming System and Paragenesis

This study aimed to identify the ore mineralogy and zonation with related alteration assemblages to interpret the ore-forming fluid characteristics and processes. The paragenetic sequence (Figure 6.3) was developed based on the findings presented in Chapter 5 and will aid in the interpretation of the system and how different parts of the system are related.

K-feldspar alteration occurs almost everywhere and is associated with all vein types. An initial K-feldspar alteration does not seem to be related to vein formation but predates ore and gangue mineral deposition as fluids percolated through fractures as evidenced by nonsymmetrical K-feldspar alteration in homogenous host rock and occurrences of K-feldspar alteration halos around hairline fractures without any vein minerals, as described in section 5.2.1. K-feldspar alteration persists through the formation of Q1 and pyrite deposition.

Figure 6.3 Paragenetic diagram demonstrating the evolution of the fluid through time. Early K-feldspar fracture-controlled pre-ore stage alteration was followed by Q1 and pyrite deposition in veins next to a K-feldspar, sericite, and chlorite alteration halo. Ankerite was deposited in veins after Q1 and pyrite. The system reached hydrostatic conditions at least once but cycled back to lithostatic conditions, repeating the above sequence. Once the system reached final hydrostatic conditions, Q2 and base metals were deposited, followed by precious metals and a late ankerite generation. Secondary minerals showing replacement textures occur with oxides and barite. Faulting and fracturing occurred post-vein formation and resulted in K-feldspar altered fractures that offset mineralized veins. Ranges of formation temperatures were determined, and illustrations show alteration and mineralization stages with relation to the hydrothermal fluids

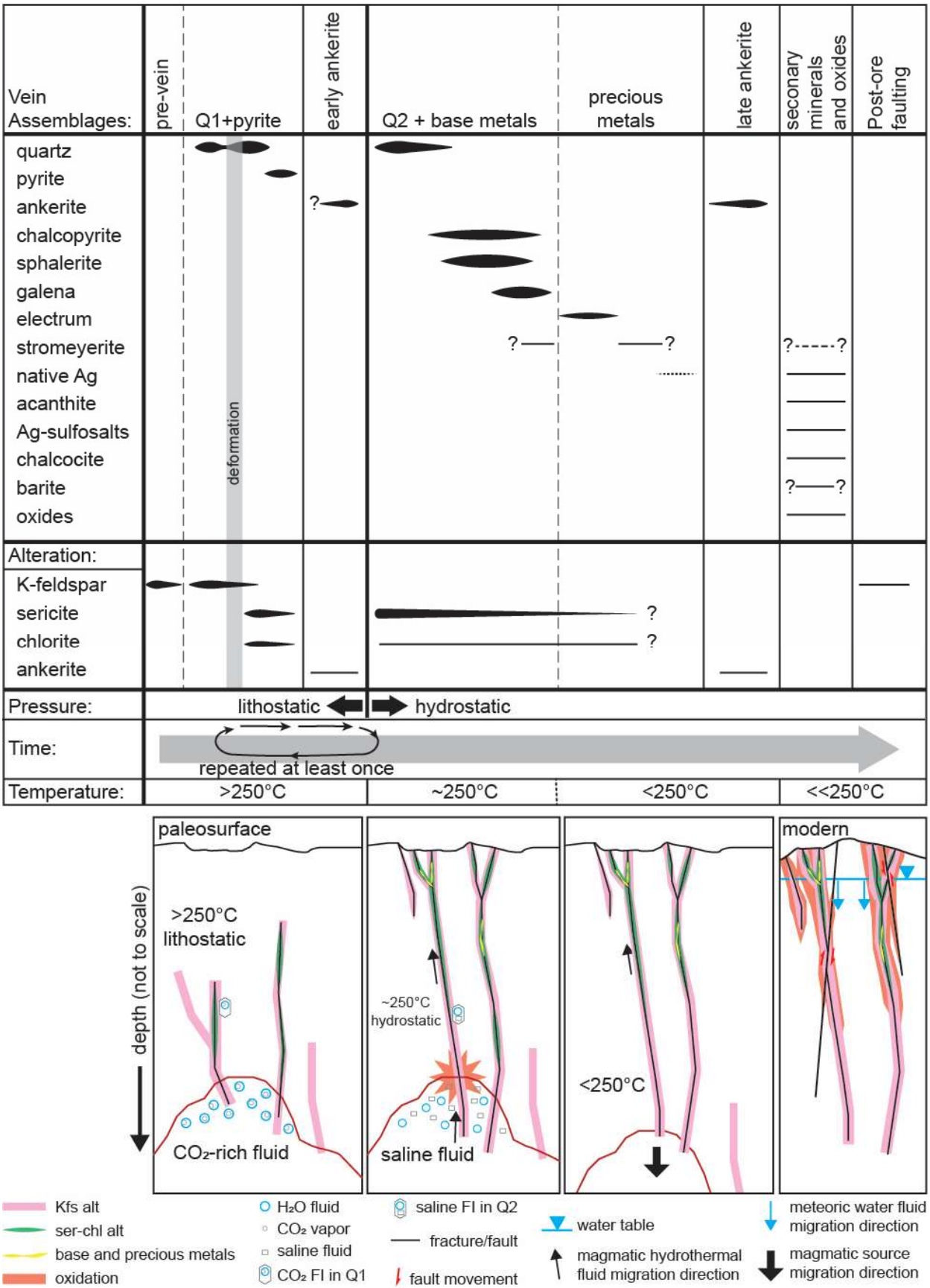
Vein Assemblages:
pre-vein
Q1+pyrite
early ankerite
Q2 + base metals
precious metals
late ankerite
seconary minerals and oxides
Post-ore faulting
quartz
pyrite
ankerite
chalcopyrite
sphalerite
galena
electrum
stromeyerite
native Ag
acanthite
Ag-sulfosalts
chalcocite
barite
oxides
deformation
Alteration:
K-feldspar
sericite
chlorite
ankerite
Pressure:
lithostatic
hydrostatic
Time:
repeated at least once
Temperature:
>250°C
~250°C
<250°C
<<250°C
paleosurface
modern
depth (not to scale)
>250°C
lithostatic
~250°C
hydrostatic
<250°C
CO₂-rich fluid
saline fluid
Kfs alt
ser-chl alt
base and precious metals
oxidation
H₂O fluid
CO₂ vapor
saline fluid
CO₂ FI in Q1
saline FI in Q2
fracture/fault
fault movement
water table
magmatic hydrothermal fluid migration direction
meteoric water fluid migration direction
magmatic source migration direction

Following this pre-ore stage, quartz (Q1) and pyrite were deposited as the first vein generation with a K-feldspar, sericite, and chlorite alteration halo. This quartz generation Q1 is represented by two textural styles (Figure 5.9): (I) strongly deformed fine- to medium-grained quartz that exhibited undulose extinction, subgrains, grain boundary migration, and lacks fluid inclusions indicating that it underwent high-temperature deformation including static recrystallization along vein margins and (II) subhedral to euhedral, unstrained, coarse-grained quartz central in the vein with tight interlocking grains with distinct growth zones containing fluid inclusions that underwent post-entrapment modification.

The two textural styles of Q1 quartz described in this study show similarities to the two distinct quartz stages distinguished by Holland (1994): a fine-grained quartz on vein margins (Holland, 1994) which appears to be similar to the first textural style of Q1 quartz, and coarse-grained quartz filling in the central portions of the vein (Holland, 1994), which appears to be similar to that of the second textural style of Q1 quartz. While the fine- to medium-grained strongly deformed Q1 quartz and unstrained coarse-grained Q1 quartz may have formed as distinct quartz generations as indicated by Holland (1994), petrographic evidence here suggests that these two quartz textures likely formed during the same fluid event (same bright blue CL response; Figure 5.33) but show varying degrees of strain resulting in strain partitioning and localized recrystallization and undulose extinction. The subhedral coarse-grained Q1 quartz grains do exhibit some minor deformation such as undulose extinction, implying that veins underwent strain partitioning where deformation was localized impacting portions of the veins more than other parts of the veins.

Quartz (Q1) in early veins show abundant implosion/explosion FI textures formed through rapid changes of cycling in overburdening pressure (section 5.4, page 71). Fluid inclusions in coarse grained Q1 quartz are CO_2 rich, suggesting a deep-seated fluid source and show post-entrapment modification, and large-scale breccias and stockwork veins at the Caribou-Cross deposit are in accordance with a major cyclical shift in pressure.

The associated K-feldspar alteration halo associated with the Q1 and pyrite vein stage, was investigated in detail. Cathodoluminescence on this K-feldspar alteration halo proximal to the veins on samples CR-21-A1-77 and CR-21-A3-11.0 (Figure 5.34) appeared bright blue. The secondary fluid inclusions in K-feldspar in the alteration halo proximal to the vein often exhibit irregular shapes indicating post-entrapment modification and some deformation with inconsistent

liquid to vapor ratios supporting the conclusion that the K-feldspar is secondary hydrothermal and likely high temperature (Jim Reynolds, pers. commun., 2022).

Following early quartz (Q1) and pyrite vein formation, fractures were reopened and ankerite was precipitated along weakness zones tracing pre-existing mineralized structures (i.e. quartz veins). Ankerite in veins exhibits various textures from euhedral crystals to crystals that are irregularly shaped and vary in size concurrently with limited ankerite alteration. Ankerite commonly replaces fine-grained recrystallized Q1 quartz and forms rhombohedrons (Figure 5.15) or is deposited along Q1 quartz filled fractures and veins forming distinct bands within Q1 quartz veins (Figure 5.15, Figure 5.18 F, Figure 5.21 C, Figure 5.25 B, C, D, and G). Although there is no explicit evidence of Q2 quartz occurring after a first ankerite stage, the banded veins suggest repetition of Q1 quartz and ankerite formation prior to formation of Q2 quartz.

After ankerite was deposited, there was a major shift from a lithostatic to hydrostatic pressure regime and back again as evidenced by multiple generations of Q1 quartz-ankerite bands. When the system reached final hydrostatic conditions, Q2 quartz and base metal sulfides were deposited in reopened veins along with sericite and chlorite alteration halos. This vein assemblage formed from a saline fluid in hydrostatic conditions as indicated by primary fluid inclusions in Q2 quartz that did not show evidence for post-entrapment modification (Figure 5.35). Q2 quartz formed contemporaneously with base metal sulfides as evidenced by inclusions of sphalerite along growth zones (Figure 5.35), indicating that the ore came with a saline fluid rather than the earlier H_2O-CO_2 fluid, although the salinity of the earlier H_2O-CO_2 fluid is unknown.

The base metals, coeval with and persisting after Q2 quartz formation, consist of chalcopyrite, sphalerite, galena, and stromeyerite that grew successively, all of which replace pyrite and fill in vugs of euhedral Q2 quartz (Figure 5.12). Chalcopyrite was the first base metal to form and continued to crystallize during and after sphalerite formation as evidenced by early chalcopyrite infilling open space and is crosscut and replaced by sphalerite followed by later chalcopyrite replacing sphalerite (Figure 5.12). Galena formed after sphalerite as evidenced by subhedral sphalerite grains that are infilled by later galena and galena replacing sphalerite in some instances mostly along grain boundaries but occasionally as inclusions throughout sphalerite (Figure 5.12). Stromeyerite exhibits multiple textures and occurs during this stage

contemporaneously with galena based on stromeyerite replacing sphalerite and chalcopyrite but shows equilibrium textures with galena (Figure 5.13).

After the deposition of Q2 quartz followed by base-metal sulfides, precious metals including Ag-bearing gold, stromeyerite, and native silver were formed. Silver-bearing gold occurs primarily at base-metal sulfide grain boundaries commonly replacing pyrite. In one instance, Ag-bearing gold occurs on a Q2 quartz grain boundary growing into galena (Figure 5.10). Evidence of Ag-bearing gold surrounding, and possibly replacing pyrite, sphalerite, and galena was found, but no evidence was found of Ag-bearing gold replacing chalcopyrite and rarely contacting chalcopyrite, which opposes Holland's (1994) suggestion that Ag-bearing gold formed with the second period of chalcopyrite formation. Silver-bearing gold Au:Ag ratios vary even across individual grains, which was also described by Holland (1994). The origin of varying Au:Ag ratios is unclear but was suggested to be due to weak oxidation and secondary processes affecting the ratios.

During the precious metal stage, stromeyerite typically encompasses vugs of sulfides, which indicates a replacement texture (Figure 5.13, Figure 5.26 A and B, Figure 5.22). In most instances it appears that stromeyerite replaced copper minerals and was in turn replaced by native Ag (Figure 5.30 A). Native silver occurs as veinlets crosscutting stromeyerite-filled vugs indicating that native silver formed after stromeyerite (Figure 5.30 B, Figure 5.26 C).

Following the deposition of precious metals, the hydrothermal fluids likely cooled and evolved to more basic pH forming late ankerite in veins and thin barren stringers (Figure 5.17, Figure 5.18 A and E, Figure 5.25 E and F, Figure 5.31 A and D).

After the magmatic-hydrothermal fluids ceased, the secondary minerals and oxides stage formed, consisting of stromeyerite, native Ag, acanthite, Ag-sulfosalts, chalcocite, barite, and various oxides formed in a supergene environment. Stromeyerite-filled vugs are often enveloped by thin Fe- or Cu- oxide minerals, which indicates formation of these minerals synchronous with the secondary minerals and oxides (Figure 5.13 B). Acanthite and other undifferentiated silver-sulfosalts most commonly occur in fractures alongside various oxide minerals and never in primary vein assemblages (Figure 5.16) indicating that these likely formed from oxidation and groundwater involvement, as described in section 6.2.

A final episode involves post-vein faulting and fracturing with the involvement of fluids. These post-ore fractures offset veins and have K-feldspar alteration halos (Figure 5.32 F).

The Caribou-Cross ore system and associated veins are fracture controlled. Hydrofracturing from built up pressures under lithostatic conditions created the breccia veins and stockwork vein textures upon transition to hydrostatic conditions. As the fluids travel through the rock, they become subject to changing geochemical parameters that cause precipitation and deposition of minerals in the paragenetic sequence described above.

6.4 District Zonation

Based on evidence found in this study, the Caribou-Cross deposit do not show any significant district-scale metal or alteration zonation, except for gold occurring at the Cross and no gold occurring at the Caribou. The deposit shows a strong structural control on mineralization, as indicated by veins showing complex relationships of the same conduits being reopened repeatedly. Alteration halos are not wide or pervasive enough to be macroscopically tracked, and there is significant K-feldspar in the host rock itself, so the geochemical (K) and mineralogical alteration zones displayed by K-feldspar and sericite may not be recognizable from large-scale exploration methods. Individual veins show small-scale (centimeter to meter) alteration zoning, but this does not persist more than 10 meters into the host rock. Metal occurrence does not appear to show any trends based on 3-D spatial observations of assay data in LeapFrog (Dave Young, pers. commun., 2021); however, identification of minerals in samples from this study may provide some insight into metal zonation.

From phase diagrams, Cu and Au are thermally hotter in the system than elements such as Ag, Pb, and Zn, so using mineralogy and metal endowment is feasible from this study to identify any potential ore zonation. Although the Caribou was not thoroughly sampled due to accessibility limitations, Ag-bearing gold was not identified in any of the Caribou samples from this study, but chalcopyrite and silver-bearing minerals are present at depth. At the Cross, the stockwork zone contains more chalcopyrite, however, only one Ag-bearing gold grain was identified. The veins exterior to the stockwork zone, which have a more definitive vein margins, have more occurrences of Ag-bearing gold grains. This could be possible to chemical parameters such as wall-rock buffering or mixing with meteoric waters or changes in pressure as the fluid moves through more channelized zones. Stromeyerite (CuAgS) occurred abundantly in the Apache-Potosi, the stockwork zone, Crown Point, and Caribou samples, but no silver-bearing minerals including native Ag or silver-sulfosalts were identified in the Hopewell. Based on Cu

endowment in the form of chalcopyrite, the stockwork zone at the Cross and the general Caribou deposit are the hotter central parts of the system, which supports to Jobodwana's (1991) conclusion that the Caribou is at the thermal center of the system and the Apache-Potosi zone at the Cross is more distal, according to his fluid inclusion microthermometry.

6.5 Deposit Model and Classification

The Caribou-Cross deposit has been historically classified as both epithermal and mesothermal, but this is outdated in modern context. This study shows early Q1 quartz contains fluid inclusions with double-bubbles (high CO_2 content), indicating that Q1 represents a deep-seated formation under high pressure. The ore-forming fluid, concomitant with quartz Q2 precipitation, was a saline fluid with homogenization temperatures (minimum temperature of entrapment) of 210 to 225°C. The temperature data from Q2 quartz along with Fe-poor sphalerite indicate a magmatic source and intermediate sulfidation state (Figure 6.4). This study indicates that the Caribou-Cross deposit is an intermediate sulfidation magmatic-hydrothermal system formed deep below the paleosurface with a deep-seated magmatic source.

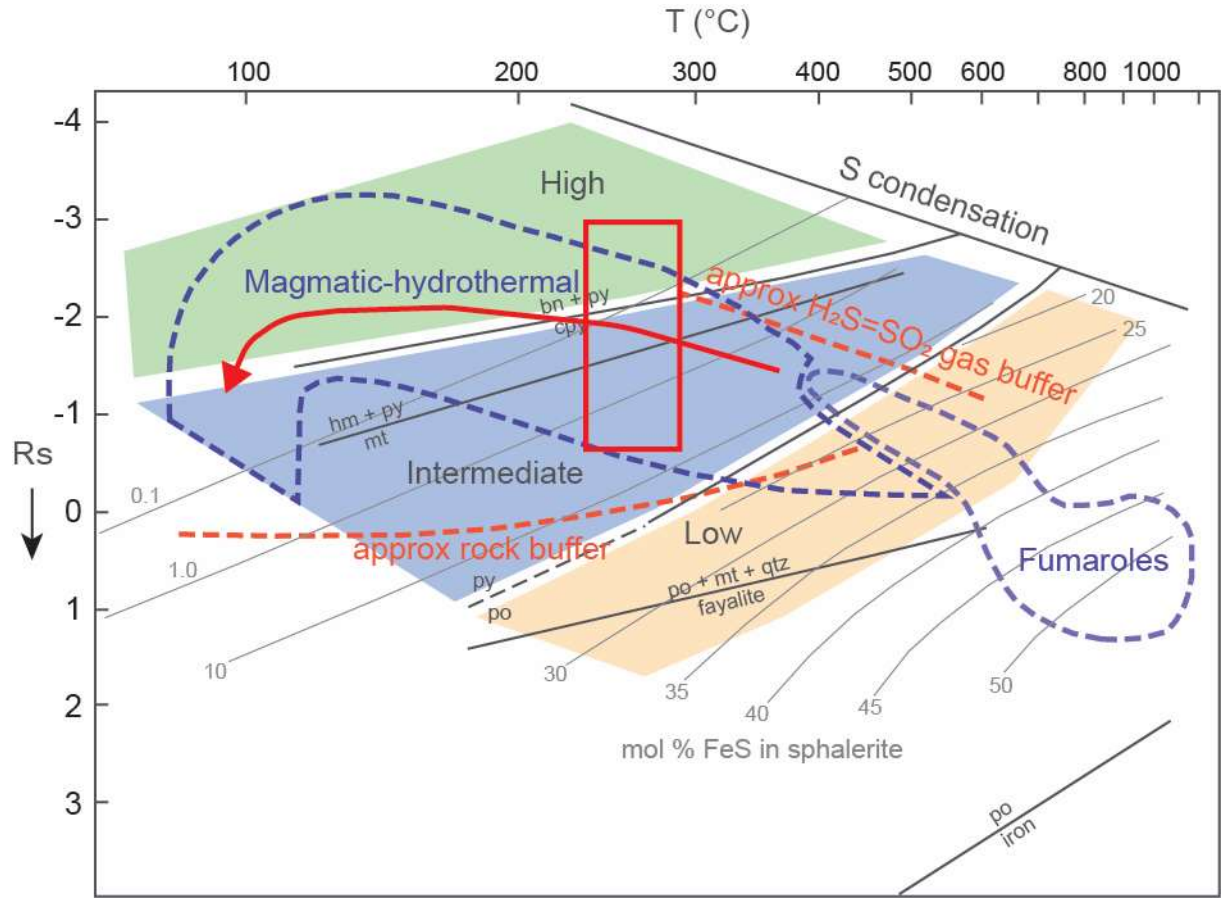

Figure 6.4 Rs-T diagram showing parameters for high, intermediate, and low sulfidation state and mineral sulfidation reactions, modified from Einaudi et al. (2003). The red box indicates the temperature of entrapment measured form FI's in Q2 and the red line showing the proposed hydrothermal fluid evolution path of the Caribou-Cross deposits. Grey contours show amount of iron in sphalerite. Because there is low iron in sphalerite at Caribou-Cross, the deposit is in the upper right portion of the diagram.

6.6 Regional Context

With increased demand for metals and economic significance of Au, understanding these deep hydrothermal systems is imperative for exploration and further understanding of magmatic hydrothermal systems. Only a few deposits within the CMB resemble the Caribou-Cross system.

The Central City Au-Ag district, approximately 12 miles (19 km) south-southeast of the Grand Island mining district, shows large-scale zoning of precious and base metal relating to a monzonitic igneous center (Lovering and Goddard, 1950; Simms et al., 1963). Alford et al. (2020) suggested that the Central City district is a porphyry-related polymetallic Au-Ag vein deposit, which is a newly recognized deposit type based on high Au and low Cu-Mo grades and

similarities with Cordilleran polymetallic-style base metal and Ag vein deposits, which are associated with Cu-Mo porphyries. The Central City district compares to the Caribou-Cross in that they both have progressive vein re-opening and overprinting, but the Caribou-Cross does not have quartz veins with molybdenite ribbons, porphyry style veining, or district-wide metal zoning as the Central City district does (Alford et al. 2020). The Central City district was primarily valued for its Au endowment (Alford et al. 2020), whereas the Caribou-Cross have been dominantly mined for Ag. Very similarly to the Caribou-Cross, the Central City deposit follows NE-trending Laramide strike-slip faults and has been thought to be related to reactivation of pre-existing Proterozoic brittle structures (Alford et al. 2019).

The Idaho Springs district, located approximately 16 miles (26 km) south of the Grand Island mining district, dominated by Precambrian gneissic, granitic, and pegmatitic rocks intruded by Laramide age irregular plutons, are cut by faults containing vein-style ore deposits (Moench and Drake, 1966). The veins in the Idaho Springs district contain Au, Ag, Cu, Pb, and Zn, and show evidence of multiple phases of movement (Moench and Drake, 1966), similar to Caribou-Cross. Quartz is the dominant gangue mineral, followed by carbonates, while barite and fluorite are rare (Moench and Drake, 1966). The sulfide assemblage generally consists of pyrite, iron-poor sphalerite, chalcopyrite, tennantite, and galena (Moench and Drake, 1966). Gold occurs as native gold and as gold telluride; enargite, pearceite, polybasite, marcasite, wolframite, pitchblende, and coffinite are also present although sparse (Moench and Drake, 1966). Deposits in the Idaho Springs district seems very similar to the Caribou-Cross deposit at the Grand-Island district in that they both have quartz and carbonate as the dominant gangue minerals and exhibit Au, Ag, base metals, and minor uranium mineralogy.

Cordilleran Pb-Zn-Cu-(Ag-Au) veins in the Montezuma district, around 30 miles (50 km) south-southwest from the Grand Island district, are interpreted to have formed from a central magmatic source as shown by district scale metal zonation (Pyanoe, 2015). The Montezuma stock is sub-alkaline quartz monzonite (Pyanoe, 2015). The veins show a systematic decline in temperatures from 341°C in the central part to 156°C at the edge of the system, and salinities range from 11.69 to 3.70 wt% NaCl equiv. This deposit is thought to be linked to a Mo porphyry in the Montezuma district (Pyanoe, 2015). Pyanoe (2015) presents a temperature decrease to be the main cause of metal precipitation. Caribou-Cross compares to the Montezuma district in that

they exhibit similar metal endowment and are both interpreted to be genetically linked to a magmatic source within similar temperatures and salinities.

The Tungsten district in Boulder County, approximately 3 miles (5 km) to 11 miles (18 km) from the Grand Island district, contains metal-bearing veins entirely within Precambrian host rocks such as the Idaho Springs gneiss and the Boulder Creek batholith. Most of the tungsten occurs as ferberite within fine-grained horn quartz (Lovering and Tweto, 1953). These veins in the Tungsten district seem to be structure controlled, similar to the veins at the Caribou-Cross deposit. The Tungsten district also includes silver-bearing copper ore and gold telluride ore. These vein systems are thought to be sourced from a volatile-rich biotite latite magma at temperatures between 200°C and 300°C (Lovering and Tweto, 1953). Ma, (1996) suggests that the tungsten ore zone overlies a gold zone as it is interpreted to be produced by magmatic tungsten-gold hydrothermal solutions moving from a deep environment (low Eh) to a sub-surface environment (low Eh). Rice et al. (2001) suggests that the tungsten district shows an overall epithermal character and that there is a connection between mineralization and monzonitic magmatism based on close spatial association between monzonitic dikes and mineralization, similar age constraints, and geochemical zoning in wolframite. Based on oxygen isotope data, these authors also suggest that the tungsten mineralization and associated alteration is a result of tungsten bearing fluids interacting with meteoric waters, based oxygen isotope data.

The nearby Gold Hill and Ward districts, just north of the Tungsten district, contain gold tellurides and uneconomic tungsten mineralization. The tungsten mineralization postdates gold mineralization and shows a lack of district-scale zoning and is thought to be an intermediate system between the Central City district which is characterized by base and precious metal veins with a clear igneous centers and zoning but no tungsten minerals, and the Tungsten district which shows evidence for igneous involvement, presence of base and precious metals, and large tungsten endowment, but no large-scale zonation (Rice et al. 2001).

While there are several deposits that show distinct similarities, the Caribou-Cross deposit seems to be unique in mineralogy and alteration characteristics. The Caribou-Cross does not show district-scale alteration or metal zonation as the Central City deposits do. The Caribou-Cross only contains trace telluride minerals, as evidenced by the presence of hessite, which are dominant minerals in the Central City and Tungsten districts. The Caribou-Cross deposit is unique in that it is dominantly Pb-Zn-Ag-rich. The greatest commonality between the Grand

Island district and the surrounding districts described above is that they are structurally controlled and are interpreted to be genetically and spatially associated with Laramide age alkaline intrusions, which is what ties them together as part of the CMB.

CHAPTER 7: CONCLUSION

The Grand Island mining district contains base- and precious-metal vein-style structurally controlled deposits hosted in the heterogenous Caribou monzonite and the Idaho Springs gneiss. This study focuses on the paragenetic sequence, ore and alteration zonation, and the causative hydrothermal fluid evolution of the Caribou-Cross deposit.

Five lithologic host rock groups were identified within the heterogeneous Caribou monzonite: magnetite dunite, monzonite and quartz monzonite, amphibolite, magnetite amphibolite, and lamprophyre. Observations found in this study suggest the igneous suite in the Grand Island mining district followed an alkaline evolutionary path and formed through magmatic differentiation.

Alteration of the Caribou monzonite consists of early-stage hydrothermal K-feldspar occurring along fractures prior to vein formation, followed by Q1 quartz vein formation with distal chlorite alteration, sericitization of plagioclase that shows increasing intensity towards the vein, and proximal K-feldspar alteration. The first vein stage consists of pyrite and early-stage quartz (Q1) with fluid inclusions indicating a CO_2-rich hydrothermal fluid from a deep-seated magmatic source. Early quartz and pyrite are followed by ankerite. Late quartz (Q2), contemporaneous with base-metals, are formed into open vugs and are clear euhedral crystals with pristine fluid inclusions along growth zones indicating a saline fluid at temperatures of homogenization from 210 to 225°C formed at hydrostatic conditions. Chalcopyrite, galena, iron-poor sphalerite, stromeyerite, and Ag-bearing gold occur along fractures through pyrite and infilling open space. Late-stage barren carbonate veins occur throughout the district. There is a late secondary mineralization stage from the effects of oxidation and circulating meteoric waters.

Integrating these observations into context, a conceptual model involving fluid characteristics and evolution of the system through time and space has been developed. The Caribou-Cross deposit is interpreted to represent an intermediate sulfidation hydrothermal deposit formed at significant depths below the paleosurface with a deep-seated magmatic source as indicated by CO_2 inclusions.

Although the complexity of the deposit makes it difficult to delineate some relationships, the findings of this study suggest that this system evolved through time and space. There are not

distinct vein types, but rather veins reopened creating overprinting relationships. There are cross-cutting relationships and textural evidence suggesting at least two cycles of vein reactivation as the fluid evolved.

CHAPTER 8: OUTLOOK

While this research provides insight into the igneous evolution, ore, and alteration mineralogy and paragenesis, and systematics of the Caribou-Cross deposit, there are still many questions that are unanswered and hypotheses yet to be proven.

The lithologies investigated in this study provide mineralogical identification and mineralogical characterization of the rocks; however, field mapping and sampling were limited. Observed in the trenches on Caribou hill, the magnetite dunite is internally weakly stratified, and although this stratification was not studied for the purposes of this thesis, it would be worth looking into to further explain the genesis of this unit. The monzonite also occasionally shows some foliation or flow banding. This may tie into the overall deformation events occurring in the district or possibly be clues to the igneous evolution. Further investigation of group 5 (lamprophyre) rocks in the district would be necessary to confidently identify this group as a lamprophyre. Xenoliths in the monzonite, which were a large part of Lovering and Goddard's (1950) evidence for their theory of the wall-rock assimilation creating the mafic rocks in the district, should also be further investigated. If they are components of the gneiss, this would indicate wall-rock assimilation. Major element geochemistry would be necessary to determine if the igneous rock suite is related from processes of magmatic differentiation or mixing. Another key piece of information that was not investigated in this study are the contact relationships of various lithologies. More field work and examination of the contacts would be necessary to fully interpret the evolution of the igneous rocks in the Grand Island district.

Because Caribou-Cross is a magmatic-hydrothermal system, the next question becomes where is the causative intrusion? Is the Caribou stock strictly the host rock for these deposits, or could it be possible that it is the source? If the Caribou monzonite is the hydrothermal fluid source rock, this would support an early pre-vein K-feldspar alteration. The low-Si chemistry and alkaline nature of the Caribou monzonite would indicate that conditions were not conductive for quartz veins to form during this early stage of K-feldspar alteration.

Age dating of the various rock units and vein assemblages or alteration minerals would provide great insight into the timing of various host rocks and vein formation. If the veins are age-dated and correspond to the age-dates of the Caribou monzonite, then that would imply that

the Caribou monzonite is the causative intrusion, and the system could be more confidently characterized as a porphyry. If the vein assemblage is significantly younger than the Caribou monzonite, then the causative intrusion is deeper below the surface and could have economic porphyry potential.

Another goal related to the host rock lithologies was to identify how vein related alteration halos and their mineralogy changes in different host rocks. Because most of the samples for this study were in the Caribou monzonite, such observations were not made in detail; however, from logging and general field work over the last year at Caribou-Cross deposit, it appears that the alteration in the Idaho Springs gneiss is more clay-rich. It also seems like there is not significant mineralization within the magnetite dunite apart from thin wavy carbonate stringers. This would need to be investigated further. Clay alteration in any host rock was not explicitly analyzed in this study, and identification of the fine-grained clay alteration minerals by means of XRD or alternative methods for fine-grained clay species would aid in deposit characterization.

Waste-rock samples were investigated for the purpose of identifying the mineralogy at the Caribou. However, in the context of mineral exploration, these waste rocks were investigated as a potential resource for ore. The next step in characterizing and analyzing the waste rock samples for potential ore and ore zonation is to assay bulk samples taken on a grid over the identified high grade waste rock piles. It is also important to keep in mind that waste rock piles are stratified, so testing the mineralization over the full depth of the waste rock pile is necessary. It is recommended that bulk samples are taken from the waste rock piles in a grid pattern to fully characterize and understand the grade that is still present in these waste rock piles.

Much more could be added to the story with more detailed fluid inclusion analysis. Although the fluid inclusions measured in this study are primary fluid inclusions that are associated with the ore-forming fluid, the fluid inclusion results are from a small population and based on a few assumptions. The first is that the salt species was assumed to be NaCl, however, these are typically much more complicated saline systems. Only the temperature of last ice melting was measured, and not the eutectic temperature, so the particular salt species cannot be accurately determined. It is suggested that ICP work be conducted to validate the composition of the salt species. The second pitfall of the evolution of the fluid is that microthermometry could not be confidently conducted on any Q1 inclusions due to post entrapment modification.

Previous studies identified ore-related minerals that were not found in this study including gersdorffite (Write, 1954), uraninite, jalpaite, bornite (Francis, 1987), chlorargyrite, stephanite (Moore et al. 1954), molybdenite, tennantite-tetrahedrite, proustite, digenite, and native gold (Holland, 1994). Because of the nature of the sulfosalts, many were undistinguishable in optical petrography, so historically some fine-grained species might have been missed or mis-identified. The SEM-EDS allowed for semi-quantitative mineral identification on the micron scale and confident mineral identification, especially of the sulfide species. It is recommended that more samples are taken targeting the fine-grained sulfide species.

A final recommendation pertains to the presence of Au in pyrite. Sampling was targeted specifically for high-grade Au intercepts based on assay data, and then specific selections were made based on visible sulfides in veins within the high-grade intervals. Many of these samples did not contain any or very minimal gold-bearing minerals. All the steps were taken to assure that if gold exists in the veins, it would be present in the samples. There could possibly be a nugget effect since the Ag-bearing gold occurs somewhat sporadically in the sulfide veins. It is also a possibility that Au exists as invisible gold in the pyrite lattice, and it cannot be macroscopically identified but would instead require microprobe or LA-ICP-MS investigation. Evidence for Au-bearing pyrite would suggest that the fluid precipitated Au much earlier than presented in this study, and Au-bearing pyrite would have huge implications for metallurgy and exploration.

REFERENCES

Alford, L., Gysi, A.P., Hurtig, N.C., Monecke, T., Pfaff, K., 2019, Porphyry-related polymetallic Au-Ag vein deposit in the Central City district, Colorado: Mineral paragenesis and pyrite trace element chemistry: Ore Geology Reviews, v. 119, p. 1-20

Barrett L.F., and Schuiling, W.T., 1988, Project status and recommendations for continued evaluation: internal report to Hendricks Mining Co., 118p.

Barrett, L.F., 1989, 1989 Exploration Program Cross Mine, Boulder County, Colorado, internal report to Hendricks Mining Co., 15 p.

Bastin, E.S., and Hill, J.M., 1917, Economic geology of Gilpin County and adjacent parts of Clear Creek and Boulder counties, Colorado: U.S. Geological Survey, Professional Paper, v. 94, 1-379.

Brodin, B.V. 1960. Galena-chalcocite myrmekitic intergrowths. Zap. Vses. Mineral. Obshst., 89, 415-423 (in Russian)

Burlingame, W.E., 1939, Report on the property of the Cross Gold Mining Company, Caribou, Colorado, internal report to Mr. W.T. Dofflemyer, 13 p.

Caine, J.S., Ridley, J., Wessel, Z.R., 2010, To reactivate or not to reactivate—Nature and varied behavior of structural inheritance in the Proterozoic basement of the eastern Colorado Mineral Belt over 1.7 billion years of earth history. In Morgan, L.A., Quane, S.L., eds., Through the Generations: Geologic and Anthropogenic Field Excursions in the Rocky Mountains from Modern to Ancient: Geological Society of America Field Guides, p. 119-140

Calias Resources, 2016, Caribou and Cross Mines, High grade gold and silver mining in the United States-Colorado, internal presentation

deKay, K.J., 1993, Gold mineralization in the Gem-Franklin vein, Idaho Springs district, Clear Creek County, Colorado, M.Sc. thesis, Golden, Colorado, The Colorado School of Mines

Dentler, P.L., 1984, Geology and ore deposits of the Cross mine, Boulder County, Colorado: M.Sc. thesis, Boulder, Colorado, University of Colorado, 108 p.

Einaudi, M.T., Hedenquist, J.W., and Inan, E.E., 2003, Sulfidation state of fluids in active and extinct hydrothermal systems: Transitions from porphyry to epithermal environments: Society of Economic Geologists Special Publication 10, p. 285–313.

Francis, K.A., 1987, Geology and geochemistry of the Caribou Mine, Boulder County, Colorado: M.Sc. thesis, Boulder, Colorado, University of Colorado, 120 p.

Gable, Dolores J., 1984, Geologic Setting and Petrochemistry of the Late Cretaceous-Early Tertiary Intrusives in the Northern Front Range Mineral Belt, Colorado: U.S. Geological Survey Professional Paper 1280, 33 p.

Hard Rock Consulting, LLC, 2017, Updated NI 43-101 Technical Report on Resources, Grand Island Resources Inc., Consolidated Caribou Project, Boulder County, Colorado, USA; prepared for Grand Island Resources Inc., February 22, 2017, 122 p.

Hedge, C.E., Peterman, Z.E., Braddock, W.A., 1967, Age of the Major Precambrian Regional Metamorphism in the Northern Front Range, Colorado: Geological Society of America Bulletin, vol. 78, no. 4, p. 551–557.

Hedenquist, J.W., Arribas, A.R., Gonzalez-Urien, E., 2000, Exploration for Epithermal Gold Deposits, Gold in 2000, Steffen G. Hagemann, Philip E. Brown

Holland, K., 1994, Structure, mineralization, and alteration of the Cross deposit, Boulder County, Colorado: M.Sc. thesis, Golden, Colorado, The Colorado School of Mines, 139 p.

Jobodwana, M., 1991, Geochemistry, ore mineralogy and hydrothermal alteration of the Cross gold mine: M.Sc. thesis, Boulder, Colorado, University of Colorado, 142 p.

Kouzmanov, K., C. Ramboz, L. Bailly, K. Bogdanov. 2004. Genesis of high-sulfidation vinciennite-bearing Cu-As-Sn (±Au) assemblage from the Radka copper epithermal deposit, Bulgaria: Evidence from mineralogy and infrared microthermometry of enargite. Canad. Mineral., 42, 1501-1521.

Burnham, C.W., 1997 in: Barnes, H.L., (ed.), Geochemistry of Hydrothermal Ore deposits, 2nd Edition, John Wiley & Sons, Inc., USA. p. 63-123.

Kramer, A.M., 1984, Paragenetic and fluid inclusion study of the Smith vein, Smith Mine, Blackhawk, CO: M.Sc. thesis, Golden, Colorado, The Colorado School of Mines, 100 p.

Lindgren, W., 1928, Mineral deposits: New York, McGraw-Hill.

Lovering, T.S., and Goddard, E.N., 1938, Laramide igneous sequence and differentiation in the Front Range, Colorado: Bull. Geol. Soc. Am. V. 49, p. 35-68.

Lovering, T. S., and Goddard, E.N., 1950, Geology and Ore Deposits of the Front Range, Colorado: U.S. Department of the Interior, U.S. Geological Survey, Professional Paper, v. 233, p. 319.

Lovering, T.S., and Tweto, O., 1953, Geology and Ore Deposits of the Boulder County Tungsten District, Colorado: U.S. Department of the Interior, U.S. Geological Survey, Professional Paper, v. 245, p. 209.

Lytle, M., 2016, The Proterozoic history of the Idaho Springs-Ralston shear zone: evidence for a widespread ca. 1.4 Ga orogenic event in central Colorado: Unpublished M.Sc. thesis, Golden, Colorado, The Colorado School of Mines, 95 p.

Ma, H., 1996, Aspects of tungsten-gold association at the Tungsten District, Boulder County, Colorado, PhD dissertation, The University of Texas at Dallas

Miller, H., 1983, Mineralogical report on the Caribou Mine, Boulder County, Colorado, internal report to Mr. Tom Hendricks, 4 p.

Moench, R. H., and A. A. Drake, 1966, Economic geology of the Idaho Springs district, Clear Creek and Gilpin Counties, Colorado: U.S. Department of the Interior, U.S. Geological Survey Bulletin 1208.

Moore, F.B., Cavender, W.S., and Kaiser, E.P., 1957, Geology and uranium deposits of the Caribou area, Boulder County, Colorado: U.S. Department of the Interior, Geological Survey Bulletin 1030-N, 34 p.

Moore, F.B. and Cavender, W.S., 1951, Geologic maps of the 380, 470, 530, 600, 670, 740, 800, and 860 levels, Caribou Mine, Boulder County, Colorado, U.S. Department of the Interior, U.S. Geological Survey

Nigbor, M.T., 1986, Petrographic data on the Cross Gold Mine: U.S. Department of the Interior, Bureau of Mines, internal report to Hendricks Mining Co., 45 p.

Pyanoe, D., 2015, Fluid inclusion and metal ratio analysis of cordilleran Pb-Zn-Cu-(Ag-Au) veins of the Montezuma district: Summit County Colorado, USA: M.Sc. thesis, Fort Collins, Colorado, Colorado State University, 138 p.

Reynolds, D.L., 1935, The genetic significance of biotite-pyroxenite and hornblendite : Min. und Petro. Mitt. 46, p. 447-490.

Rice, C.M., Harmon, R.S., Boyce, A.J., Fallick, A. E., 2001, Assessment of grid-based whole-rock δD surveys in exploration: Boulder County epithermal tungsten deposit, Colorado, Economic Geology, v. 96, p. 133–143.

Rock, N.M.S., 1977, The nature and origin of lamprophyres: some definitions, distinctions, and derivations: Earth-Sci. Rev., 13: p. 123-169.

Sillitoe, R. H., 2010, Porphyry copper systems: Economic geology and the bulletin of the Society of Economic Geologists, v. 105, no. 1, p. 3–41.

Smith, W., 1938, Geology of the Caribou stock in the Front Range, Colorado: American Journal of Science, p. 161-196.

Smith, D.A, 2003, Silver Saga: The Story of Caribou, Colorado, Revised Edition, University Press of Colorado, 230 p.

SRK, 2011, Updated NI 43-101 Technical Report on Resources, Calais Resources, Inc., Consolidated Caribou Project, Boulder County, Colorado, USA; prepared for Calais Resources, Inc., 100 p.

Tweto, O., and Sims, P.K., 1963, Precambrian ancestry of the Colorado Mineral Belt: Geological Society of America Memoir 144, 44 p.

Wang, H., Lan, T., Chen, Y., Hu, H., and Shu, L., 2022, Mobilization of Au and Ag during Supergene Processes in the Linglong Gold Deposit: Evidence from SEM and LA-ICP-MS Analyses of Sulfides: Minerals (Basel), v. 12, no. 3, p. 367.

Wilson, A., and Sims, P.K., 2003, Colorado Mineral Belt Revisited- An Analysis of New Data: USGS Open File Report 03-046

Winter, J.D., 2014, Principles of igneous and metamorphic petrology, second edition, Pearson Education Limited.

Write, H.D., 1954 Mineralogy of a uraninite deposit at Caribou, Colorado: Economic Geology, v. 49, p. 129-174.

APPENDIX A: WASTE ROCK FIELD DESCRIPTIONS

Table A.1. Field descriptions of the waste rock piles

Station Name	Waste rock pile Name	Field Notes
SW Pandora Dump	Minor pit just SW of the main Pandora dump	No sulfides observed on the dumps, but there is oxidized and silicified or sericitized material that has some Cu-carbonates and reddish oxide veins
Old Mill by 505 parking lot	Unknown mill by the 505 parking lot	Pyrite veins and stockworks throughout; the main material is oxidized stockwork monzonite
659	Unknown dump off of the 505, about 200 ft N of the Grey Eagle vein dump	Moderately oxidized felsic monzonite with limonitic stockworks and pyrite in veins throughout; local jarosite alteration, some box works
651	Isabel vein dump- also San Isabel dump (SI-#)	Mostly red oxidized and white fresher felsic monzonite, abundant hematite intermixed with chalcopyrite or tarnished pyrite, possibly bornite; all sulfides seen are along veins, vuggy qtz slightly less common, magnetite float abundant. There was abundant magnetic dike with amphibole, epidote, and pyroxene. The sulfides were abundant and dominantly chalcopyrite occurring in vugs and veins. The sulfides often occurred in very oxidized quartz veins. Malachite was common. There were stockworks, but not a lot of breccia, only in minor veins. The mafic rocks are not oxidized. Alteration was dominantly sericite and oxidation
647	Amazon vein dump	Dump had fair amount of vuggy quartz and jarosite altered material with abundant pyrite
656	Unknown dump	Exploratory shaft near Isabel dumps, lots of hematite and oxides; magnetite and pyrite, and a specularite rich boulder near the top of the dumps
667	Unknown dump	Mostly oxides at this dump, but some isolated sulfide rich material, including pyrite veins within silicified and oxidized monzonite. Some pyritic material with oxidized and possibly brecciated monzonite.
NS	Near Native Silver Vein	Mostly altered monzonite with less than 5% fresh rock. Strongly oxidized with limonite and hematite staining. Veins are dominantly quartz gangue with pyrite and chalcopyrite. Veins are often stockwork and some breccia. Alunite occurs in vugs on the surfaces of the rocks. Euhedral quartz grows in open vugs and veins. Microcrystalline quartz also occurs. Specular hematite, malachite, chlorite, slicken lines, and thin black veins occur throughout the pile.